

**CHARACTERIZATION OF WEAK ROPE THROUGH THE  
DESIGN AND CONSTRUCTION OF A  
PORTABLE TENSILE TESTING MACHINE**

BY

**GLENN M<sup>C</sup>GILLICUDDY**

B.S. Mechanical Engineering, University of New Hampshire, 2001

**THESIS**

Submitted to the University of New Hampshire  
In partial fulfillment of  
The Requirement for the Degree of

Master of Science

In

Ocean Engineering

December 2005

This thesis has been examined and approved.

---

Thesis Director, Kenneth C. Baldwin  
Professor of Mechanical and Ocean  
Engineering

---

Lloyd C. Huff  
Research Professor of Center for Coastal  
And Ocean Mapping

---

Scott Kraus  
Vice President for Research,  
New England Aquarium

---

Yuri Rzhanov  
Research Associate Professor of Center  
For Coastal and Ocean Mapping

---

Date

## **DEDICATION**

To my family, friends, and colleagues.

## **ACKNOWLEDGEMENTS**

This work is a result of research sponsored in part by the New England Aquarium and the National Ocean and Atmospheric Administration, U.S. Department of Commerce under grant number: 14N372 through the University of New Hampshire.

I would like to take this opportunity to thank the following people for their support throughout this project. To Paul Lavoie, thank you for your engineering and fabrication support for which the project depended on. To Dr. Lloyd Huff, for his endless knowledge on every topic encountered for the duration of the project (and then some) and for giving me direction when the correct path seemed to be unclear.

Appreciation is extended to Dr. Yuri Rzhanov as well, for his video image processing techniques in extracting the high resolution elongation data. To Dr. Ken Baldwin, thank you for your guidance as a graduate advisor and for providing feedback and revisions on this work. To Dr. Barbara Kraft, thank you for answering countless Matlab questions and providing direction to appropriate data processing techniques.

To Dr. Scott Kraus, a thanks for the background insight as to why the project is important and the years of knowledge of whale behavior and entanglements. Thanks to Jud DeCew, Chad Turmelle, and Glen Rice for the splicing lessons, the occasional helping hand, and reality checks. To Dr. Norm Holy and Bob Ames of Seaside Inc., thank you for the development of WSR and providing a sample for testing. Last but not least, to the whole of CCOM, especially Director Larry Mayer, for providing the

facilities and the flexibility in the daily work schedule to complete this milestone in my education. I am greatly in debt to you all. Thank you.

## TABLE OF CONTENTS

DEDICATION .....	iii
ACKNOWLEDGEMENTS .....	iv
LIST OF TABLES .....	ix
LIST OF FIGURES .....	x
NOMENCLATURE.....	xiii
ABSTRACT .....	xv
CHAPTER I: INTRODUCTION.....	1
1. Background .....	1
2. Goals / Objective.....	5
3. Approach.....	5
CHAPTER II: CORDAGE INSTITUTE GUIDELINES .....	7
CHAPTER III: MACHINE DESIGN .....	10
1. General .....	10
2. Mechanical .....	14
3. Hydraulics .....	26
CHAPTER IV: FABRICATION .....	33
1. Part Specification .....	33
2. Assembly.....	36
3. Apparatus Testing and Modification.....	39
CHAPTER V: INSTRUMENTATION .....	44

1. General System Overview.....	44
2. Measurement System Error Analysis.....	48
3. Instrument Calibrations.....	52
CHAPTER VI: ROPE TESTING .....	57
1. Experimental Design.....	57
2. Procedure .....	60
CHAPTER VII: DATA PROCESSING .....	69
1. General.....	69
2. Video Data Processing.....	70
3. Matlab Data Processing .....	73
CHAPTER VIII: RESULTS AND DISCUSSION .....	76
1. General.....	76
2. Physical Properties.....	78
3. Engineering Properties.....	80
CHAPTER IX: CONCLUSIONS .....	86
REFERENCES.....	89
APPENDICES .....	91
APPENDIX A: DESIGN CALCULATIONS.....	92
APPENDIX B: AUTOCAD FABRICATION DRAWINGS .....	106
APPENDIX C: MATLAB CODE .....	122
APPENDIX D: ENGINEERING STRESS-STRAIN PLOTS.....	140
APPENDIX E:	
FIRST DERIVATIVE OF STRESS WITH RESPECT TO TIME.....	144

APPENDIX F:	
SECOND DERIVATIVE OF STRESS WITH RESPECT TO TIME.....	148



## LIST OF TABLES

Table 3.1: Location of centroids for the composite beam.....	23
Table 3.2: Estimated weight of apparatus components.....	25
Table 3.3: Hydraulic piston characteristics.....	29
Table 3.4: Estimated hydraulic losses and heat generation.....	32
Table 5.1: Calculated measurement uncertainties.....	52
Table 7.1: Input arguments for RopeMovie program .....	72
Table 8.1: Strands remaining after breaking.....	76
Table 8.2: Location of breaks within the center section .....	77
Table 8.3: Physical properties.....	78
Table 8.4: Physical expected mean estimate error .....	79
Table 8.5: Engineering properties.....	81
Table 8.6: Engineering expected mean estimate error .....	84
Table A.1: Anchor pin calculation results.....	95

## LIST OF FIGURES

Figure 1.1: Vertical buoy line weak link.....	3
Figure 1.2: Gill net weak link .....	3
Figure 3.1: Flow chart of the design process .....	10
Figure 3.2: Scissor design concept.....	11
Figure 3.3: Custom Cordage testing apparatus .....	12
Figure 3.4: Hydraulic design concept .....	13
Figure 3.5: AutoCAD drawing of the UNH testing apparatus.....	15
Figure 3.6: Free body diagram of an anchor plate .....	19
Figure 3.7: Cross section of the structural members.....	23
Figure 3.8: Structural member free body diagram.....	24
Figure 3.9: UNH wave tank hydraulic power pack.....	26
Figure 3.10: Schematic of the testing apparatus's hydraulic circuit .....	28
Figure 4.1: Assembly drawing showing the placement of the thrust plate .....	37
Figure 4.2: Assembly drawing of the crosshead .....	38
Figure 4.3: Original method for securing the load cell .....	40
Figure 4.4: Modified stationary anchorage .....	41
Figure 4.5: Fray location in relation to thimble .....	42
Figure 4.6: Yarn comparison .....	42
Figure 5.1: Block diagram showing data flow .....	45

Figure 5.2: Gauge mark placement .....	47
Figure 5.3: Crosshead speed calibration setup .....	53
Figure 5.4: Calibration plot for crosshead speed .....	54
Figure 5.5: Bridgesensor calibration setup .....	55
Figure 5.6: Calibration curve for the bridgesensor .....	55
Figure 5.7: Final calibration curve for the load cell bridgesensor setup .....	56
Figure 6.1: Student's t-distribution .....	59
Figure 6.2: Setup for determining Physical properties .....	61
Figure 6.3: Masking used during black stripe application .....	63
Figure 6.4: Masking used during white stripe application .....	64
Figure 6.5: Saltwater soak .....	65
Figure 6.6: Setup for determining Engineering properties .....	65
Figure 7.1: Front panel for Lens Correct program .....	71
Figure 8.1: Comparison plot for dry and wet WSR engineering properties .....	82
Figure 8.2: Comparison plot for polypropylene and dry WSR engineering properties .....	83
Figure D.1: Engineering Stress-Strain of WSR-Dry .....	141
Figure D.2: Engineering Stress-Strain of WSR-Wet .....	141
Figure D.3: Engineering Stress-Strain Comparison of Wet and Dry WSR .....	142
Figure D.4: Engineering Stress-Strain of Polypropylene .....	142
Figure D.5: Engineering Stress-Strain Comparison of WSR-Dry and Polypropylene .....	143
Figure E.1: First Derivative of Stress for WSR-Dry .....	145
Figure E.2: First Derivative of Stress for WSR-Wet .....	145

Figure E.3: First Derivative of Stress Comparison of Wet and Dry WSR .....	146
Figure E.4: First Derivative of Stress for Polypropylene.....	146
Figure E.5:	
First Derivative of Stress Comparison of WSR-Dry and Polypropylene .....	147
Figure F.1: Second Derivative of Stress for WSR-Dry .....	149
Figure F.2: Second Derivative of Stress for WSR-Wet.....	149
Figure F.3: Second Derivative of Stress Comparison of Wet and Dry WSR .....	150
Figure F.4: Second Derivative of Stress for Polypropylene .....	150
Figure F.5:	
Second Derivative of Stress Comparison of WSR-Dry and Polypropylene .....	151

## NOMENCLATURE

A:	Cross-sectional Area
$A_s$ :	Cross-sectional Area at Maximum Stress
B:	Unit Measure for Width of the Confidence Interval
c:	Unit of Measure from the Centroid
d:	Unit Measure for Diameter
E:	Young's Modulus of Elasticity
f:	Friction Factor
F:	Applied Force
$F'$ :	Primary Shear Force
$F''$ :	Secondary Shear Force
g:	Gravitational Constant
$h_l$ :	Head Loss
I:	Area Moment of Inertia
$IT_p$ :	Initial Tension per CI Guidelines
$K_t$ :	Stress Concentration Factor
l:	Unit Measure for Length
$LD_p$ :	Linear Density per CI Guidelines
M:	Moment
$M_{max}$ :	Maximum Bending Moment
n:	Number of Samples
NA:	Neutral Axis
$N_r$ :	Reynolds Number
P:	Pressure
$P_{hyd}$ :	Hydraulic Horsepower
$P_n$ :	Pressure Drop across the component specified by n
Q:	Hydraulic Flow Rate
r:	Unit Measure for Radius
$RT_p$ :	Reference Tension per CI Guidelines
$S_g$ :	Specific Gravity of Hydraulic Oil
t:	Unit Measure for Thickness
V:	Transverse (Shear) Force or Hydraulic Fluid Velocity
$V_{max}$ :	Maximum Transverse (Shear) Force
w:	Unit Measure for Width
$\bar{x}$ :	Centroidal X-Axis Distance from the Origin
$\bar{y}$ :	Centroidal Y-Axis Distance from the Origin
$y_{max}$ :	Maximum Deflection
$Z_{\alpha/2}$ :	Z-statistic

$\alpha$ :	Form Factor based on Cross-sectional Area
$\Delta P$ :	Pressure Drop
$\beta$ :	Angle between Primary and Secondary Shear Forces
$\gamma_{H_2O}$ :	Specific Weight of Water
$\nu$ :	Kinematic Viscosity
$\theta_{max}$ :	Deflection Angle of a Beam
$\sigma$ :	Tangential Stress and Statistical Standard Deviation
$\sigma_{max}$ :	Maximum Tangential Stress
$\sigma_o$ :	Nominal Normal Stress
$\tau$ :	Transverse (Shear) Stress
$\tau_{max}$ :	Maximum Transverse (Shear) Stress

## **ABSTRACT**

### **CHARACTERIZATION OF WEAK ROPE THROUGH THE DESIGN AND CONSTRUCTION OF A PORTABLE TENSILE TESTING MACHINE**

by

Glenn McGillicuddy

University of New Hampshire, December, 2005

The North Atlantic Right Whale (NARW) is considered to be one of the world's most endangered whale species. Dr. Scott Kraus of the New England Aquarium extensively reviewed the available data and concluded that although ship/whale collisions are more deadly than entanglements it is entanglements that happen more frequently and should raise concern (Kraus 1990). Whale Safe Rope (WSR) has been developed on the premise that a whale collision with the fixed fishing gear using WSR will cause a localized point of high stress and the WSR will theoretically break at the point of impact.

This study involves the design and construction of an apparatus for evaluating the characteristics of WSR, as well as, the development of a robust experimental methodology for future evaluations of WSR or similar rope. Video image processing and typical data acquisition techniques were employed. This lead to precise engineering stress-strain curves being developed for the WSR and standard polypropylene rope. The engineering stress-strain curves of WSR indicate that the

WSR exhibited properties that more closely match that of a brittle material when compared to engineering stress-strain curves of standard polypropylene. Statistical analysis of the data supported the conclusion that the experimental methodology was robust. The results of this experimental test, as well as the development of the fixture and methodology, will allow future researchers and end-users of small size rope/line to better understand the behavior of the most common piece of equipment which impacts cost and safety in the marine industry. That is to say, rope.



# CHAPTER I

## INTRODUCTION

### 1. Background

The North Atlantic Right Whale (NARW *Eubalaena glacialis*), is considered to be one of the world's most endangered whale species. Prior to the introduction of whaling, NARW was believed to be numbered in the thousands. The large decline in past years is attributed to whaling, although the NARW has not made a significant recovery since its placement on the endangered species list in 1936.

In response to the repeated endangerment and neglect of marine mammals the United States established the Marine Mammal Protection Act (MMPA) in 1972. The act put a moratorium on all marine mammal products, foreign and domestic, to further prevent the exploitation of marine mammals and to conserve them for future generations.

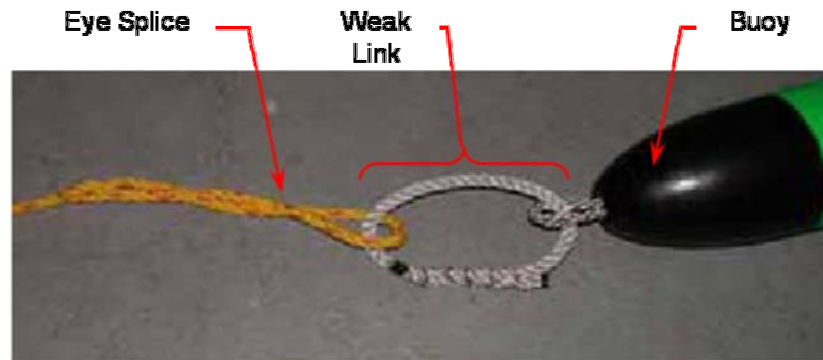
However despite these efforts, the growth rate of the NARW in recent years has been declining such that it is predicted that the NARW will likely become extinct in the year 2190 (Caswell, Fujiwara, and Brault 1999). Three factors which have been identified as major contributors to the troubled status of the NARW are: (1) water quality, (2) ship collisions, and (3) entanglements in fixed fishing gear. Kraus (Kraus 1990) extensively reviewed the available data and concluded that although ship/whale

collisions are more deadly than entanglements, it is entanglements that occur more frequently.

Of the known fifty plus deaths of NARWs between 1970 and 2001, nine percent were a direct result of entanglements in fishing gear (Knowlton and Kraus 2001). Over seventy percent of the present NARW population exhibit signs of past entanglements. More importantly, the number of potentially fatal and fatal entanglements has risen in recent years (Cavatorta et al. 2003). Cavatorta concluded that fixed traps and gill nets, as well as, the vertical buoy lines pose the most serious class of entanglement hazard.

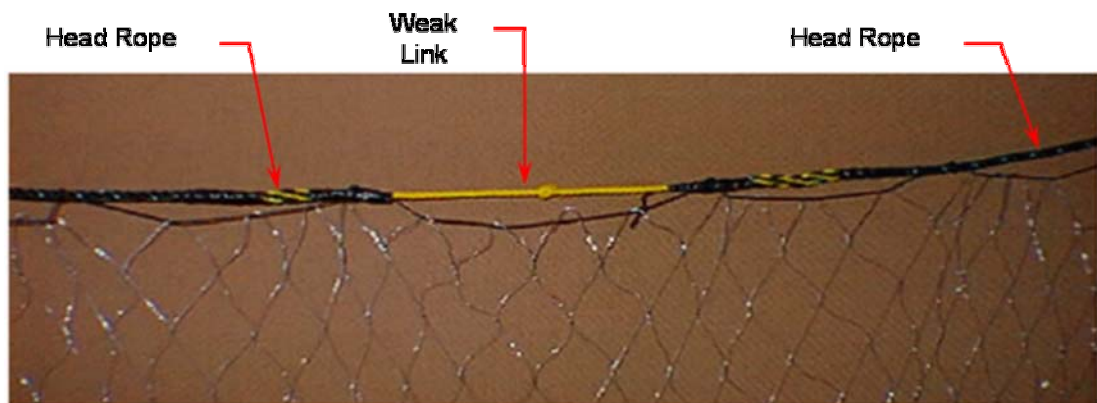
The Atlantic Large Whale Take Reduction Plan (ALWTRP) was established in response to the growing negative trend in the well-being of all large whales. The first stage of ALWTRP, which went into effect in 1997, restricted where and when commercial fixed fishing gear can be deployed. In February 1999, ALWTRP further dictated requirements on rigging and deployment methods of commercial fixed fishing gear in these restricted areas by introducing the weak link concept.

The weak link concept in commercial fixed fishing rigging consists of a weak element which is designed to fail in the event that a whale collides with the gear or somehow becomes entangled with the gear. The weak element is placed on the vertical buoy lines, specifically where the buoy is tied to the upper end of the vertical line (Figure 1.1).



**Figure 1.1: Weak link connecting surface buoy and hauling line (a.k.a. vertical buoy line weak link). Photograph courtesy of NOAA Bulletin: “Techniques for Making Weak Links and Marking Buoy Lines”.**

The reasoning behind placing the link there is that the buoy will break away thereby allowing the line to slip through the mouth of the whale, free from any obstructions, i.e. knots. Weak links are also incorporated into the float lines and net panels of the commercial gill net rigs, as seen in figure 1.2.



**Figure 1.2: Weak link installed in a gill net panel. Note the knot in the weak link to reduce the breaking strength of the weak link. Photograph courtesy of NOAA Bulletin: “Techniques for Making Weak Links and Marking Buoy Lines”.**

Although this is a huge step forward in rigging fixed fishing gear in order to improve the safety of all marine mammals, there still exist problems with these methods. The first problem being that obstacles remain attached to the line after the weak link fails and can act as points that add to the friction already experienced by the

rope in contact with the animal. These obstructions come in many shapes and forms that include but, are not limited to, intact weak links, knots used in weak links, splices (eye and/or end to end), and anything else that may be attached below the weak link which alters (increases) the overall diameter of the line used.

In an attempt to alleviate this problem, Dr. Norm Holy and Bob Ames of Seaside, Inc. developed a product called Whale Safe Rope (WSR). WSR is a polypropylene based rope with varying amounts of barium sulfate mixed into the polymer chain to control (reduce) the breaking strength of the rope. WSR was developed to avoid the difficulties with discrete weak links. Deploying WSR in all the rigging lines would eliminate the need for discrete weak links because the rigging itself is a continuous weak link. The intended advantage of using WSR is that when a large whale collides with the fixed fishing gear the resulting localized point of high stress will break there rather than at a weak link device that may be some distance away from the point of impact. The theoretical risk of entanglement in the line goes down due to the fact the animal would not be dragging anything that may get wrapped around any body appendages on the whale.

The exact interactions between large whales and fixed fishing gear are unknown because none have been observed. An effort is presently underway at the University of New Hampshire (UNH) in cooperation with the New England Aquarium (NEAq) to study the potential interactions between large whales and fixed fishing gear in the water column on a model scale. It is suggested that when the entanglement process is understood it will be evident that WSR is a viable alternative to the present combination of discrete weak link and line. This study involves determining the

engineering properties of WSR in order to better characterize it for modeling purposes. The WSR characteristics will be compared to 3/8” standard polypropylene line that is commonly used by the fixed fishing gear industry.

## **2. Goals / Objectives**

The specific goals of this research are:

- 1) Research and gather appropriate technical material to conduct the following tests on the WSR:
  - a. Physical Properties
    - i. Reference Tension
    - ii. Initial Tension
    - iii. Size Number
    - iv. Linear Density
  - b. Engineering Properties
    - i. Uncycled Strength (Breaking Strength)
    - ii. Uncycled Strain
- 2) Design and construct a portable low cost rope testing apparatus to test not only dry rope specimens but also specimens that have been soaked in salt water.
- 3) Develop the methodology and verify the degree of robustness through the analysis of experimental data. Robustness was defined in two parts:
  - a. The ability of the testing apparatus to perform without deflections or malfunctions and the measurement systems to provide consistent, accurate results.
  - b. The ability of test to be preformed by an average person without specialized training and obtain high quality and high precision results.
- 4) Characterize WSR for the UNH effort in modeling whale-gear interactions.
- 5) Compare WSR to the commercial fixed fishing industry standard 3/8” polypropylene rope.

## **3. Approach**

A critical need exists for the ways and means to evaluate varying kinds of rope, specifically Whale Safe Rope, in order to justify potential modifications to fishing

gear and in order to establish a basis for ongoing whale-gear research at UNH Ocean Engineering. This study focuses on the evaluation of WSR through the development of a testing apparatus for use in the laboratory and, if necessary, in the field. In March 2004, the Fifth International Rope Technology Workshop was attended. This provided a working knowledge of terminology, testing procedures, and the acknowledged authorities in the field of tension member research. As a compliment to the knowledge gained in the work shop, the Cordage Institute (CI) through its technical references provided detailed guide lines and valuable insights into the principals of manufacturing, testing, and application.

The information gained from the workshop and from the CI influenced the design of the rope testing apparatus. The design hinged on the general design specifications provided by Seaside, Inc. as well as the suggested testing methods of the CI and the criterion set forth by the UNH initiative. Construction began in August 2004. The rope testing apparatus which in the end underwent a series of preliminary evaluation tests followed by modifications, produced acceptable and repeatable breaks of the WSR.

After the apparatus was demonstrated to produce consistent acceptable breaks, an evaluation was conducted on the process. The evaluation verified the manufacture's load cell calibration and calibrated the cross head travel velocity. These two calibration processes ensured a known baseline for the subsequent rope testing.

A comparison of the WSR and traditional 3/8" polypropylene line, as tested on the rope testing apparatus, was made to determine what were the notable differences beyond the obvious difference in ultimate breaking strength.

## **CHAPTER II**

### **CORDAGE INSTITUTE GUIDELINES**

The Cordage Institute (CI) was founded in 1920 and is composed of manufactures and sellers of cordage, rope, and twine. The institute developed and published, in 1980, the first known testing standards for fiber ropes. The American Society for Testing Materials (ASTM) produced standards three years later which were revised in 1989. It is widely accepted that the CI's methods are the industry standards (Flory 1997). The CI revised their testing method guidelines in the early 1990's and again in 2002. The guidelines produced by the CI are so widely accepted nationally and internationally that ASTM withdrew their guidelines in June of 2002 (ASTM 1993). The CI guide lines that were followed during this study.

Several of the CI guidelines were essential to the design process which includes test specimen length, force application rate, strain rate, and minimum measurement accuracies. Compliance with these basic standards is essential to produce industry accepted results.

Specimen length plays a vital role in the design of the UNH rope testing machine because it defines not only the minimum distance between attachment points but also the dynamic range that the specimen must be stretched to break. The institute specifies two specimen sizes that are based on the overall diameter of the rope being tested. If the sample is less than 5/8" then the required length between gauge marks is

one foot. For any sample over 5/8" the required length between gauge marks is six feet. The CI also requires that there be two gauge marks which are simply non-intrusive marks placed as reference points on the rope under test. Given that the WSR has a manufacturer specified nominal diameter of 3/8", this study used a one foot measure between gauge marks. In addition to the distance between gauge marks, the CI also specifies that there must be at least one-half foot clearance at each end of the gauge marks before the terminations to the testing apparatus occur. Consequently the minimum specimen length is two feet.

The application of force to the specimen under a breaking force test is also regulated by the institute, but not as stringently. The CI states that during testing, the time allowed for the specimen to be loaded to 20% of its estimated breaking force must be in the range of two to two hundred seconds. Having established the speed for the loading, it must be maintained throughout the test in order to provide a constant and uniform strain rate. The speed for the loading helps identify the hydraulic specifications discussed in the following chapter.

Lastly, the Cordage Institute specifies minimum accuracies for all force, length, and weight measuring instrumentation. The force measurements must be accurate to  $\pm 5\%$  of the calculated reference tension unless an elongation/extension test is done. If the elongation test is to be completed, the required tolerance on accuracy is  $\pm 1\%$ . The length and changes of length must be accurately measured to  $\pm 1/16"$ . The measurement accuracy for the weight of a specimen must be measured to an accuracy of  $\pm 0.25\%$  of the total specimen weight. All these measurement systems



must have calibrations that are traceable, well documented, and conducted within one year of the date of the rope testing.

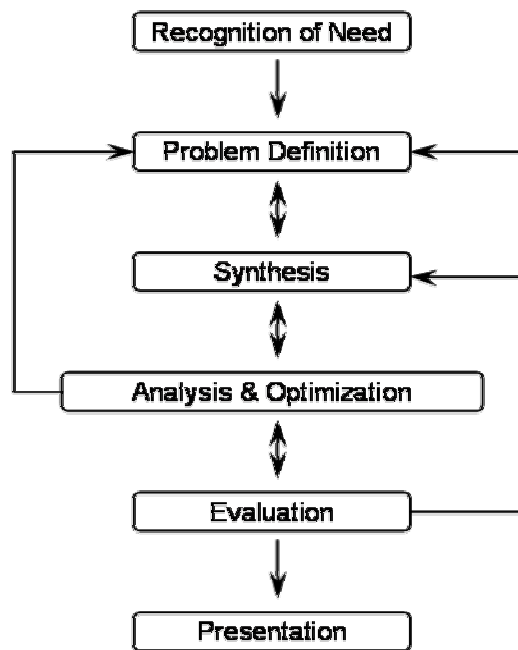
These criterion set forth by the CI are crucial to obtaining test results that are acceptable within the industry. The design, construction, and evaluation of the rope testing machine were conducted in a manner that was consistent with the CI criterion.

## CHAPTER III

### MACHINE DESIGN

#### 1. General

The design process followed a traditional mechanical engineering design process as outlined below in figure 3.1.



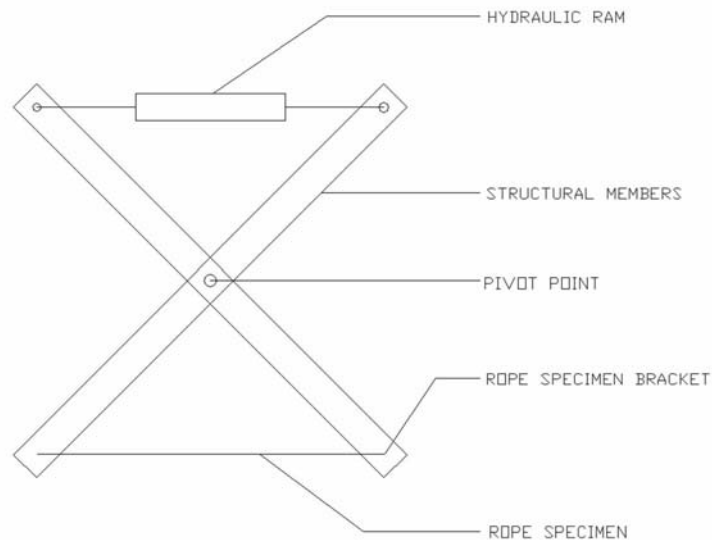
**Figure 3.1:** Flow chart of the design process employed during the design portion of the project.

The recognition of need and problem definition were clearly outlined in the introduction chapter. The third, fourth, and fifth steps, which include synthesis, analysis and optimization, and evaluation, are the discussion in this chapter.

The guidelines of the Cordage Institute were used as a basis for establishing a set of design criterion for the development of the UNH rope testing apparatus. The three categories were established for the design. They were mechanical, hydraulic, and instrumentation and were governed by CI guidelines for specimen size, force application rate, and measurement accuracies, respectively.

Working within these guidelines, a series of three initial design concepts were investigated. The three conceptual designs for the apparatus were called scissor, capstan, and hydraulic ram.

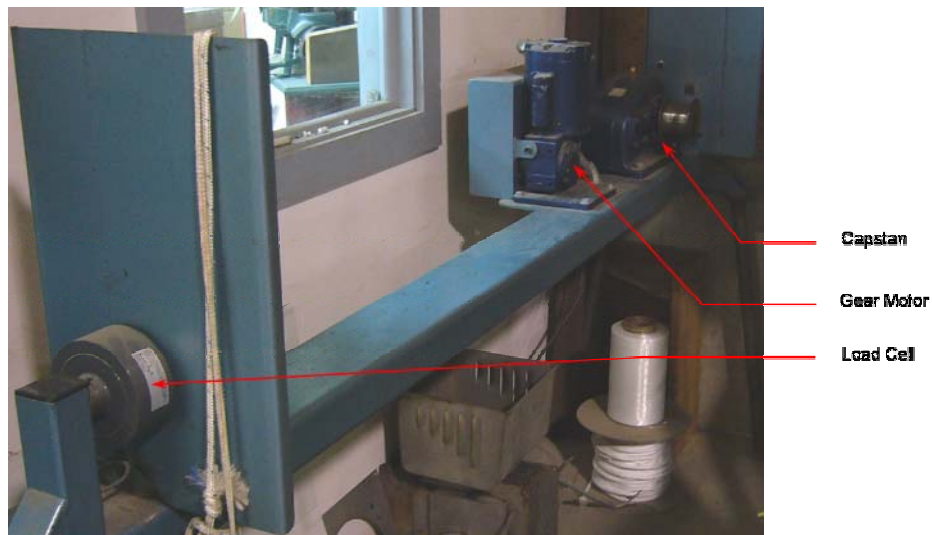
In the first design called scissor, it was conceptualized as having two strength members, probably constructed from steel box beam, that were pinned together at their centers. At one end, the two strength members would be linked via a hydraulic piston. At the opposite end of the scissor, the specimen under test would be mounted. The scissor concept is visualized in the conceptual drawing presented as figure 3.2.



**Figure 3.2: Scissor design concept (backing plate not shown).**

A structural plate for mounting the entire scissor is not shown in figure 3.2. The structural backing plate would serve to constrain the device to actions in one plane of motion. During testing, the hydraulic piston would be extended thus applying a tension force to the specimen. The idea of this design is that it could be secured to a dock with the structural members extending into the water to conduct tests while the rope specimen was under water. However, initial calculations indicated that the apparatus would be too bulky to meet a portable criterion. Furthermore considerable complexity of moving parts would be needed to constrain the scissor to one plane of action.

The second design, called capstan, was considered after a field visit to Custom Cordage of Waldoboro Maine. Custom Cordage possessed a similar apparatus to that shown, figure 3.3, which was used to conduct quality assurance tests when producing cordage for government institutions.

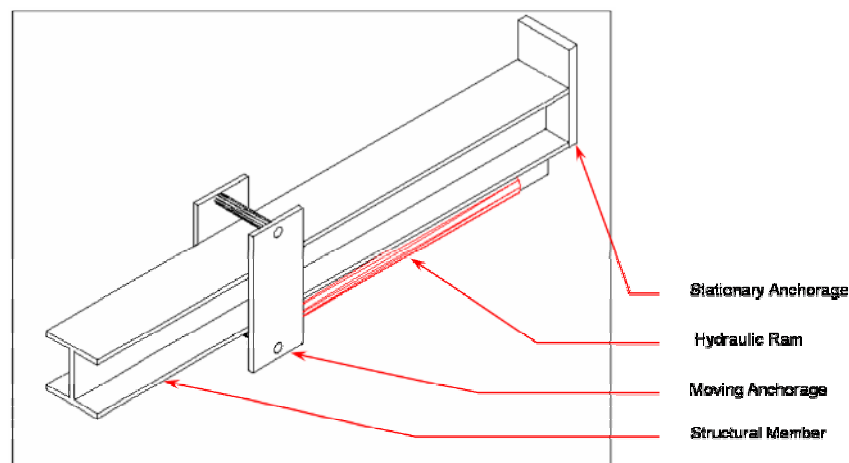


**Figure 3.3: Custom Cordage testing apparatus for quality assurance testing.**

A specimen would be secured to the load cell by taking a few wraps around a drum attached to the load cell. The other end of the specimen would be wrapped around the

rotating drum of the capstan and allowed to accumulate on the drum thus applying a tension force to the specimen. This concept had several drawbacks. When observing tests being conducted with their apparatus it was noted that the specimen would continually settle on the drum of the capstan as the tension was gradually increased until the specimen broke. It was recognized that the continual settling actually violates the Cordage Institute guidelines CI 1500-02:9.4.2 and CI 1500-02:9.4.3, which state that once a test is in progress the strain rate must continue at the same rate at which it started.

The third design, hydraulic ram, consisted of a combination of the two previous designs. The conceptual design consisted of a structural member with a fixed anchorage at one end and a moving anchorage in the opposite one-third of the structural member (Figure 3.4).



**Figure 3.4: Hydraulic design concept.**

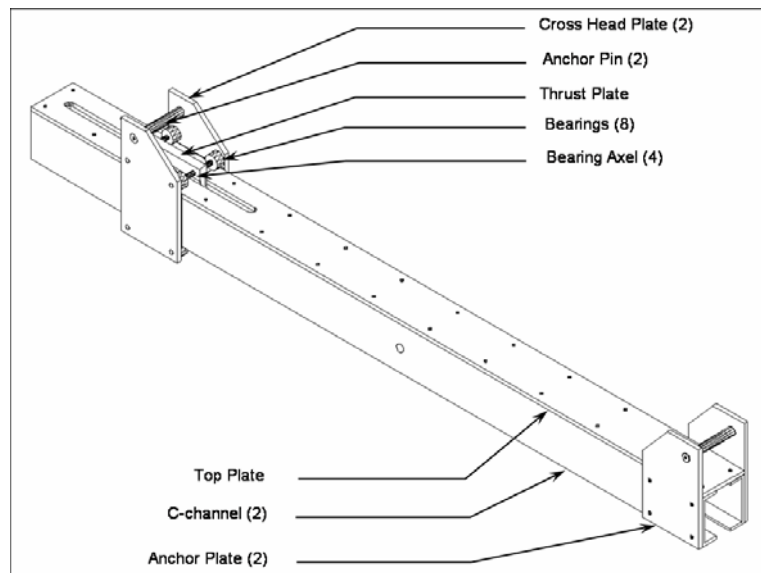
A hydraulic ram would provide the driving force for the moving anchorage. The rope member under test would be placed between the anchorages and a tensile force applied

by the ram. The only foreseeable drawback to this system was the cost associated with the hydraulic power pack needed to actuate the system.

The third conceptual design was eventually chosen over the other two designs. The mechanical category which initially took into account the specimen size was expanded to include other issues like portability, maximum design load, specimen behavior, and specimen mounting. The hydraulic category was also expanded to include limitations. In addition to the rate of force application, these limitations included specifications on several in-house preexisting hydraulic power packs. As with the other two categories, the instrumentation design category was expanded to include additional parameters above and beyond the guidelines laid out by the Cordage Institute. Based on these additional design considerations, a series of design iterations were completed prior to construction of the UNH testing apparatus. The final design evaluation is outlined in the following Mechanical and Hydraulic sections.

## **2. Mechanical**

The fundamental objective of this apparatus is simple: break the specimen of rope that is under test. However, interactions between all of the mechanical parts must be understood to confidently conclude that a test will be adequately conducted and that the measurements acquired will truly represent the conditions undergone by the specimen. The general components of the tensile testing apparatus are illustrated in figure 3.5.



**Figure 3.5: Final AutoCAD drawing of the UNH test apparatus showing the various parts. Note that the hydraulic piston is hidden inside between the C-channels.**

The mechanics of the UNH testing apparatus can be broken down further by starting with the specimen under test, progressing on to the specimen anchor points, then to the anchorages, followed by the transmission of force to the main structural member (the backbone of the apparatus), and finally to the portable supporting structure.

As previously stated, the specimen length must have a minimum length between the terminations. However, the CI specifications do not describe the type or length of the end terminations. For example when eye splices are used as specimen terminations, great care must be taken in choosing the angle at which the working end re-enters the running end of the rope. Typically in a thimble, this angle is in the neighborhood of 20 degrees off the centerline of the rope for a total spread of about 40 degrees. Also, the number of tucks must be sufficient to not cause a stress concentration in the specimen. A general rule of thumb suggests that the number of tucks must be at least five although no scientific evidence was found to validate this.

Another option for the specimen end terminations would be to take a couple of wraps around a drum and mechanically pinch the end such that the drum reduces the force to zero at this point. However, this allows the specimen to continually settle during the test which is in violation of the CI's guidelines as mentioned earlier. For this reasoning it was decided to terminate the specimen with eye splices.

The length of the specimen was crucial to sizing the design of the testing apparatus. The amount of elongation that occurs before the rope actually breaks was important because the apparatus needed to be designed with a limited amount of throw. Review of the various rope compounds indicated that nylon exhibits the greatest elongation under tension. Three-eighths inch three strand nylon, for example, has a 15% stretch at 30% of its ultimate breaking strength, which is around two tons (Sampson 2003). This suggests that if a three-foot specimen were used that it would elongate 5.5" at 30% of its ultimate breaking strength, not including any settling of the terminations. On this basis, the maximum specimen length was established at three feet and the apparatus was expected to have a working tension of 5000 pounds with a throw of at least one foot.

The design tension was set at 5000 lbs however the hydraulics (which are discussed in 3. Hydraulics) are capable of producing roughly three times that force. A second set of calculations were preformed, and thus the design revised to include this factor of safety to the system

Once the length and terminations of the specimen were considered, the design work turned to securing the specimen using eye splices. It was decided to secure the specimen using a simple pin mounted in the anchorages. The pins would have to



withstand the design tension of 5000 pounds. The pins must not only sustain this tension force but must also have a small deflection.

The anchor pins were considered as rigidly fixed ended circular beams with a single force applied to the midpoint of the span. Based on Roark's formulas for stress and strain (Young 1989), the maximum bending moment ( $M_{\max}$ ), maximum transverse shear ( $V_{\max}$ ), and maximum deflection ( $y_{\max}$ ) on the anchor pins are represented by the following expressions:

$$M_{\max} = \frac{F \cdot l}{8} \quad \text{at } \frac{l}{2} \quad (1)$$

$$V_{\max} = \frac{F}{2} \quad \text{when } F \text{ is at } \frac{l}{2} \quad (2)$$

$$y_{\max} = \frac{-F \cdot l^3}{192 \cdot E \cdot I} \quad \text{at } \frac{l}{2} \quad (3)$$

where  $F$  is the load (Force),  $l$  is the point of application of the force from an end,  $E$  is Young's Modulus of Elasticity, and  $I$  is the area moment of inertia about the centroidal axis of the beam's cross section. From general mechanics (Beer and Johnson 1996) the maximum bending moment and the maximum transverse shear equations can be written as follows for the maximum tangential stress ( $\sigma_{\max}$ ) and the maximum transverse (shear) stress ( $\tau_{\max}$ ):

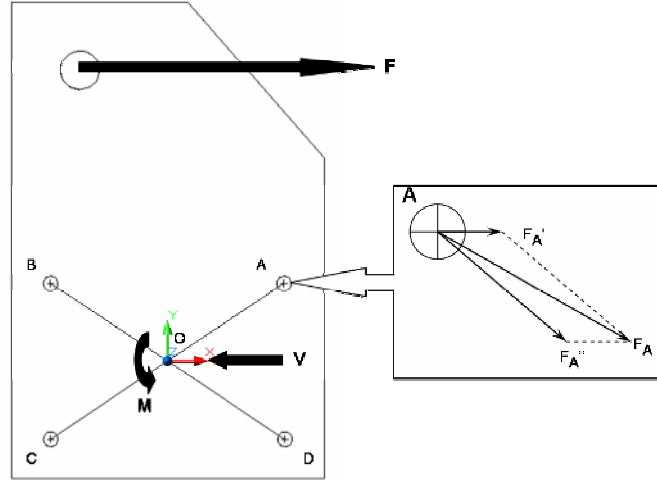
$$\sigma_{\max} = \frac{M_{\max} \cdot c}{I} \quad (4)$$

$$\tau_{\max} = \alpha \cdot \frac{V_{\max}}{A} \quad (5)$$

where  $c$  is the maximum distance from the neutral axis,  $\alpha$  is the form factor of the cross section (typically equal to  $4/3$  for a cylindrical cross section), and  $A$  is the cross sectional area.

Calculations for the pins were made for various cross sectional sizes and lengths for loads of 5000 lbs and 15000 lbs. The calculations are tabulated, in Appendix A. In the final design, a one-inch diameter by six-inch long, W1 tool steel was chosen for the anchor pins. This decision was based on the factor of safety of about 1.5 between the tangential stress and the yield stress at the design load. The fact that the theoretical deflection of the anchor pin was only four thousandths of an inch was influential in concluding the final design sizes and material.

The anchor pins tie into what is known as the anchor plates, shown in figure 3.5. These anchor plates must secure the pins such that minimal movement is allowed. The anchor plates must also withstand and transfer the forces produced during the test to the structural member of the apparatus. The anchor plate connections must be made to minimize any deflections by the apparatus's structural components that would falsify the results. Stress calculations to determine the appropriate size of the anchorages were conducted, using the coordinate system presented in the free body diagram of figure 3.6.



**Figure 3.6: Free Body Diagram (not to scale) of the anchor plate illustrating the applied force (F) and the resulting forces on the bolt pattern (A, B, C, D). The callout shows the convention used for determining the shear loading on each individual bolt.**

The initial stress calculation used a fixed plate with the design load acting along the x-axis or tangential of the plane of the plate. General thin-plate theory would have been applied in this case except that the assumption that the load is applied normal to the midsurface plane would have been violated. The flexure of straight bars can not be used because the span to height ratio (the width of the plate) in this case, is less than eight which violates a basic assumption of beam theory. Therefore, a geometric approach was taken (Frocht and Hill 1940) to compensate for the stress concentration of a one-inch hole in the anchorage plate that must accommodate the anchor pin. The stress concentration factor for the normal ( $K_t$ ) stress can be written:

$$K_t = \frac{\sigma_{\max}}{\sigma_o} \quad (6)$$

where  $\sigma_{\max}$  is the maximum normal stress, and  $\sigma_o$  is the nominal normal stress. The stress concentration factor is obtained by interpolating a graph of stress concentration

factors versus the dimensionless ratio of the hole diameter ( $d$ ) to width of the plate ( $w$ ). The nominal stress is defined as follows:

$$\sigma_o = \frac{F}{(w - d) \cdot t} \quad (7)$$

where  $t$  is the thickness of the plate. Once the nominal stress and the stress concentration factor are known, equation (6) can be solved for the maximum stress experienced based solely on the geometric properties of the hole in the plate.

Next, the forces were examined at the connection of the anchor plates to the structural backbone of the apparatus. This connection is made by a pattern of bolts. The bolt pattern that secures the anchor plates was investigated for failure in pure shear loading, bearing stress, and critical bending stress of the bolted plate (Shigley and Mischke 1989).

Figure 3.6 illustrates the name convention given to the bolt pattern along with the centroid of the bolt pattern (O) and the convention used for examining the shear load of the individual bolts. The centroid is the point at which the moment reaction is about and the shear reaction would pass through. Thus, the primary shear load ( $F'$ ), also known as the direct load, can be written:

$$F' = \frac{V}{n} \quad (8)$$

where  $n$  is the number of bolts in the bolt group. The loading on each bolt due to the moment, called the secondary shear load ( $F''$ ), can also be written:

$$F'' = \frac{M \cdot r_n}{r_A \cdot r_B \cdot r_C \cdot r_D} \quad (9)$$

where  $r$  is the radial distance between the centroid and the bolt center. Since the geometry is symmetric in both axes, the secondary shear forces are the same and can be written:

$$F'' = \frac{M}{4 \cdot r} \quad (10)$$

Through the introduction of the parallelogram rule, as seen in the call out of figure 3.6 the two vectors ( $F'$  and  $F''$ ) can be added to yield the resultant load ( $F_n$ ) on each respective bolt.

$$F_n = \sqrt{F'^2 + F''^2 + (2 \cdot F' \cdot F'' \cdot \cos \beta_n)} \quad (11)$$

where  $\beta_n$  is the angle between  $F'$  and  $F''$ . This shows the bolts that are closest to the point of application of the load experience the greatest force, in this case bolts A and B.

The bolts used to connect the anchor plates to the structural members of the apparatus are flat hex head countersunk bolts of size 3/8" – 16 x 1" composed of Grade 5 steel. Since these bolts come fully threaded, the maximum shear stress will be applied over the minor pitch diameter of the threads. By American National Standards Institute (ANSI) standards, the area at this location ( $A_s$ ) is 0.0678 in<sup>2</sup> and the maximum bolt shear stress can be written:

$$\tau_{\max} = \frac{F_{A \text{ or } B}}{A_s} \quad (12)$$

Since the thickness of the web ( $t_w$ ) of the c-channel used for the structural members of the apparatus is thinner than the thickness of the anchor plates ( $t$ ), the largest bearing stress will occur where the bolt presses against the web of the c-channel. Based on the

American Standard Channel parameters, the bearing stress ( $\sigma_{bear}$ ) can be calculated using the general stress equation with the area equal to:

$$A_{bear} = d_{bolt} \cdot t_w \quad (13)$$

The critical bending stress was calculated through the bolts A and B, where the stress is the greatest. The results of this calculation should be viewed as an approximation due the assumption that the anchor plate is indeed a bar, which as discussed earlier, violates beam theory. Equation (5) is employed with the second moment of area obtained by the implementation of the transfer formula:

$$I = I_{bar} - 2 \cdot (I_{holes} + d^2 \cdot A) \quad (14)$$

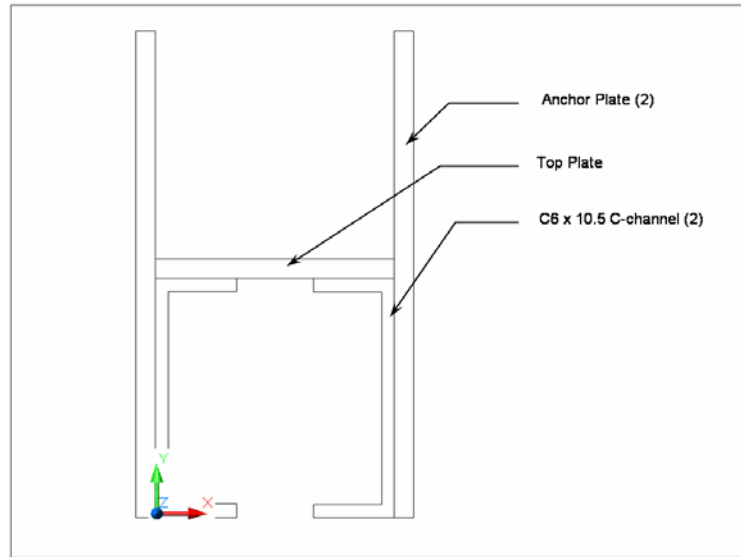
where d is the horizontal distance between the bolt pattern centroid and the bolt center.

“A” in equation (14) is the bearing area between the bolt and the anchor plate.

After these calculations were completed, a comparison was made to determine which element of the anchor plate would fail first, the stress concentration due to anchor pin hole or the shearing of the bolts due to the eccentric loading. The result was that the bolt group will fail prior to failure due to the stress concentration produced by the hole for the anchor pin. Similar, calculations were also made for the moving cross head attached to the hydraulic piston. In addition to ensuring that the bolts securing the stationary anchorage would not fail, the aforementioned set of calculations were utilized to determine the load rating of bearings needed in the cross head.

When the analysis of the anchor plates was complete, attention was moved onto the analysis of the backbone or structural members of the apparatus. The main structural member of the apparatus is actually composed of two C6 x 10.5 C-channels

with a top plate, 0.5” thick and 6” wide. As shown in the cross section depicted in figure 3.7, those items are bolted such as to create a 6.5” x 6” semi-closed U-channel.



**Figure 3.7: Cross section of the structural members in relation to the anchor plates.**

The numbering convention used for calculations assigned a #1 to the top plate, a #2 to the left hand C-channel, and a #3 to the right hand C-channel. The coordinate origin is located in the lower left corner of the composite with a right hand positive sign convention, as seen figure 3.7. The overall length of the apparatus was set at eight feet in part to accommodate potential future work on larger specimens in both the length and diameter dimension. The centroid of the cross-sectional geometry of the composite, was determined and tabulated in table 3.1.

**Table 3.1: Location of centroids for the composite beam.**

<b><i>First moments of the component areas</i></b>					
<b><u>Component</u></b>	<b><u>Area</u></b> <b><i>(in<sup>2</sup>)</i></b>	<b><u>xbar</u></b> <b><i>(in)</i></b>	<b><u>ybar</u></b> <b><i>(in)</i></b>	<b><u>xbarA</u></b> <b><i>(in<sup>3</sup>)</i></b>	<b><u>ybarA</u></b> <b><i>(in<sup>3</sup>)</i></b>
1	3.000	3.000	6.250	9.000	18.750
2	3.090	0.499	3.000	1.542	9.270
3	3.090	5.501	3.000	16.998	9.270
<b><u>Sums</u></b>	9.180	N/A	N/A	27.540	37.290

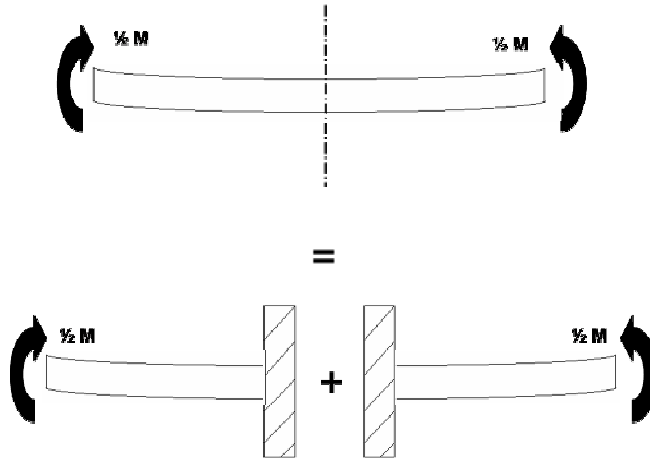
The position of the neutral axis was computed using the lower left corner of the composite as the origin:

$$\bar{x} = \frac{\sum \bar{x}A}{\sum A} \quad (15)$$

$$\bar{y} = \frac{\sum \bar{y}A}{\sum A} \quad (16)$$

The next step was to calculate the moment of inertia ( $I_{1,2,3}$ ) for each of the components and sum all the components to achieve the moment of inertia ( $I$ ) for the composite beam. Using both the maximum force output of the hydraulics and the design force based on the tensile strength of the cordage, the maximum ( $M_{max}$ ) and design ( $M_{design}$ ) moments were calculated respectively.

The principal of superposition was then applied to the length of the composite beam such that it could be divided into two equal halves as seen in figure 3.8.



**Figure 3.8: Structural member free body diagram. Illustration showing the analysis technique to determine the stress and deflections of the test apparatus's structural members.**



This allows for each half section to be represented as a member loaded by a concentrated intermediate moment. Furthermore, the boundary conditions of a fixed end can be applied at the end where the full length beam was cut in half and a free end can be applied at the ends of the full length beam. This is possible because in the middle of the full length beam, the deflection angle is zero and the moment is zero. The worst case scenario for the two equal halves is when the moment is applied at the free end, so these are the conditions that define the calculations. The deflection magnitude ( $y_{max}$ ) and deflection angle ( $\theta_{max}$ ) are represented by the equations:

$$y_{max} = \frac{M_{max} \cdot l^2}{2 \cdot E \cdot I} \quad (17)$$

$$\theta_{max} = \frac{-M_{max} \cdot l}{E \cdot I} \quad (18)$$

where  $l$  is the length of the half composite beam. Equation (4) can also be applied at this point substituting the location of the neutral axis ( $y_{bar}$ ) for “c” to yield the stress in the composite.

A table of weights was constructed as the final phase of the design analysis on the mechanical elements of the UNH apparatus.

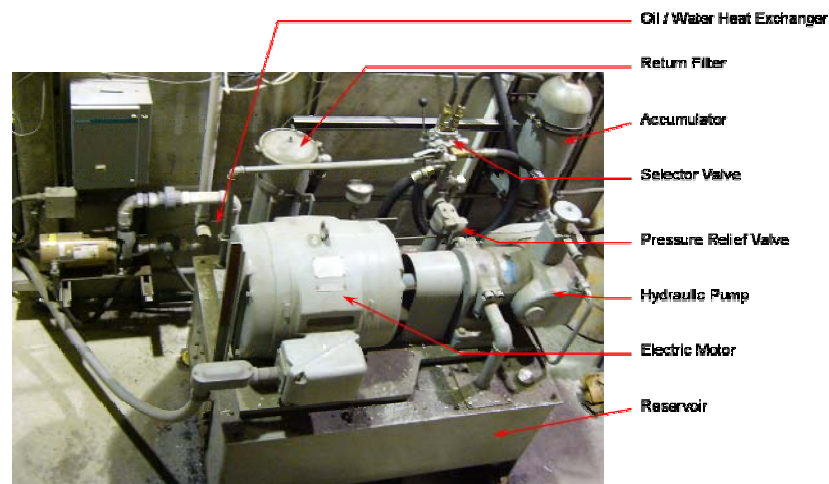
**Table 3.2: Table of weights for mechanical components only.**

<b><i>Estimated weight of apparatus components</i></b>			
<b><u>Component</u></b>	<b><u>Calculated Weight</u></b>	<b><u>Number Needed</u></b>	<b><u>Total Weight</u></b>
	<b><i>(lb)</i></b>		<b><i>(lb)</i></b>
Anchor Pin	1.61	4	6.42
Anchor Plate	13.82	2	27.64
Cross Head Plate	15.79	2	31.58
Thrust Plate	22.56	1	22.56
Top Plate	81.22	1	81.22
C-channel	84	2	168
		<b><u>Grand Total (lb)</u></b>	337.42

This indicates that the legs which support the apparatus must support about 340 lbs, not including any of the hydraulic parts. It was decided to construct the legs at a 45 degree angle to offer the most support against tipping and to place scaffolding casters under the legs so that it can easily be rolled around. The structural members were also place at a height above the floor such that the bottom edge was relatively the same height of a standard pickup truck bed for ease of transportation to a remote site. The attention to mechanical design and the sizing of critical elements that are subject to stress was important to achieve the mechanical aspect of robustness.

### 3. Hydraulics

The Jere A. Chase Ocean Engineering Laboratory houses a variety of hydraulic equipment. The largest being the custom power pack for the Tow/Wave tank wave generator pictured below.



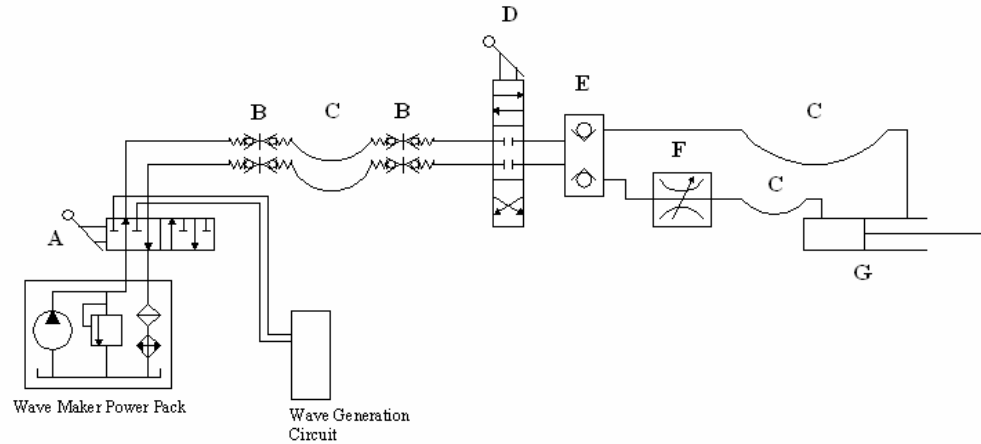
**Figure 3.9: Hydraulic Power Pack used for the generation of waves in the Jere A. Chase Ocean Engineering Laboratory. Note the placement of the selector valve installed to switch between wave generation and power take off (PTO) circuit.**

This power pack has a maximum flow capacity of 19.8 gallons per minute (GPM) at a maximum output pressure of 5000 psi. The adjustable pressure relief valve is currently set at 1950 psi with an inline accumulator with a pressure setting of 650 psi. The hydraulic horsepower ( $P_{hyd}$ ) produced by a power pack (Cundiff 2002) is written:

$$P_{hyd} = \frac{P \cdot Q}{1714} \quad (19)$$

where  $P$  in psi is the output pressure and  $Q$  in GPM is the flow rate. In this case the power pack is capable of generating 22.5 hp at the current settings or 57.7 hp at maximum capacity. Although it constituted a violation of the portability goal, it was decided to use this power pack for the actuation of the UNH rope testing apparatus. The decision was largely based on economics. If portability becomes a major issue then a different power pack will be required.

It was purposed to modify the current setup, by incorporating a power take off (PTO) point. This would create a point where by the rope testing apparatus's hydraulic circuit could be connected and disconnected with ease. The selection between the wave generation circuit and the PTO is accomplished using what is known as a selector valve, marked by the letter "A" in figure 3.10.



**Figure 3.10: Schematic showing the rope testing apparatus's hydraulic circuit and the insertion of the selector valve to create a PTO point.**

When the PTO circuit is selected via the selector valve, hydraulic power is transmitted through quick disconnects (B) into flexible hydraulic hoses (C) to the apparatus where an identical set of quick disconnects are located. The hydraulic fluid then flows to a directional control valve (D) to control the actuation direction of the hydraulic piston (G). The allowable actuation direction can be either extend, contract, or neutral. Beyond the directional control valve (DCV), a load check valve (E) was placed to prevent the hydraulic piston from moving when the DCV is in the neutral position. Since the Cordage Institute specifies a constant strain rate, a flow control valve (F) is placed in-line with the line that supplies hydraulic pressure to the extension of the hydraulic cylinder.

To determine the implications of this circuit on the operation of the hydraulic power pack, a theoretical analysis was conducted (Cundiff 2002) of the expected requirements and losses for pressure, flow, and the amount of heat production. A piecewise approach was taken to analyze the circuit starting with the requirements of the hydraulic piston. As stated before, the travel rate of the hydraulic cylinder must

remain constant throughout the test. It was decided that the rate should be 144 inches per minute. Multiplying the flow rate by the surface area of the hydraulic piston yields a flow rate of hydraulic fluid to move the piston at the desired velocity. The pressure output from the power pack required to produce the design tension on the specimen was found by dividing the required tension by the surface area of the piston. These calculations were made for various piston surface areas and are tabulated below.

**Table 3.3: Table of varying piston surface areas and the required flow rates and pressure inputs.**

<b>Hydraulic piston characteristics</b>					
<b>Geometric Characteristics</b>			<b>Hydraulic Characteristics</b>		
<b>Velocity</b>	<b>Diameter</b>	<b>Surface Area</b>	<b>Flow Rate</b>	<b>Pressure Input</b>	
<i>(in/min)</i>	<i>(in)</i>	<i>(in<sup>2</sup>)</i>	<i>(gal./min)</i>	<i>Design (psi)</i>	<i>Maximum (psi)</i>
144.00	1	0.79	0.49	6366.2	19098.59
	1.5	1.77	1.1	2829.42	8488.26
	2	3.14	1.96	1591.55	4774.65
	2.5	4.91	3.06	1018.59	3055.77
	3	7.07	4.41	707.36	2122.07
	3.5	9.62	6	519.69	1559.07
	4	12.57	7.83	397.89	1193.66

Based on these calculations and the geometric restrictions imposed by the strength member of the apparatus it was decided to use a 2-1/2" diameter hydraulic piston.

Working backwards towards the hydraulic power pack and leaving the lines and hoses for later analysis, attention was turned to the flow control valve. This valve is designed to regulate the flow to the linear actuator while maintaining the system pressure on the relief valve ( $P_r$ ). Consequently it is called a pressure-compensated flow control valve. As the pressure required to actuate the linear actuator ( $P_L$ ) is increased, the pressure drop across the valve ( $P_{fc}$ ) decreases and therefore maintains a constant load on the pump as expressed by equation (20).

$$P_r = P_{fc} + P_L \quad (20)$$

This can be considered the worst case scenario because it assumes zero pressure drop across the pressure relief valve in the system. Anytime there is a pressure drop across a component, heat is generated. This generation of heat can be calculated by using equation (19) wherein “ $P$ ” in the equation can be attributed to the pressure drop across the component. Using the pressure calculated from equation (20), it can be seen that in the worst case the heat generated by this flow control valve is equivalent to eleven horsepower.

A similar process was used to determine the operating characteristics of the load check valve. A load check valve simply locks the hydraulic piston in position whenever the DCV is in the neutral position. This is achieved through the use of two pilot-operated check valves with the pilot line of one valve connected to input line of the other. According to the manufacturer’s documentation, the typical pressure drop across this component is five psi at the design flow rate.

The directional control valve, quick disconnects, and selector valve have manufacturer defined pressure drops of two, three and three pounds per square inch respectively. Equation (19) was employed to predict the potential heat generation of those three system components. The final major losses in the system are due to the lines and hoses. It was assumed that the majority of these losses can be contributed to the two fifty-foot lengths of hose because the remaining lines and hoses in the system are very short compared to them. Estimating the losses incurred by the fluids traveling through the lengths of hoses were less straight forward than the estimates for other component losses in the system. The first step was to determine the type of flow that was expected in the hoses. That was accomplished through an examination of the

dimensionless Reynolds Number. The Reynolds Number ( $N_r$ ) is defined (Cundiff 2002) as:

$$N_r = \frac{7740 \cdot \nu \cdot d_{ID}}{V} \quad (21)$$

where  $\nu$  is the kinematic viscosity (expressed in centistokes),  $d_{ID}$  is the inside diameter of the hose (expressed in inches) and  $V$  is fluid velocity (expressed in ft/s) in the hose. The Reynolds Number was found to be greater than 4000, therefore by definition the fluid flow is considered to be turbulent. Once the type of flow and the Reynolds Number was established, the Blasius equation can be applied to determine the friction factor of the inside of the hose due to the surface roughness. The Blasius equation is defined (White 1999) as:

$$f = \frac{0.3164}{N_r^{0.25}} \quad (22)$$

yielded a friction factor of 0.037. This led to the application of the Darcy-Wabaush equation (Cundiff 2002) to determine the equivalent head loss ( $h_l$ ) as defined below:

$$h_l = f \cdot \left( \frac{l}{d_{ID}} \right) \cdot \left( \frac{V^2}{2 \cdot g} \right) \quad (23)$$

where  $g$  is the gravitational constant in Imperial units. The head loss was converted to a pressure drop ( $\Delta P$ ) utilizing the head loss ( $h_l$ ), specific gravity of the hydraulic oil ( $S_g$ ), and the specific weight of water ( $\gamma_{H2O}$ ) in the following form:

$$\Delta P = \gamma_{H2O} \cdot S_g \cdot h_l \quad (24)$$

It is important to note that the specific weight of water must be expressed in units of lbf/in<sup>2</sup> for the equation to yield  $\Delta P$  in units of psi. Equation (19) was applied to compute the heat generated by this drop in pressure.

Following the calculations for the individual components, the pressure losses and heat generation parameters were summed to provide an estimate of the overall system characteristics that are presented in table 3.4.

**Table 3.4: Summarization of the pressure losses and heat generation parameters for each individual component and the estimated system wide parameters.**

<b><i>Estimated hydraulic loss and heat generation</i></b>					
<b><u>Component</u></b>	<b><u>Quantity</u></b>	<b><u>Pressure Loss (psi)</u></b>		<b><u>Heat Generation (hp)</u></b>	
		<b><i>Per Unit</i></b>	<b><i>Total</i></b>	<b><i>Per Unit</i></b>	<b><i>Total</i></b>
<b><i>Individual Parameters</i></b>					
Flow Control Valve (FCV)	1	150	150	0.268	0.268
Load Check Valve (LCV)	1	5	5	0.009	0.009
Directional Control Valve (DCV)	1	2	2	0.004	0.004
Quick Disconnect (QD)	8	3	24	0.005	0.043
Selector Valve (SV)	1	3	3	0.005	0.005
50' of Rubber hose	2	2.85	5.7	0.005	0.01
<b><i>System Wide Parameters</i></b>					
Hydraulic System	1	189.7	189.7	0.339	0.339

It is important to note that any pressure losses that may occur due to the flow through the fittings was ambiguous at this point but not neglectable. From basic fluid mechanics and empirical data, it is known that head losses in fittings are proportional to the square of the velocity. Since all the fittings to be used in the hydraulic circuit were unknown at this point, a factor of safety approach was used. The factor of safety used was two, therefore doubling the expected pressure loss and the amount of heat generated by the circuit. This conservative estimate was consistent with the robustness criteria of being able to repeatedly control the testing without damage to the machinery.



## **CHAPTER IV**

### **FABRICATION**

#### **1. Part Specification**

Many of the structural components of the rope testing apparatus were defined during the final iteration of the design process. The steel used in the fabrication of the anchor plates, cross head plates, thrust plate, top plate, and left and right c-channels were specified to be 1018 hot rolled steel. The anchor pins, cylinder pins, and bearing axels were also specified by the apparatus design calculations to be fabricated of water hardened tool steel. The bolts securing the anchorages to the c-channel must each withstand the calculated shearing force of approximately 1200 pounds. Since that value is approaching the upper limit for a  $\frac{1}{4}$ "-20 bolt, a  $\frac{3}{8}$ "-16 steel alloy flat head cap bolt was specified. The same bolts were also specified to secure the top plate to the left and right c-channels and to be placed every eight inches on center. It had been calculated that the radial bearings which guide the crosshead during actuation must be capable of withstanding a radial force of 1200 pounds and required a  $\frac{1}{2}$ " bore to accept the bearing axels. Based on availability and specifications, a  $\frac{1}{2}$ " plain bore 1" flat track radial bearing with a load rating of three tons was chosen.

The process of specifying hydraulic parts was a bit more elusive. The selection of parts depended not only on the hydraulic calculations but also on the

requirements imposed by space and mounting requirements. The hydraulic part specification followed the logic of starting with the linear actuating piston and working back to the hydraulic power pack, while leaving the lines and hoses to be the last items that were specified.

In the hydraulic section, it was shown that a hydraulic piston with a two and a half inch bore and a minimum pressure rating of 1950 psi would be well suited for the design. Based on the elongation characteristics of standard 3/8" polypropylene and the minimum specimen length, the stroke length of the hydraulic piston was determined. A stroke length of 18" was determined to be adequate. The piston was required to fit between the two c-channels. These two factors led to the design selection of a 2.5" x 18" 2500 psi rated, double acting, tie rod hydraulic cylinder manufactured by Prince Hydraulics (Model # SAE-9118).

The extension rate of the piston is controlled with a flow control valve. The flow control valve also must adhere to the minimum operating pressure rating of 1950 psi. The flow rate for this component is based on that required to extend the piston at a speed of 144 inches per minute. These requirements led to the flow control valve being specified as the Prince Hydraulic model number RD-150-8. The RD-150-8 flow control valve has a maximum pressure rating of 3000 psi and a variable flow rate between zero and eight GPM.

Addressing a safety concern that was identified during the design phase, a load check valve was added between the flow control valve and the directional control valve. This prevents movement of the piston while the directional control valve is in the neutral position. As with the previous hydraulic parts, the load check valve must

withstand a minimum pressure rating of 1950 psi and a maximum flow rate of 19.8 gpm that will be experienced during piston extension or retraction. Prince Hydraulic model number RD-1450 double pilot operated load check valve met the requirements with a maximum operating pressure of 3000 psi and a flow rate of 30 gpm.

Control for the direction of actuation was to be accomplished through use of a directional control valve (DCV). The DCV must be able to withstand a minimum of 1950 psi of hydraulic pressure and a flow rate of 19.8 gpm experienced during extension or retraction of the piston. Prince Hydraulic DCV part number RD512CB5A1B1 met these specifications and additionally provided a safety relief valve set at 2000 psi that would avoid accidental over pressurization of the system. This particular DCV also allows for power beyond (the ability to add extra DCVs with minimal plumbing) for future expansion of the apparatus to involve cyclic loading tests.

The selection between operation of the tow tank wave generator and operation of the rope testing apparatus is accomplished through a Prince Hydraulic selector valve (DS-4A4E). This valve has a maximum flow rate of 40 gpm and an operational pressure range up to 2500 psi. Since this selector valve transfers hydraulic power to either the tow tank wave generator or the rope testing apparatus, it is critical that it does not restrict the wave generators' ability to produce waves of the amplitude and frequency that are requested by the tank user.

The hoses that connect the rope testing apparatus to the hydraulic power pack via the selector valve are attached at each end using quick connects. The return line hose has a maximum working pressure of 2000 psi while the supply line has a

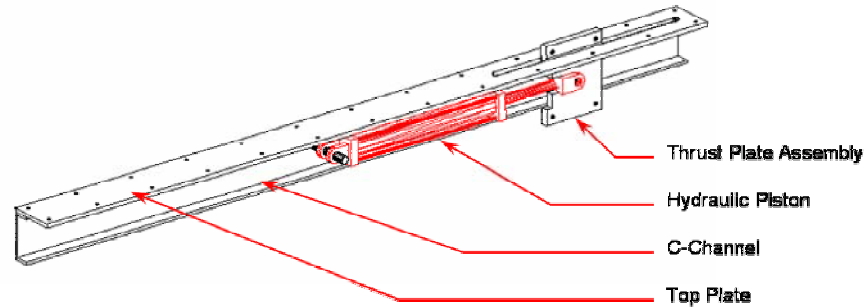
maximum working pressure of 3500 psi. These hoses, both of which are ½ inch diameter, were pre-existing parts from a previous Ocean Engineering initiative. All steel lines and fittings on the rope testing apparatus were specified to have a maximum working pressure of 3000 psi. The careful selection of components was deemed critical to meeting the requirement that the rope testing apparatus be robust and to ensuring that the operation of the tow tank wave maker, which shares the hydraulic power pack, would not be negatively impacted.

## **2. Assembly**

Prior to assembly the structural steel components were fabricated. The engineering drawings that were prepared during the design phase were subject to a design review process to produce a set of fabrication drawings. The resulting fabrication drawings, Appendix B, were used to fabricate all the necessary components. The appropriate machining practices were used during the fabrication of all parts. Additionally, good assembly techniques were employed which include, but are not limited to, the application of sealants, lubricants, torque, etc. Assembly of the structural members and the hydraulic components occurred in parallel as the hydraulic piston required encasement within the two c-channel sections and top plate.

First, one of the c-channels was attached to the top plate using the 3/8” flat hex head bolts. The thrust plate bearing material was attached to the thrust plate using the specified apparatus screws. The thrust plate was slipped into the moving clevis end of the hydraulic piston and then secured using the manufacture’s clevis pin. This sub

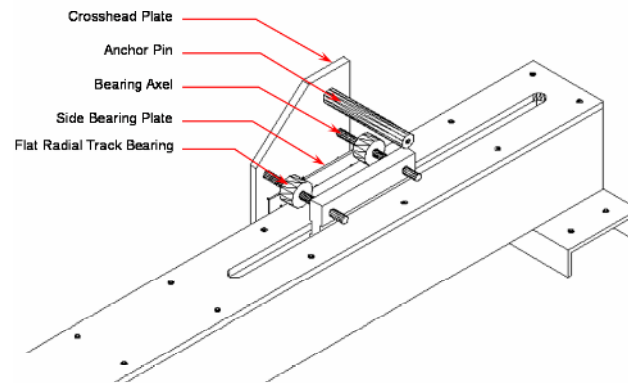
assembly was fitted into the pre-assembled c-channel and top plate where it was secured with the cylinder pin.



**Figure 4.1: Assembly drawing showing the placement of piston-thrust plate assembly in the c-channel-top plate assembly.**

The second c-channel was slipped over the cylinder pin and secured to the top plate and the leg plates were added to each end of the assembly using 3/8" flat hex head bolts. Finally the stationary anchorage was assembled by bolting the anchor plates to the two c-channels and slipping the anchor pin through the 1" hole in both plates. This completed the assembly of all the stationary structural components.

Moving onto the crosshead components, the side bearing plates were attached to each of the two crosshead plates. The four bearing axels were placed in the appropriate holes in one of the two crosshead plates. Four of the eight flat track radial bearings were then slipped onto each of the bearing axels followed by four bearing spacers. This assembly was slipped onto the rope testing apparatus ensuring that each of the bearing axels passed through the appropriate holes in the thrust plate. This stage of assembly is illustrated in figure 4.2.



**Figure 4.2: Assembly drawing of the crosshead. Note the spacer bearings to isolate the flat radial track bearings from the thrust plate.**

The remaining four bearing spacers were added to the bearing axels followed by the remaining four flat track radial bearings. The second crosshead plate was slipped over the bearing axels while taking care to ensure proper alignment. Finally the crosshead plate was secured. The leg and caster assemblies were constructed and upon their attachment to the under side of the leg plates, the mechanical assembly of the rope testing apparatus was completed.

The hydraulic components other than the piston were mounted to the apparatus in their respective positions.  $\frac{1}{2}$ " alloy steel tubing was bent to make connections between components. Hoses, not steel lines, were used to connect the hydraulic piston. This was intended to alleviate fatigue of the steel lines that may otherwise have occurred due to motion of the piston. The selector valve was mounted by the hydraulic power pack as seen in Figure 3.6 and plumbed into the existing tow tank wave generator circuit according to the manufacture's recommendations. A male and female set of quick disconnects sets were connected to two of the ports on the selector

valve. Two other male and female sets of quick disconnects were placed on the rope testing apparatus such that the hoses connecting the power pack and the testing apparatus could be removed from either or both the power pack and the rope testing apparatus. The completed assembly of the rope testing apparatus and was followed by a performance evaluation period for the apparatus. The careful attention to details during the assembly was part of the intent and design for robustness.

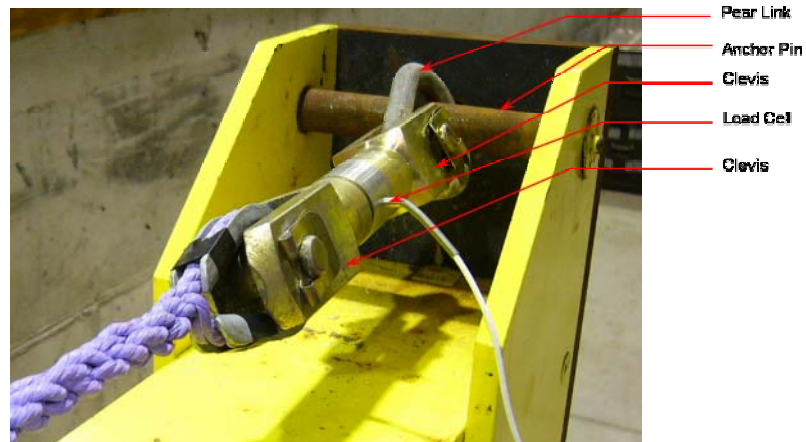
### **3. Apparatus Testing and Modification**

The preliminary testing of the rope apparatus was both qualitative and quantitative. The purpose of these tests was not to gather data on the rope but to investigate how the apparatus should be operated to satisfy the robustness criteria of being operated without extensive training. These tests provided positive insight for the general operational characteristics of the apparatus and the construction of the specimens.

The first set of tests involved a qualitative analysis during and after a test specimen had been loaded to the point of breaking. Items that were considered included deformation of structural components, check for hydraulic leaks, proper operation of all valves, relative location of the specimen break, and the extent of elongation that occurred prior to breaking the specimen.

Although the load cell was in place for the first set of tests, data was not collected. This was done in order to focus solely on the operation of the apparatus and construction of the test specimen. The load cell was attached to the anchor pin in the

stationary anchorage using a pear link and a clevis which treaded onto the load cell as shown in figure 4.3.



**Figure 4.3: Original method for securing the load cell to the stationary anchorage with clevises and a pear link. Note that the weight of the securing method is entirely supported by the tension in the specimen.**

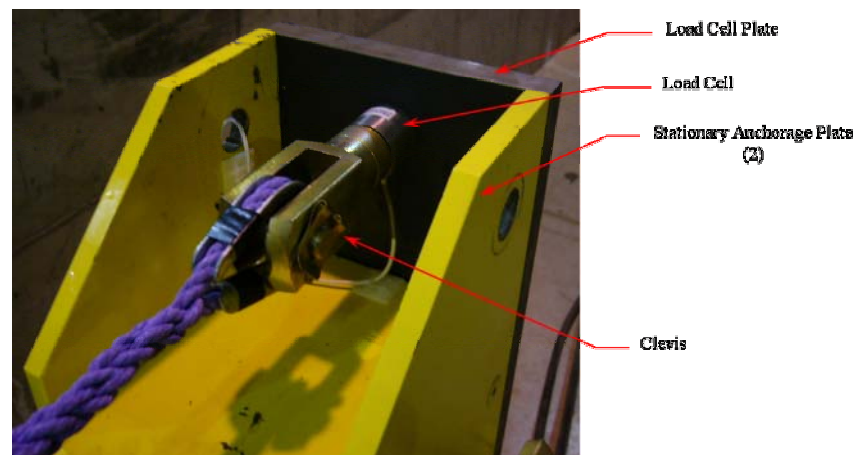
One end of the rope specimen was attached to the load cell using a second clevis threaded onto the other end of the load cell, as depicted above. The other end of the specimen was simply attached to the anchor pin of the moving anchorage via an eye splice and heavy duty thimble. The two eye splices were constructed in accordance with the recommended procedures of the CIs' manual. The splices were each constructed around a heavy duty thimble, to prevent any flattening of the rope around the anchor pins, and finished with a series of five tucks. Once the specimen was secure, the piston was actuated in the extend mode until the specimen broke or the piston reached the full extent of its stroke.

This test was repeated several times and resulted in the following observations and speculation about the potential causes. First and foremost, no deformations, yielding, or failure of any structural components were observed. Likewise, no hydraulic problems were observed with the exception that the selector valve was



observed to have some blow-by into the wave generation circuit which caused a build up of back pressure on the return line of the wave generation circuit. The relative location where the specimen broke did, however, raise some concerns. All specimens broke at the end that was attached the load cell. Even more concerning was the observation that the break occurred either in the splice or the eye. It was suspected that the weight of the load cell, in conjunction with the weight of the clevises and pear link, were contributing factors adding to the break occurring at the stationary anchorage end.

The attachment of the load cell to the stationary anchorage was reconfigured such that the weight of the load cell was supported by the apparatus and not by the specimen under test. The modification consisted of fastening a steel plate, called the load cell plate, on the end of the stationary anchorage with the load cell attached at the same height as the anchor pin. This is depicted in figure 4.4.



**Figure 4.4: Modified stationary anchorage to support the entire weight of the load cell and termination.**

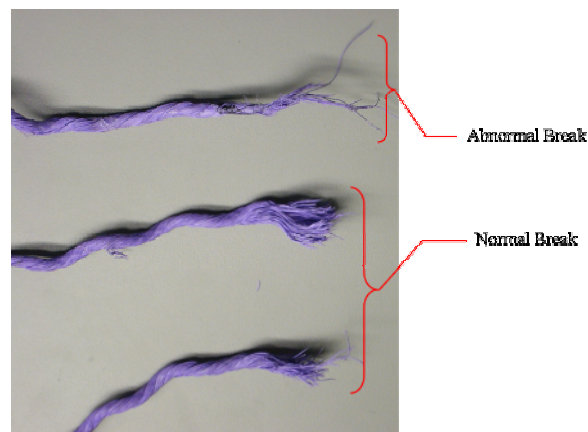
Another series of tests were conducted to evaluate the modified anchorage for the load cell. Although the new tests revealed that the end at which the specimen broke

seemed to be random in nature, the break still occurred within the tuck section or the eye section of the splice. Examination of the specimens at their point of failure indicated that the majority of the breaks occurred where the “working” end of the rope re-enters the “running” end of the specimen. This was manifested as a fray in the throat of the thimble, as seen in figure 4.5.



**Figure 4.5: Fray location in relation to the thimble. Notice the fray occurring in the strand closest to the throat of the thimble.**

Closer investigation of the three strands at the throat of the thimble showed that two strands had broken cleanly in the expected manor. The third strand however, looked as if it had been crushed. This dissimilarity of breaks became even clearer when the ends of the three strands underwent a side by side comparison, as shown figure 4.6.



**Figure 4.6: Yarn comparison. The two lower yarns exhibit a typical failure mode while the top yarn seems to have been crushed. The top yarn is the same one showing a fray in figure 4.5.**

Based on these visual results, it was decided that increasing the length of the eye should help decrease the angle at which the “working” end re-enters the “running” end. This also moved the “throat” of the eye splice away from the end of the thimble which was seen to rotate during testing conditions and thereby place pressure against the splice.

Additional rope specimens were broken to ensure that the modifications to the rope testing apparatus and to the specimens were adequate. This demonstrated that the failure point of the specimen had migrated from the splices (as seen in prior cases) toward the center of the specimen. With this success, it was concluded that the preliminary testing of the rope testing apparatus and the construction technique for the specimens had met its objective. The rope testing apparatus was instrumented and one final test was conducted with all of the system components fully functional. The lessons that were learned in the preliminary testing were critical to meeting the robustness criteria that the rope testing apparatus would provide results that were predictable and repeatable.

## **CHAPTER V**

### **INSTRUMENTATION**

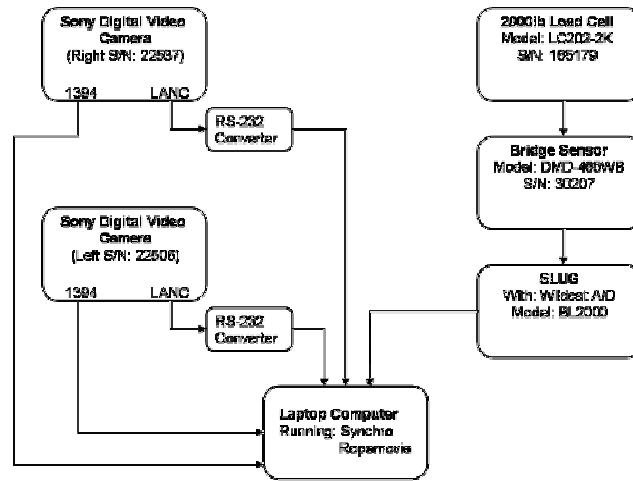
#### **1. General System Overview**

Two primary parameters remained that needed to be characterized. These included the loading of the specimen and the relative change in length between the gauge marks on the specimen. These two parameters must be measured throughout the duration of the experiment. Typically a load cell, in conjunction with an extensometer, is used to record the load and extension over time. A potential safety hazard exists with this technique, because the extensometer must be removed prior to the parting of the rope to prevent instrument damage. The removal of the extensometer must be done by reaching over the specimen while it is under tension that is close to the breaking load.

During these experiments a load cell was used in line with the specimen to acquire the load information. The important deviation from prior practice was removing the extensometer by using video cameras and imagery tracking software to extract the changes in distance between the gauge marks.

The measurement system consists of four parts: (1) a load cell with analog output, (2) an analog to digital (A/D) converter, (3) two digital video cameras, and (4)

a laptop running a customized logging program called Synchro. The data flow can be seen in the block diagram of figure 5.1



**Figure 5.1: Block diagram showing the data flow during the experiment and the transfer of video data via 1394 protocol to the laptop.**

The load that was being applied to the specimen under test with the rope testing apparatus was measured using an industry standard tension/compression load cell. The load cell, an Omegadyne Inc. (Part number: LC202-2K) had a calibrated dynamic measuring range between zero and two thousand pounds. The LC202 model series load cells are constructed of stainless steel and are environmentally sealed. These two features are advantageous during testing of salt water soaked specimens. The manufacturer provides each load cell with a NIST certified five-point calibration at 0(twice), 50(twice), and 100(once) percent of full scale load. This provides traceability and confidence in measurements that are acquired during tests. The load cell outputs an analog voltage in the microvolt range. A bridgesensor (Omegadyne Model number DMD-465WB) was used in conjunction with the load cell. The bridgesensor provides the excitation voltage required by the load cell and amplifies the load cell output voltage. This provided the load cell with a stable output voltage that

was on the order of millivolts per pound rather than the native output which would have been on the order of microvolts per pound.

The millivolt per pound output levels allowed the data to be measurable with an existing A/D converter. The A/D converter is housed in a device known as the “SLUG”. The SLUG, incorporates a BL2000 Wildcat single board computer. The BL2000 digitizes the load cell’s output analog signal at 15 Hz into 4096 quantization levels representing voltages between  $\pm 10$  volts and outputs a NMEA string containing the information. This string, along with the Local Application Control Bus System (LANC) information from each camera is sent via RS232 serial protocol to the laptop running SYNCHRO software where it is time tagged and recorded.

The elongation data was extracted using digital videography. For simplicity, image processing that is designed to track linear changes, usually is set to track a particular feature such as the transition from a black stripe to an adjacent white stripe. Therefore black and white stripes were placed next to each other on the specimen to serve as gauge marks. Note that in figure 5.2 it is readily observed that the left gauge mark is distinguishable from the right gauge mark by the “sense” of the transition. One being from black to white compared to the other being from white to black.



**Figure 5.2: Gauge mark placement. The distance between the black white and white black transitions (top) is one foot which is equal to the CI guidelines recommendations. Also in accordance with CI guidelines the minimum distance from the end of the splice (bottom) is also one foot.**

Two Sony Hi8 Digital video cameras (Model number DCR-TVR230) were employed. Each camera was trained onto one of the two gauge marks and used to record the movement of that individual set of stripes as a function of time. This method does not produce immediate elongation data, however through post-processing, this method produces highly accurate changes in length over the 1-foot gauge length. This method will be discussed further in the data processing portion of this thesis.

The correlation between the load cell data and the elongation data is provided by a data logging program developed at the University of New Hampshire's Center for Coastal and Ocean Mapping called Synchro. Synchro, developed by Dr. Yuri Rzhhanov is a serial port logging program that continually polls the user specified serial ports and immediately responds to the arrival of new data. After the serial ports are sampled the information and corresponding time are then streamed to a user specified file. Three serial ports were used for acquiring the necessary data during the testing: (1) load cell data via the SLUG, (2) "right" camera LANC information, and (3) "left"

camera LANC information. In addition to the precise logging of the load cell data, the time synchronization of the LANC information with the load cell data is crucial for accurate quantitative results. The LANC information contains the frame number, referenced to the beginning of the digital media, which is recorded synchronously with the load cell data readings. This allows the elongation data measured via the video cameras to be matched in time with the load data during post processing. This provides the ability to develop stereotypical plot of engineering stress-strain which completely characterizes the rope up to breaking as opposed to just determining the ultimate breaking strength. Without the ability to make measurements up to the breaking point, it would not have been possible to make measurements of the strain hardening region of the engineering properties. That would have obscured one of the important findings of the experiment (as discussed in 8.3 Engineering properties) which was the brittle-like property of the WSR near the breaking load.

## **2. Measurement System Error Analysis**

Each element of the measurement system contributes an inherent error that must be associated with each data point that is reported. The errors propagate through the various measurements and calculations to generate a level of uncertainty for every measurement made and every value computed. Starting with the load cell and continuing through the image analysis, the uncertainty will be calculated for each component as well as for the entire system based upon manufacturer specifications and laboratory measurements conducted prior to the experimental runs.



The load cell was provided with a certified calibration by the manufacturer. Beyond this certification, the manufacture specifies that the accuracy of the load cell is  $\pm 0.25\%$  of the full scale output. This means for a cell with a maximum load limit of 2000 lbs the measured load will be within plus or minus five pounds of the true value. This correlates to a voltage uncertainty of  $\pm 60.5 \mu\text{V}$  for the native analog voltage output of the load cell. Since this was fed into the bridgesensor, any error associated with amplification of the signal must be included. A laboratory exercise was conducted to determine the gain factor applied to the bridgesensor's input signal (see 3. Instrument Calibration). This showed that the bridgesensor was amplifying the input signal by a factor of 267.8, with a coefficient of determination of 99%. The error associated with the gain uncertainty equated to  $\pm 0.12\%$  of the full scale output voltage of the bridgesensor.

The Wildcat BL2000 analog to digital converter housed in the SLUG also impacts the accuracy and precision of the individual load measurements. The Wildcat BL2000 is a 12 bit A/D converter with a maximum input range of  $\pm 10$  volts. This means that the quantization level, or voltage resolution, is 0.005 volts. The error associated with a recorded A/D voltage is plus/minus one-half of the quantization level.

The errors associated with measuring the lateral movement of the gauge marks are affected by several factors. These factors include the distortion due to the curvature of the lens, the field of view, and the processing technique of extracting the transition point between the black and white stripes. Lens distortion errors will cause objects to appear to move more in the center of the frame of view and less along the

edges of the frame of view. This distortion can be removed by mathematically applying a radial correction factor to each of the frames of the video. However, even this correction has errors associated with it. Based on the worst case scenario seen during the lens calibration process, the residual errors after the distortion correction were on the order of  $\pm 0.5$  pixels.

The second factor affecting the resolution of the lateral movement measurement is the camera's field of view. Since the lateral movement of the gauge marks from right to left is in a single horizontal plane, the conversion between horizontal distances and image pixels is of primary interest. If both gauge marks were to be captured by one camera the horizontal field of view at the gauge marks would have to be up to 30 inches width. Since the camera segments the horizontal field of view into 720 pixels, the image resolution in that case would at best be  $\pm 0.042$  inches per pixel. If two identical cameras are utilized, one for tracking each gauge mark independently, the horizontal distance resolution of each camera increases to  $\pm 0.021$  inches per pixel.

Post processing of the video data to extract the transition point between the black and white stripes of each gauge mark exhibits the greatest uncertainty of the three factors. This is due in large part to the compounded effect of lens distortion correction errors and field of view resolution. Additionally, the processing method, which is described in the data processing section, is only estimating the black-white or white-black transition between the stripes to the nearest pixel. Together the three factors lead to a horizontal distance measurement resolution of  $\pm 0.022$  inches per pixel per camera. The key here is per camera. Remember in order to achieve elongation

data from the two-camera method, the movement of the gauge mark in one camera must be differenced with the movement of the other gauge mark in the other camera. This leads to a combined measurement error of  $\pm 0.031$  inches per pixel.

The last error associated with the experiment is timing or matching of the load data with the elongation data via the Synchro program. The Synchro program effectively samples the LANC data available at the communication ports of the computer at a rate of 15Hz. The LANC information changes at the frame rate of the cameras which is essentially 30Hz. Therefore the sampling rate of the Synchro program is the limiting factor in resolving the correspondence between a load cell measurement and the video frame capture. This does not negatively impact the load measurement error except for the load at breaking. Since the load is nominally continually increasing at a fixed rate, the actual load at the breaking point, which obviously occurs between two of the 15 Hz samples, must be larger than the load that was measured on the sample just before the sample that detailed the break. This results in a bias of half the nominal change in load between two measurements and increases the variance of the measurement by  $q^2/12$  where  $q$  is the nominal change in load between measurements. Therefore an additional uncertainty of  $\pm 0.024$  volts needs to be summed in quadrature with the error associated with the A/D quantization level to estimate the uncertainty in the load at the breaks. This combination of the sampling error and the A/D quantization error produces a calculated uncertainty of the breaking point of  $\pm 0.026$  volts. For all other load values the  $\pm 0.012$  volts uncertainty is that associated with just the load cell amplification and the A/D conversion. The

measurement uncertainties for the physical and engineering properties of the experiment are easily seen in table 5.1

**Table 5.1: Measurement uncertainties associated with all equipment used during experimentation.**

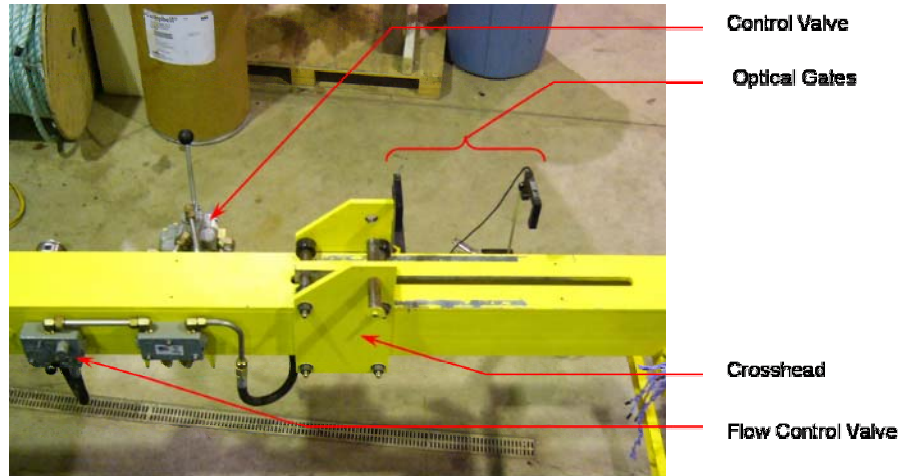
<b>Calculated measurement uncertainties</b>		
<b>Measurement Parameter</b>	<b>Measurement Uncertainty</b>	<b>Unit of Measure</b>
<b>Physical properties</b>		
Diameter	0.001	inch
Length	0.016	inch
Mass	0.002	lbs
<b>Engineering properties</b>		
Length	0.063	inch
Diameter	0.001	inch
Load Cell	0.25% Full Scale	volts
Bridge Amplifier	0.12% Full Scale	volts
Wildcat BL2000	0.005	volts
Breaking point	0.026	volts
Lens Correction	0.5	pixels
Pixel Resolution	1	pixels

### **3. Instrument Calibrations**

Calibration of several instrumentation packages were required to ensure accurate results and to keep the propagation of error to a minimum. The actuation (extension) speed of the hydraulic ram was measured several times to ensure that the rate was indeed 144 inches per a minute and that the speed was consistent time after time. The bridgesensor's amplification stage was determined. Finally, the calibration constants for the video camera lens distortion were computed.

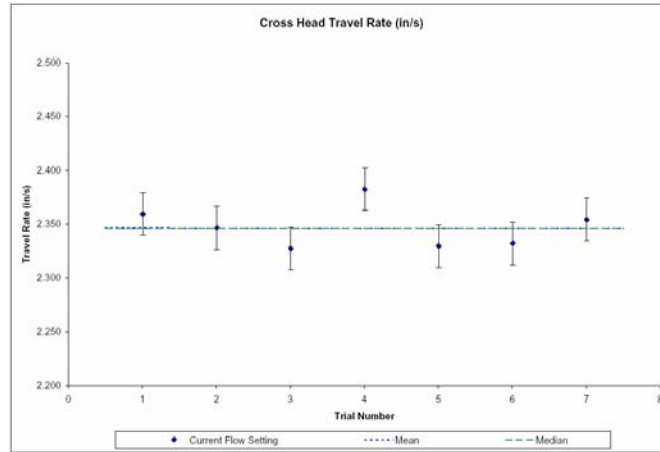
The actuation (extension) speed of the crosshead needed to be calibrated in order to assure compliance with the Cordage Institute's guidelines. These guidelines require the uncycled strength and strain test to be conducted under a constant strain rate. The speed of the crosshead was calculated based on the time it took the

crosshead to travel a specified distance. The time measurements were made with a pair of PASCO Scientific optical gate timers (Model number ME-9215A) and were implemented as seen in figure 5.3



**Figure 5.3: Setup used to calibrate the crosshead speed. The final setting was assured to be at a rate of 144 inches per minute.**

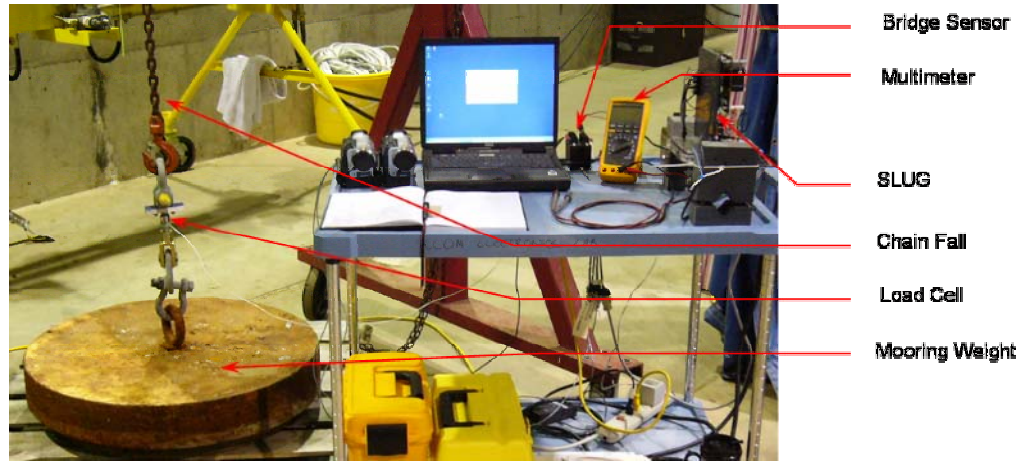
A series of five trials were run at each setting of the flow control valve. It was determined that with the flow control valve set to “number four”, the crosshead traveled at the desired rate. This was re-checked prior to the start of testing. The results are presented in figure 5.4 with the trial number plotted against the measured crosshead travel rate.



**Figure 5.4: Calibration plot of the crosshead travel rate. The final setting was at a level of 145.44 inches per minute.**

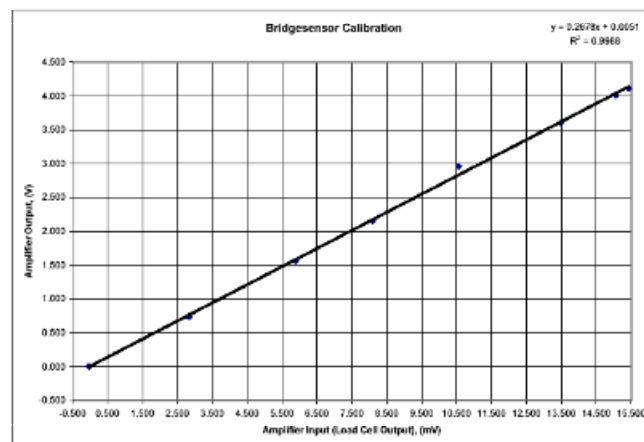
The flow control valve was set on “number four” to provide a crosshead travel rate at 144 inches per minute for all the experimental runs.

The bridgesensor was calibrated to relate the input voltage to the output voltage in terms of a gain factor. This is necessary in order that the manufacturer’s certified calibration can be used during the post processing of the data. The load cell was connected to the bridgesensor in the manor described by the manufacturer. The load cell was attached between a mooring weight at one end and an overhead chain fall at the other. The chain fall was incremented until a portion of the force due to gravity acting on the weight had been taken up by the chain fall in figure 5.4.



**Figure 5.5: Bridgesensor calibration setup.**

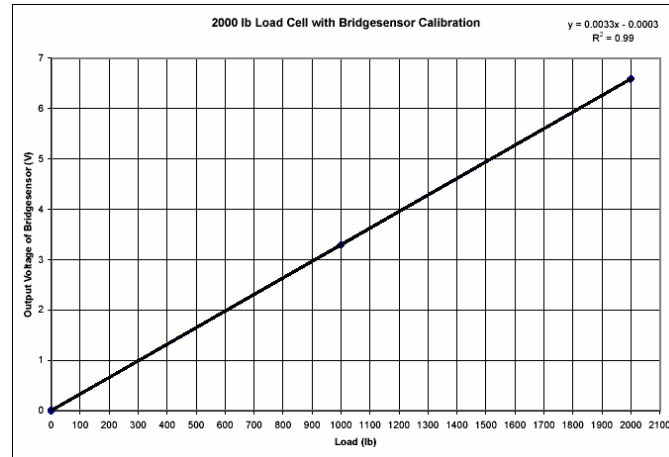
The output voltage from the load cell was measured to  $\pm 0.001$  mV with a Fluke (Model 189) multimeter and compared with a similar measurement made with the Fluke multimeter at the output terminals of the bridgesensor. This was repeated several times until the weight was lifted off the floor. The weight was returned to the floor and the set of input-output voltage measurements were repeated at zero load. The ratios of the outputs to the inputs were plotted to obtain the gain curve for the bridgesensor, figure 5.6.



**Figure 5.6: Calibration curve for the amplification stage of the bridgesensor.**

This curve was combined with the manufacturer's calibration to produce a curve associating the load applied to the load cell with the output voltage of the

bridgesensor, figure 5.7. A curve fit was then applied to this data to establish an equation that can be used to convert the A/D voltages back to loads during post processing.



**Figure 5.7: Load cell calibration combined with bridge sensor calibration. This relates final output voltage to load experienced by the load cell**

Prior to recording the video data, a calibration was performed to determine the distortion characteristics of the lens on each camera. This step was completed so that the distortion affects of the lens can be removed during post processing. The video cameras were set in their final test positions and the zoom made equal in both cameras and equal to what would be used in the tests. A video image capture was performed such that a checker board of black and white blocks was oriented in a variety of angles. A Matlab tool box for camera calibrations, developed in open source code by the California Institute of Technology and Intel, was implemented. This program produced correction coefficients for the lens focal length, principal point, lens distortion, pixel error and the uncertainties for each correction coefficient.



## **CHAPTER VI**

### **ROPE TESTING**

#### **1. Experimental Design**

The objective of these experiments was to characterize Whale Safe Rope and show the robustness of the experimental procedure. The characterization process involved both the definition of the physical properties and the engineering properties of dry WSR as well as saltwater soaked WSR. This lead to defining the experimental factors to be: (1) the properties of dry WSR compared to polypropylene and (2) the effects saltwater soaked WSR cordage. These experimental factors lead to the development of three treatment combinations.

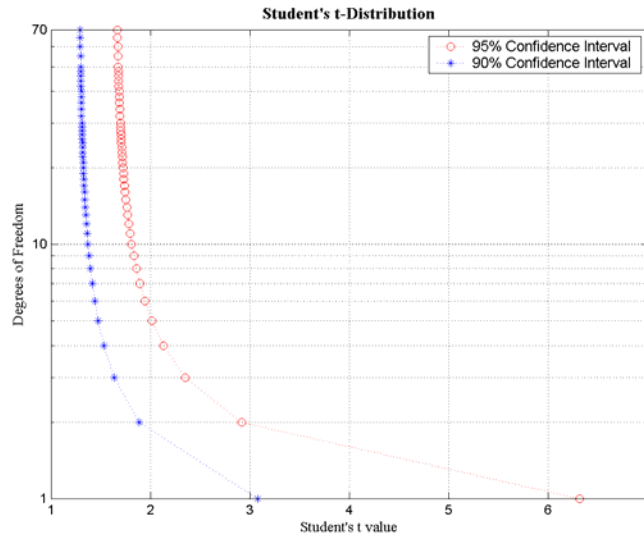
These treatment combinations are: (1) Dry WSR, (2) Wet WSR, and (3) Dry Polypropylene. A conscious effort was made to reduce the categorical factors by purchasing the WSR and the polypropylene rope from the same manufacturer, the construction of all the specimens by a single person, and keeping the test conditions constant in all experimental runs. This should provide more accurate and precise definition of the continuous factors through the physical and engineering properties of the rope specimens.

Before starting the tests it was necessary to quantify the number of replicate specimens to use in each of the experimental runs. The characteristics of the

specimens in the sample population must adequately represent the characteristics of the parent population. Since Whale Safe Rope is brand new and not a continually produced product, the statistical parameters of the parent population are unknown. In short there is no production history at this juncture. As a start, the nonexistent parent WSR population was considered to exhibit the characteristics of a well behaved standard normal distribution. With this assumption, the Central Limit Theorem applies and the determination of the number of samples ( $n$ ) need to represent the parent population (Vining 1998) can be written:

$$n \geq \left( \frac{z_{\alpha/2} \cdot \sigma}{B} \right)^2 \quad (25)$$

where  $z_{\alpha/2}$  is the probability standard random variable based on the degrees of freedom,  $\sigma$  is the population standard deviation, and  $B$  is the measure of the width of the confidence interval. Since the standard deviation of the population is unknown, the 'z' statistic and the standard deviation are replaced by the student's t-distribution and the variance to determine a sample size (Schenck 1961). If the student's t is plotted against the degrees of freedom with varying confidence levels, as shown in figure 6.1 a cost benefit analogy can be conducted to determine the number of replicates required to yield creditable results.



**Figure 6.1: Graph of the Student's t-distribution with varying confidence levels. Note that as the degrees of freedom goes above 32 it can be shown that the Student's t-distribution approaches the 'z' statistic.**

Figure 6.1 reveals that there is not much to be gained by conducting more than 32 replicates per treatment combination. For this study it was decided that 40 replicates would be conducted to provide a safety buffer in case of machine malfunction, data collection errors, or ill behaved statistical data distributions.

These parameters defined that this study should conduct three sets of experimental runs: a dry WSR run, a wet WSR run, and a reference run using standard polypropylene. All samples must come from the same manufacturer and must be prepared by the same individual to ensure consistency. The number of samples for each experimental run was set at 40 for a total of 80 WSR specimens and 40 standard polypropylene specimens.

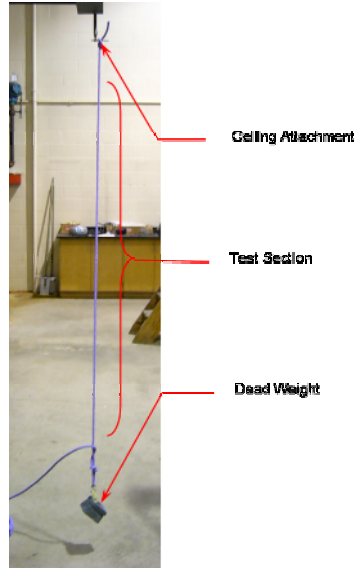
## 2. Procedure

There are two important factors in the identification and classification of new types of cordage material. These are (1) the physical properties and (2) the engineering properties. The physical properties include the calculation of the reference tension, initial tension and the measurement of the size number and linear density of the line. The engineering properties include the uncycled strength and strain measurements. While the Cordage Institute Guidelines outline many of the procedures for conducting these tests, the procedures actually used for conducting all the aforementioned tests will be discussed along with any idiosyncrasies associated with the setup in this study.

The first set of tests to be completed involved the determination of the physical properties of the Whale Safe Rope. Before any tests could be completed the reference tension, a low tension that does not change the properties of the specimen, needed to be calculated. The Cordage Institute defines the reference tension ( $RT_p$ ) as:

$$RT_p = 50 \cdot d^2 \quad (26)$$

where  $d$  is the nominal diameter of the specimen. If the nominal diameter is not known a measure can be conducted under light hand tension. The UNH method used a nominal diameter of 3/8 of an inch as a first iteration. In accordance with the CI guidelines, a section of WSR rope was secured to an overhead beam and a weight, dictated by the calculated reference tension, tied to the opposite end to provide the necessary tension, as seen in figure 6.2.



**Figure 6.2: Setup for determining the Physical properties (nominal rope diameter, rope number, and linear density).**

Measurements of the diameter were acquired with the use of a machinist vernier calipers ensuring that at least two strand crowns were in contact with each side of the caliper jaws at all times. The measurements were repeated at a spacing of typically three inches but no less than two inches. At this point according to CI guidelines if the average measured nominal diameter varied more than 10%, the process must be iterated. The iteration must start with the recalculation of the reference tension using the average nominal diameter value.

Once the nominal diameter met the criterion of less than 10% variation, the size number was calculated by multiplying the measured nominal diameter by Pi.

Additionally, the initial tension ( $IT_p$ ), in units of pounds was calculated by:

$$IT_p = 200 \cdot d^2 \quad (27)$$

The amount of weight at the end of the specimen was then adjusted to meet the initial tension criterion. One gauge mark was then placed one inch from the top termination

and a second placed ten inches below the first to an accuracy of  $\pm 1/16$  of an inch. Since the length of the specimen under tension was greater than the one foot requirement by the CI guidelines for this test, a series of ten inch increments were marked out with a minimum of one inch separation between them. A utility knife was used to cut on these marks to produce a ten inch specimen for the measurement of linear density. This is repeated until the proper number of linear density specimens are produced. The linear density specimens were then weighed to an accuracy of  $\pm 1\%$  with a Mettler 1200 electronic balance. With the precise weight (P) in pounds and length (F) in feet known, the linear density per 100 feet ( $LD_p$ ) of WSR is calculated by:

$$LD_p = 100 \cdot \left( \frac{P}{F} \right) \quad (28)$$

The ends of the specimens were then taped to prevent any fiber loss or unwrapping. Additionally, the specimens were numbered, bagged, and inventoried until all processing was complete. This ensured that any question that may arise during post processing might be resolved by reviewing any particular specimen.

The next portions of the experimental test were aimed at defining the engineering properties of the WSR. This began with preparation of the samples that would be tested as dry WSR, wet WSR, and standard polypropylene. As mentioned in the experimental design section, 40 specimens were prepared for each of these tests. Each specimen length was marked on the axis to which it was unraveled from the spool and cut to a length of approximately 90 inches. The cut specimen was then transferred to a jig in order to set the length of the eye splices and to ensure that no twists were introduced. The length of each eye splice was controlled to be 6.5" in

length and was constructed with five tucks securing the splice. The final length of the test specimens, center to center between eye splices, was 62 inches

Each of the newly spliced specimens was placed under the specified initial tension. Two marks were placed on the specimen with a permanent black marker. One mark was 12 inches from the end of the splice that was to be secured onto the stationary anchorage and another one was 12 inches from the first mark. These two marks indicated where the black to white, or white to black transition would occur between the stripes. Tape was applied to mask the rope during the painting of the black stripes, which extended one inch along the rope as seen in figure 6.3.



**Figure 6.3: Depiction of masking for the painting of the black stripes.**

It is important to note that in the above figure that the black stripes occur on the outside of the black marker marks placed on the specimen. After the black stripes had thoroughly dried, tape was applied one inch inside the black marker marks to mask the rope for the painting of the white stripes. A clear tube was slid over the black painted stripes to protect them from over spray during the painting process. This is illustrated in figure 6.4.



**Figure 6.4:** Depiction of methodology used to paint white stripes. Notice the clear plastic tubes over the black stripes (outside).

A latex based paint was used so that the addition of the paint to the rope would have minimal affects, if any to the properties of the rope.

The specimens for the dry WSR and the standard polypropylene were ready to undergo testing at this point. However, the samples slated for use in the wet WSR tests required soaking in a bath of saltwater. This was accomplished by combining twenty gallons of cold tap water with 2365.8 mL of an artificial sea salt concentrate. Using a Fisher Scientific hydrometer (model 11-529-A), a Neslab Instruments thermometer, and an Odem Hydrographic digibar pro sound velocimeter (model DB1200), the salinity was estimated as 31.49 PSU. The specimens that were slated for wet testing were draped into the saltwater solution ensuring that the eye splices were kept out of the water, as seen in figure 6.5

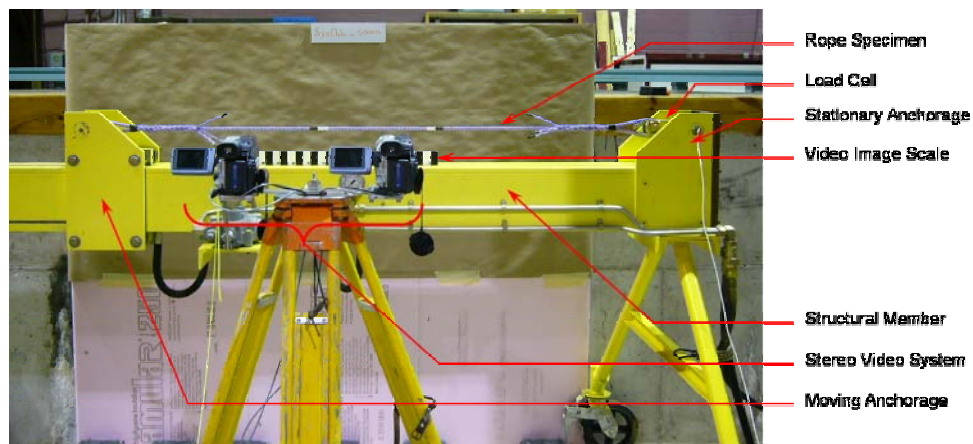




**Figure 6.5: Rope specimens soaking in a bath of saltwater.**

These specimens were soaked approximately 48 hours prior to testing and were kept in the saltwater solution until they underwent testing.

The next step was to setup the machine and data collection systems. They were setup electronically, as in figure 5.1, and physically as shown in figure 6.6.



**Figure 6.6: Final setup used to run all experimental runs for the determination of the Engineering properties. Notice the sign, on the background depicting the specimen under test, the horizontal arrangement of black and white calibration blocks, and the black to white and white to black transitions of the gauge marks.**

It is important to note that the video image scale with its horizontal alternating blocks of black and white is directly under the center line of the specimen and the right hand edge is vertically aligned with the right hand white black transition point. The distance between the camera lenses and the video image scale was set to 32 inches and the height of the camera lenses were aligned on the center line of the rope specimen. The separation distance between centers of the camera lenses was one foot, the same as the distance between the gauge marks on the specimen. The two cameras were turned on and the zoom on each was adjusted to ensure that the field of view would be equal on both video recorders. Also at this point, the tripod is moved right to left such that gauge marks are guaranteed to be located in the right hand side of the individual cameras field of view.

A background was placed behind the test machine to reduce the possibility of vertical lines of contrast in the video. This was done to reduce contrast changes in the background which improved the tracking of the white-black and black-white transitions. This also allowed a small sign to be placed on the background indicating which sample specimen was under test.

Once the setup was completed, a series of system checks were preformed. A video calibration was conducted for each camera as outlined in chapter five. Prior to mounting the specimen, the load cell zero point was checked for any DC offset and adjusted if necessary. The logging software was tested for proper port and channel trigger settings. A dry run of the experiment was preformed where an extra rope specimen was placed in the testing machine. The acquired data was checked for validity before moving on to the actual experimental testing stage.

All the rope specimens that were tested and used to determine the characteristics of the WSR and the reference industry standard polypropylene were tracked. Each specimen was given a unique serial number. For example, the serial number S000D was assigned to a dry WSR specimen number zero that was used in the dry run test. These serial numbers are affixed to plastic storage bags that contain the specimen before and after the test run. In addition, the serial number was used for the basis of associating collected video and data files to a particular specimen. During the experiment a log sheet was used to track various items. These items include the starting frame numbers of the left and right cameras, data file names, date, time, position of break, qualitative break data, and other pertinent information about each of the experimental runs.

Finally, the experiment was ready to commence. In this particular study, the dry WSR tests were conducted first, followed by the saltwater soaked WSR tests and finally the reference polypropylene. The specimen under test was mounted in the grips of the machine with one gauge mark located 12 inches from the eye splice on the stationary anchorage end. The experimental protocol required that the mark which indicated how the rope was taken off the coil, was facing up on both ends and that no twists were added to the specimen. Once set in the anchorages the specimen's termination points were restrained from rotating around the axis of the rope. Since the gauge marks were applied to the specimens while the samples were under initial tension, the application of the initial tension, which is part of the procedure outlined by the Cordage Institute was passed. The Synchro program was reset from standby to recording mode as were the left and right digital video cameras. The directional

control valve was set to put the crosshead into the extension motion. The crosshead was kept in motion, with all personal at a safe distance, until the specimen parted. The direction of crosshead motion was reversed and ran until the hydraulic piston was fully retracted. The specimen was removed from the grips, bagged, and cataloged. The log sheet for the specimen test was filled out and placed in the serialized bag with the specimen.

## **CHAPTER VII**

### **DATA PROCESSING**

#### **1. General**

The data on the physical properties of the WSR and the reference polypropylene rope were examined. The mean and standard deviation of the nominal diameter was computed, followed by the size number classification as outlined in the procedure section. The reference and initial tensions were calculated based on the measured diameter in accordance with the CI guidelines. Finally the mean and standard deviation of the linear density was determined in accordance with the CI guidelines.

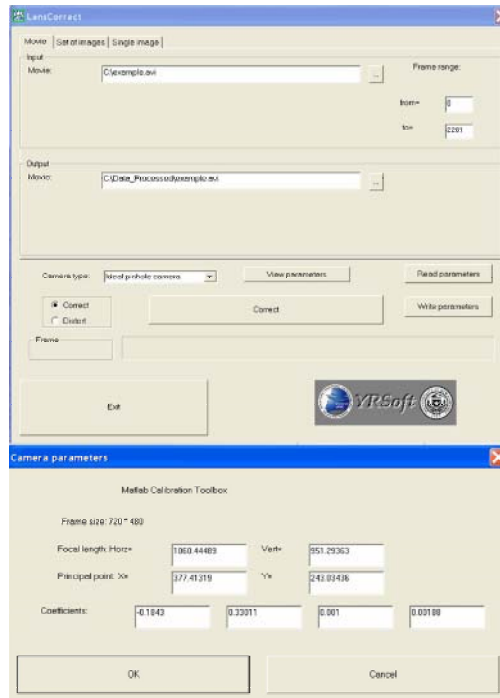
The raw data for determining the engineering properties was collected in two forms. A text file was collected by a laptop containing the LANC information for the right and left digital video cameras which was matched in time with the data obtained from the load cell. The two cameras recorded the relative movement of the gauge marks over time. The digital image data was downloaded to a computer for post processing. In the post processing stage, the video imagery was corrected for the lens distortion then a specialized image processing program was used to extract frame by frame the change in pixels of the white-black or black-white transition of the gauge mark. The displacements, measured in each of the two cameras along with the

corresponding video frame information, were saved to a text file. The load cell text file and the imagery text file were time aligned and the engineering stress-strain information was extracted.

## **2. Video Data Processing**

The lens calibration constants were obtained from the lens calibration software as outlined in the calibration section. The individual replicate runs' left and right video captures were downloaded using WinDV and corrected for lens distortion using the lens calibration constants. The hour, minute, second, and frame number for each replicate and each camera at which the video captures were started were recorded to preserve the time link between the load cell data and the elongation (video) data. This information was collected on the same log sheet that had been used during the experiments for each replicate specimen and later entered into an MS Excel spreadsheet for use in the automated Matlab data processing.

The Lens Correct program requires its input be uncompressed video files while the output of WinDV's compression format is based on Digital Video (DV) compression. Therefore the downloaded video captures needed to be resaved in an uncompressed format. The Lens Correct program could then be used to remove any distortions in the video capture created by the inaccuracies in the curvature of the camera lens. The Lens Correct program, whose GUI is shown in figure 7.1 has two inputs, (1) the uncompressed video in \*.avi format and (2) the calibration constants in a \*.txt format.



**Figure 7.1: Front Panel of the Lens Correct program. The lower window appears when the View Parameters button is clicked.**

The program outputs an uncompressed \*.avi file to which the camera lens correction constants have been applied.

Having systematically removed distortion due to inaccuracies in the curvature of the camera lens, the captured video frames were ready to be processed for extracting the horizontal movement of the black-white gauge mark transition point. A DOS application, called RopeMovie written by Dr. Yuri Rzhanov was used to extract the pixel location of the black to white and white to black transition points in a single frame of the video capture file. The program basically moves from pixel to pixel looking at the change in contrast between horizontal neighboring pixels. The location where the contrast slope is the greatest is defined as the transition point between the different colored stripes on the rope. The program then advances to the next frame and repeats this process, recording the pixel location of the transition with the frame

number. The program also characterizes the robustness of the determination of the transition point. In addition to the input and output file names, several input parameters listed in table 7.1 were optional that could be specified to increase the accuracy, precision and speed of tracking the transition point.

**Table 7.1: Input arguments for the Ropemovie program which extracts the transition point of the gauge marks as a function of time. The pixel position is recorded in a text file along with the associated frame number.**

<i>Input arguments for RopeMovie program</i>			
<u>Argument</u>	<u>Input Limits</u>	<u>Default Values</u>	<u>Description</u>
-bw	0 or 1	0	Order of transition sequence (black white or white black)
-d	0 or 1	0	Debugging level (zero is off)
-r	0 to infinity 0 to infinity	0 10000	Range of frames to be processed (starting and ending frame number)
-R	0 to 480	-1	Height of video image scale in pixels (Feature is off when -1)
-s	0 to 720 0 to 480	10 11	Width and Height of either the white or black stripe in pixels
-x	0 to 720 0 to 720	200 500	Range (pixels) in the horizontal where the transition is located
-y	0 to 480 0 to 480	100 400	Range (pixels) in the vertical where the transition is located
in.avi	N/A	N/A	Input file name in avi format
out.txt	N/A	N/A	Output file name in txt format

Importantly, the program measures the pixel width of the alternating white and black blocks on the video image scale (seen in figure 6.6) to provide a link between pixel space and actual measurable distance. This scaling value is determined for every frame in the video capture and is included in the output text file.

The Ropemovie program was run for every replicate in the three treatment combinations for both cameras. This yielded two text files for each replicate, left and right for a total of 240 text files. The left and right image processing text files were matched in Matlab with the associated load cell text file for each individual replicate.



### **3. Matlab Data Processing**

Once all the video captures had been processed down to their respective text files, they along with the corresponding load cell data file and the frame reference Excel file were processed in Matlab. The objective of the Matlab processing was to produce an engineering stress-strain plot of the data along with an appropriate curve fit that would accurately represent each of the treatment combinations.

The first step was to align the displacement text files from the video images with the load cell data in time. Since the LANC information was preserved throughout the video analysis and it was also recorded with the load cell data, a logical way to align the three files, (right camera displacement, left camera displacement, and load cell data) was to match up the hour, minute, second, and frame numbers within each file. The data was then filtered and only the data points containing the left displacement, right displacement, and load cell data were kept.

The aligned data needed to be accurately and precisely converted from output load cell voltages and pixel displacements into actual loads in pounds and displacements in inches, respectively. The load cell data was converted from volts into pounds using the calibration curves that were obtained during the load cell calibration process. The conversion from pixels to distance in inches was a bit more involved. The change in specimen length between the two gauge marks from one frame to the next was initially computed in the pixel domain. Delta length in pixels was converted to inches by taking the mean of the number of pixels in each of the alternating black and white blocks contained in the ruler column of the Ropemovie text file for each camera. The right camera length measurements, which was tracking

the gauge mark closest to the stationary anchorage of the machine was subtracted from the left camera length measurements. This yielded the delta length across the entire gauge length of the specimen, or specifically the elongation. The engineering stress and strain were calculated by dividing the load and the delta length by the cross sectional area of the rope at initial tension and the original one foot gauge length, respectively. This process was repeated for each replicate in each of the three treatment conditions.

The engineering stress-strain raw data was curve fitted to determine the mechanical settling, linear elastic, and strain hardening regions. This was achieved through a piecewise fitting routine. The first and second derivatives of stress with respect to time were computed to determine concavity and their associated inflection points. The first derivative revealed a parabolic shape with some data spikes present that could obviously be considered as outliers. These spikes were detected and removed from the first derivative of stress. A centered five point boxcar filter was implemented to smooth the data. The second derivative was computed on the smoothed data. This revealed a relatively flat data set with a slight negative slope. A first-round estimate of the mean and standard deviation around the zero crossing of the filtered second derivative was computed and used to determine limits for the section of data that could be considered to have a constant slope. The starting and ending indices of this section of data were acquired and used as the data limits in determining a linear fit to the engineering stress-strain raw data. The data prior to the starting index and following the ending index were each fitted with a second order polynomial fit. This process was repeated for all replicates in the three treatment conditions.

All of the curves and their associated statistics in a particular treatment condition were combined into a single curve that represents the forty replicates in the treatment condition group. Finally the two WSR curves dry and wet, were plotted on the same graph for comparison purposes.

## CHAPTER VIII

### RESULTS AND DISCUSSION

#### 1. General

Qualitatively, the results of all the experiments exceeded the initial expectations of the project. The rope breaks were clean, as shown in the lower portion of figure 4.6 and exhibited a typical failure mode. Table 8.1 shows that a majority of strand failures occurred simultaneously in 2 or 3 of the strands.

**Table 8.1: Number of strands remaining after the point of failure. Note that all tests yield a break therefore there are no failures at which all, three, strands remain.**

<u>Type</u>	<b><i>Strands remaining after breaking</i></b>					
	<u>Zero</u>		<u>One</u>		<u>Two</u>	
	<b><i>Number</i></b>	<b><i>Percentage</i></b>	<b><i>Number</i></b>	<b><i>Percentage</i></b>	<b><i>Number</i></b>	<b><i>Percentage</i></b>
WSR - Dry	13	32.5	27	67.5	0	0
WSR - Wet	3	7.5	37	92.5	0	0
Polypropylene	25	62.5	13	32.5	2	5
Total	41	34.2	77	64.2	2	1.7

The load for a failure with one strand remaining compared to the load for a failure with no strands remaining was virtually the same. Table 8.1 does however indicate possible trends. When the percentage of breaks occurring with zero and one strand remaining in the dry WSR condition were compared to the wet WSR condition, it is seen that in 92.5% of the cases one strand remained in the wet case as compared to only 67.5% in the dry case. This may be attributed to many factors including, but not

limited to, the rate of heat dissipation during the loading of the specimens. The WSR cases were compared to standard polypropylene and it was seen that the polypropylene was more apt to have a failure of all three strands. A possible explanation of the tendency for instantaneous failure of all strands of the polypropylene was the higher tensile load at failure. As the failure propagates the transfer of load from one strand to the next occurs at a faster rate than the rate of elongation. Therefore the machine does not have to “play catch up” to break all three strands.

Further stratification of the specimen failures brings up the question of the locations of the breaks. None of the 120 specimens tested broke in the terminations. However, the relative location of the break that occurred within the center section did vary. These variations are outlined in table 8.2.

**Table 8.2: Table showing the varying location of the breaks between the splices. Note that none of the 120 specimens broke in the terminations.**

<b><i>Location of breaks within the center section</i></b>				
<b><u>Type</u></b>	<b>Closer to Moving Anchorage</b>		<b>Closer to Stationary Anchorage</b>	
	<b><i>Number</i></b>	<b><i>Percentage</i></b>	<b><i>Number</i></b>	<b><i>Percentage</i></b>
WSR - Dry	16	40	24	60
WSR - Wet	21	52.5	19	47.5
Polypropylene	21	52.5	19	47.5
Total	58	48.3	62	51.7

The location of the breaks in all the experimental runs seemed to be fairly evenly distributed between breaking closer towards the moving anchorage and closer towards the stationary anchorage. This implied that the experimental process, the rope machine, and in particular the terminations did not effect the location of the break. The failure points did not seem to be predetermined by external factors beyond the specific specimen under test.

## 2. Physical Properties

The physical properties for the Whale Safe Rope were measured. The physical properties of the Polypropylene were those published by the manufacture. Table 8.3 presents the physical properties of the two types of rope.

**Table 8.3: Results of the physical properties tests showing the mean value, standard deviation of the mean, the associated measurement uncertainty with a single measurement, and the percent error between the standard deviation and the mean. Note that the Polypropylene data is from the manufacturer.**

<b>Physical properties</b>		
<b>Experimental Test</b>	<b>Treatment Combinations</b>	
	<b>Whale Safe Rope</b>	<b>Polypropylene</b>
<b>Size Number</b>		
Mean	1.13	1.18
Standard Deviation	0.010	N/A
Measurement Uncertainty	0.003	N/A
Coefficient of Variation	0.8	N/A
<b>Linear Density (lbs / 100ft)</b>		
Mean	3.39	2.8
Standard Deviation	0.243	N/A
Measurement Uncertainty	0.020	N/A
Coefficient of Variation	7.1	N/A

The size number of the WSR is approximately 4.2% smaller than that of the Polypropylene even though both ropes were considered to be in the 3/8" diameter class. This was in part due to WSR having a much tighter weave as compared to the polypropylene. The difference in the linear density between the two ropes was due to the addition of barium sulfate to reduce the breaking strength of the polypropylene based WSR.

The robustness of the experimental procedure can be examined through analysis of the standard deviation and the measurement uncertainty. The measurement

uncertainty showed the effective resolution of each of the individual measurement that made up the mean value of a parameter, where as the standard deviation is a measure of how an individual measurement differs from the expected mean calculated from the sample set. Table 8.3 shows that all the observed standard deviations were greater than the calculated measurement uncertainties. This indicates that the instrumentation used to obtain the parameters for determining the rope properties was not the limiting factors.

The data closely resembles a well behaved standard normal distribution, therefore the standard deviation and the ‘z’ statistic was used to determine the number of measurements in future experiments (as seen in equation (25)) with this procedure and instrumentation that are required to bound the expected mean within a desired confidence limit, called the expected mean estimate error. Table 8.4 shows the expected mean estimate error with various sample sizes for two confidence limits.

**Table 8.4:** Table of expected mean estimate error used to determine future sample sizes using the present data set as an accurate representation of the parent population.

<b><i>Physical expected mean estimate error</i></b>				
<b>Number of Rope Samples</b>	<b>Rope Number</b>		<b>Linear Density</b>	
	<b>Confidence Level</b>		<b>Confidence Level</b>	
	<b>90%</b>	<b>95%</b>	<b>90%</b>	<b>95%</b>
2	0.012	0.014	0.284	0.337
4	0.008	0.010	0.200	0.238
8	0.006	0.007	0.142	0.168
16	0.004	0.005	0.100	0.119
32	0.003	0.003	0.071	0.084
64	0.002	0.002	0.050	0.060

The table 8.4 shows that in future experiments a relatively small sample set is required to reliably estimate the expected mean of each of the physical parameter.

### **3. Engineering Properties**

The ultimate breaking strength was extracted from the uncycled strength and elongation data. As seen in table 8.5, Seaside Inc., who manufactures the WSR, suggested that the ultimate breaking load of WSR is in the region of 1050 lbs. When this is compared to the acquired mean seen in table 8.5, along with the associated standard deviation, it fell within the two standard deviation limit of the UNH data. Seaside Inc. did not provide an estimate for wet breaking strength of the WSR. However, there was a marketed difference between the WSR dry and wet breaking strengths. This difference was attributed to the dissipation of heat by the salt water contained in the wet combination. The mean ultimate breaking strength for the polypropylene reflected the published values which range from 2440 to 2900 pounds.



**Table 8.5: Engineering results showing the ultimate breaking strength, elongation, and elastic modulus.**

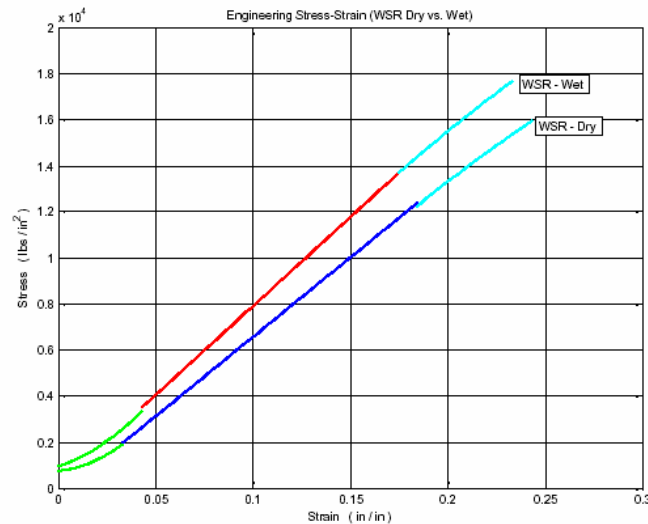
<b>Engineering properties</b>			
<b>Experimental Test</b>	<b>Treatment Combinations</b>		
	<b>Whale Safe Rope</b>		<b>Polypropylene</b>
	<i>Dry</i>	<i>Wet</i>	<i>Dry</i>
<b>Ultimate Breaking Strength (lbs)</b>			
Mean	1019.5	1132.4	2784.2
Standard Deviation	34.9	35.5	60.2
Measurement Uncertainty	7.83		
Coefficient of Variation	3.4	3.1	2.2
<b>Elongation (in)</b>			
Mean			
Percent Full Load			
10	0.341	0.267	0.104
50	1.457	1.354	1.627
90	2.593	2.478	2.834
Standard Deviation			
Percent Full Load			
10	0.072	0.143	0.104
50	0.101	0.102	0.087
90	0.138	0.109	0.101
Measurement Uncertainty	0.024		
Coefficient of Variation			
Percent Full Load			
10	21.1	53.6	100.0
50	6.9	7.5	5.3
90	5.3	4.4	3.6
<b>Elastic Modulus (psi)</b>			
Mean	68897	77169	102490
Standard Deviation	3070	2455	3431
Measurement Uncertainty	218		
Coefficient of Variation	4.5	3.2	3.3

The elongation measurements were determined at three separate load conditions, 10%, 50%, and 90% percent of the ultimate breaking strength. These three percentages were intended to give a general feel of the data in the three regions of mechanical settling, elastic, and strain hardening.

These regions, as outlined in the data processing section, can be seen overlaid on the raw engineering stress-strain data in appendix D. These plots show dotted lines demarcating the 95% confidence limits of the fit parameters. In the linear region of the fits, the slope parameter represents the modulus of elasticity as reported in the

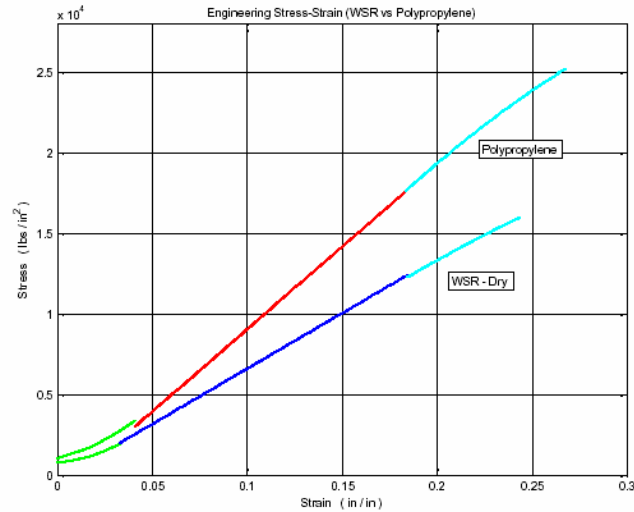
lower portion of table 8.5. No published comparison values exist for the WSR. However, the measured polypropylene's elastic modulus is about half of the values reported by the plastics industry. It is theorized that this reduction of elastic modulus is due to having constrained the specimen to prevent rotation during the test and due to the multiple strand construction of the WSR. The non-rotational constraint adds a torque force (based on the helical angle of the weave) to what would otherwise be a pure tensile force. The test is a valid representation of the condition in which the rope is deployed in fixed fishing gear without mechanical swivels.

The comparison of the different treatment combinations shows some interesting results. The first comparison was preformed on the engineering stress-strain curves between the wet and dry cases of the WSR as seen in figure 8.1.



**Figure 8.1: Comparison plot of the curve fits for the WSR dry and wet cases. The green color represents mechanical settling, the cyan color is the strain hardening region, and the linear sections (red and blue) are the elastic regions.**

It can be concluded from figure 8.1 and the values for the elastic modulus in table 8.5 that the salt water soak had a measurable effect on the performance of the whale safe rope. The dry cases for the WSR and the polypropylene were compared in figure 8.2.



**Figure 8.2: Comparison plot of the curve fits for the whale safe rope (dry) and polypropylene (dry).**

The ultimate breaking strength and the elastic modulus were obviously very different between the WSR and the polypropylene. Furthermore, the strain hardening regions of the two exhibited distinctively different slope characteristics. Appendix E presents the first derivative of stress verses the linear index number for the various treatment conditions and comparisons. It is clearly seen that slope of the strain hardening region for the WSR is much flatter than that of the polypropylene. It is suggested that this indicates an increase in the brittle properties of WSR compared to the polypropylene.

The second derivative of stress was also computed. The second derivative of stress plotted against the linear index exhibited a flat region with a slight negative slope (Appendix F). This is suggestive of “necking” or reduction of the cross-sectional area of the specimens during the experimental runs. The extraction of the increase in the brittle properties of WSR as compared to standard polypropylene and the measurement of the reduction of the cross-sectional area over time from the data is a unique quality of the implemented data acquisition systems and techniques. The

aforementioned points cannot be extracted while using the stereotypical extensometer to measure elongation.

The consistent extraction of data from the engineering stress-strain, and the derivatives of stress are a direct result of the accuracy and precision of the experimental methodology. An analogous process to that outlined in the physical properties results section was followed to further show the robustness of the methodology. A table of expected mean estimate errors was constructed to determine the number of samples necessary in future experiments of this type to measure a parameter within a specific confidence limit. This is seen in table 8.6.

**Table 8.6: Table of expected mean estimate error used to determine future sample sizes using the current data set as an accurate representation of the parent population.**

Engineering expected mean estimate error								
Number of Rope Samples	Ultimate Breaking Strength		Elongation				Elastic Modulus	
	Confidence Level		Confidence Level				Confidence Level	
	90%	95%	90%		95%		90%	95%
			Percentage Full Load					
			50%	90%	50%	90%		
Whale Safe Rope - Dry								
2	40.7	48.4	0.118	0.161	0.140	0.191	3582	4255
4	28.8	34.2	0.083	0.114	0.099	0.135	2533	3009
8	20.4	24.2	0.059	0.081	0.070	0.096	1791	2127
16	14.4	17.1	0.042	0.057	0.049	0.068	1266	1504
32	10.2	12.1	0.029	0.040	0.035	0.048	895	1064
64	7.2	8.6	0.021	0.028	0.025	0.034	633	752
Whale Safe Rope - Wet								
2	41.4	49.2	0.119	0.127	0.141	0.151	2864	3403
4	29.3	34.8	0.084	0.090	0.100	0.107	2025	2406
8	20.7	24.6	0.060	0.064	0.071	0.076	1432	1701
16	14.6	17.4	0.042	0.045	0.050	0.053	1013	1203
32	10.4	12.3	0.030	0.032	0.035	0.038	716	851
64	7.3	8.7	0.021	0.022	0.025	0.027	506	601
Polypropylene - Dry								
2	70.2	83.4	0.102	0.118	0.121	0.140	4003	4755
4	49.7	59.0	0.072	0.083	0.085	0.099	2831	3362
8	35.1	41.7	0.051	0.059	0.060	0.070	2002	2378
16	24.8	29.5	0.036	0.042	0.043	0.049	1415	1681
32	17.6	20.9	0.025	0.029	0.030	0.035	1001	1189
64	12.4	14.7	0.018	0.021	0.021	0.025	708	841

Table 8.6 shows that only a small number of samples are required to achieve the expected mean of a parameter within limits based on the selected confidence limit. The claim of a robust process, with the exception of the elongation at the 10% full load case, is further supported by the reported coefficient of variation experienced in table 8.5. The elongation within the mechanical settling region is excluded due to the high variability of the settling of the newly formed splices and transient vibrations of the machine when first actuated from rest.

## **CHAPTER IX**

### **CONCULSIONS**

This study successfully investigated the properties of Whale Safe Rope (WSR) in an effort to establish a robust experimental methodology for the accurate and precise testing of rope. The process started with the research, design and construction of a rope tension testing apparatus and data measurement systems that would yield accurate and consistent results. The robust experimental methodology that was devised for testing the rope to ultimate failure achieved high accuracy of the elongation measurement through the implementation of digital image processing making it easy for an operator to safely achieve high repeatability without having extensive specialized training.

The physical and engineering properties of WSR presented in tables 8.3 and 8.5, respectively, show various parameters that are required in order to make informed decisions about the design and implementation of offshore gill net and lobstering rigging. It is noteworthy that WSR shows evidence of properties that are analogous to those of a material with brittle characteristics. This means that the WSR might very well break at the location of a point (whale) load. The aforementioned charts and figures show a high degree of precision which allows insight into the mechanics of the specimen under test.

Statistical analysis of the experimental data, as presented in tables 8.1, 8.2, 8.4, and 8.6, show both qualitatively and quantitatively the robustness of the experimental methodology. These tables show that future experiments can achieve significant results by testing only four replicates per treatment combination and still guarantee that 95% of the data will contain the expected value of a particular parameter to within the same standard deviations as noted in the physical and engineering properties tables. This outstanding result stems directly from the methods that were devised and then used to gather and process the data.

The data in tables 8.1 and 8.2 further demonstrates that the bed length chosen for the testing machine was reasonable. This directly reflects the fact that the design process correctly weighed the design criterion to minimize the fabrication cost and maximize the data quality and repeatability.

There are, however, a few points worth addressing for future testing. The errors of the measurements deemed to be in the mechanical settling region of the engineering stress-strain curves were higher than those exhibited elsewhere. The high standard deviation is largely attributed to the video cameras having been mounted to a tripod that was independent and remote from the frame of the rope testing apparatus. Affixing the cameras directly to the frame of the testing apparatus will likely reduce these errors and possibly provide greater insight into the mechanical settling characteristics of the terminations.

The method of attaching the specimens to the machine may possibly be redesigned to eliminate the need to construct an eye splice at each end of the specimen. This would allow for quicker testing and the nondestructive testing of field

deployed line, which typically is hard to splice. It is also arguable that this method of attachment, if done carefully, will settle no more than that of an eye splice. However, care must be taken to assure that if any extended settling of the rope on the termination does occur, it can be neglected in favor of the other benefits that this type rope attachment would bring to the operation. This modification to the test apparatus could be beneficial for gaining insight into the performance characteristics of WSR, or any line, over time. The addition of a cyclic loading test should also be considered to give a further basis for comparisons between different types of ropes. This possibility of including cyclic load testing was foreseen in the design stage of the testing apparatus and consequently provisions were made that would make it relatively easy to exchange the present direction control valve for a computer controlled solenoid control valve. These additional modifications and experimental tests will allow future researchers and end-users of any rope/line to better understand the most common piece of equipment which impacts cost and safety in the marine industry. That is to say, rope.



## REFERENCES

- ASTM. (1993). *Standard Methods of Testing Fiber Ropes*. Annual Book of American Society for Testing and Materials Standards, Vol. 7, D4268 – 93, 397 – 403 p.
- Beer, F.P., and Johnston, E.R. (1996). Vector Mechanics for Engineers: Statics. McGraw-Hill, Inc., New York. 599 p.
- Caswell, H., Fujiwara, M., and Brault, S., (1999). *Declining survival probability threatens the North Atlantic right whale*. Proceedings of the National Academy of Sciences. 3308 – 3313 p.
- Cavatorta, D., Starczak, V., Prada, K., and Moore, M. (2003). *Friction of Different Ropes in Right Whale Baleen: a Potential Strategy to Reduce Entanglement Mortality*. North Atlantic Right Whale Consortium Annual Meeting, Feb 4&5.
- CI. (1999). *CI 1301-96: Polypropylene Fiber Rope*. Cordage Institute Standards, Ver. 2, Wayne, PA.
- CI. (2002). *CI 1500-02: Test Methods for Fiber Rope*. Cordage Institute Standards, Ver. Feb 2002, Wayne, PA.
- Cundiff, J.S. (2002). Fluid Power Circuits and Controls. CRC Press LLC, Florida. 533 p.
- Flory, J.F., and Mercer, D.E. (1997). *The New Cordage Institute Fiber Rope Test Methods*. Oceans '97 MTS/IEEE Conference Proceedings, Vol. 1, 308 – 313 p.
- Fraday, T. (2004). *Guide to: The Atlantic Large Whale Take Reduction Plan*. NOAA/NMFS/NER, <http://www.nero.noaa.gov/whaletrp/>.
- Frocht, M.M., and Hill, H.N. (1940). *Stress-Concentration Factors Around a Central Circular Hole in a Plate Loaded Through Pin in the Hole*. Journal of Applied Mechanics (Transactions of the American Society of Mechanical Engineers), Vol. 7, No. 1, A-7 to A-9 p.
- Higgins, J., Kenney, J., and Salvador, G. (2003). *Techniques for Making Weak Links and Marking Buoy Lines*. How to comply with the ALWTR Plan, <http://www.nero.noaa.gov/whaletrp/>.

- Knowlton, A.R. and Kraus, S.D. (2001). *Mortality and serious injury of northern right whales (*Eubalaena glacialis*) in the western North Atlantic Ocean*. Journal of Cetacean Research and Management, Vol. 2, Special Issue, 193 – 208 p.
- Kraus, S.D. (1990). *Rates and potential causes of mortality in North Atlantic right whales (*Eubalaena glacialis*)*. Marine Mammal Science, Vol. 6, No. 4, 278 – 291 p.
- Mangonon, P.L. (1999). The Principles of Materials Selection for Engineering Design. Prentice- Hall PTR, New Jersey. 824 p.
- Oberg, E. et. al. (2000). 26<sup>th</sup> Edition Machinery's Handbook. Industrial Press Inc., New York. 2630 p.
- Sampson Rope Technologies. (2003). *Industrial Rope Catalog*. <http://www.sampsonrope.com> .
- Schenck, H. Jr. (1961). Theories of Engineering Experimentation. McGraw-Hill, Inc., New York. 239 p.
- Shigley, J.E., and Mischke, C.R. (1989). Mechanical Engineering Design. McGraw-Hill, Inc., New York. 779 p.
- Taylor, J.R. (1997). An Introduction to Error Analysis: The Study of Uncertainties in Physical Measurements. University Science Books, California. 327 p.
- Ugural, A.C., and Fenster S.K. (1995). Advanced Strength and Applied Elasticity. Prentice- Hall PTR, New Jersey. 570 p.
- United States. (1972). *Marine Mammal Protection Act (MMPA) of 1972*. United States of America Congress. 119 p.
- Vining, G.G. (1998). Statistical Methods for Engineers. Duxbury Press, Pacific Grove, CA. 479 p.
- White, F.M. (1999). Fluid Mechanics. McGraw-Hill, Inc., New York. 826 p.
- Young, W.C. (1989). Roark's Formulas for Stress and Strain. McGraw-Hill, Inc., New York. 764 p.

## **APPENDICIES**

**APPENDIX A:**  
**Design Calculations**

## *Calculations for Anchor Pins*

Given:	$E := 2.9 \cdot 10^7 \frac{\text{lb}}{\text{in}^2}$	Young's Modulus of Elasticity for W1 Tool Steel
	$\sigma_{\text{yield}} := 5.8 \cdot 10^4 \frac{\text{lb}}{\text{in}^2}$	Yield strength of W1 Tool Steel
	$l := 6.5 \text{ in}$	Anchor pin length
	$d := 1 \text{ in}$	Anchor pin diameter
	$c := \frac{d}{2}$	Max distance from the Netural Axis
	$F := 15000 \text{ lb}$	Max design load

- Find:
- (1) Bending Moment,  $M_{\text{max}}$
  - (2) Transverse Shear,  $V_{\text{max}}$
  - (3) Displacement,  $y_{\text{max}}$
  - (4) Tangential Stress,  $\sigma_{\text{max}}$
  - (5) Transverse (shear) stress,  $\tau_{\text{max}}$
  - (6) Factor of Safety, FS

Solution: Part (1)

$$M_{\text{max}} := \frac{F \cdot l}{8}$$

$$M_{\text{max}} = 1.219 \times 10^4 \text{ lb} \cdot \text{in}$$

Part (2)

$$V_{\text{max}} := \frac{F}{2}$$

$$V_{\text{max}} = 7.5 \times 10^3 \text{ lb}$$

Part (3)

First determine the Moment of Inertia about the Netural Axis

$$I := \frac{\pi \cdot \left(\frac{d}{2}\right)^4}{4}$$

$$I = 0.049 \text{ in}^4$$

$$y_{\text{max}} := \frac{-F \cdot l^3}{192 \cdot E \cdot I}$$

$$y_{\text{max}} = -0.015 \text{ in}$$

Part (4)

$$\sigma_{\max} := \frac{M_{\max} \cdot c}{I}$$

$$\sigma_{\max} = 1.241 \times 10^5 \frac{\text{lb}}{\text{in}^2}$$

Part (5)

First determine the cross sectional area

$$A := \pi \cdot \left(\frac{d}{2}\right)^2$$

$$A = 0.785 \text{ in}^2$$

$$\alpha := \frac{4}{3}$$

Form Factor for Circular Cross Section

$$\tau_{\max} := \alpha \cdot \frac{V_{\max}}{A}$$

$$\tau_{\max} = 1.273 \times 10^4 \frac{\text{lb}}{\text{in}^2}$$

Part (6)

$$FS_{\sigma} := \frac{\sigma_{\text{yield}}}{\sigma_{\max}}$$

$$FS_{\sigma} = 0.467$$

$$FS_{\tau} := \frac{\sigma_{\text{yield}}}{\tau_{\max}}$$

$$FS_{\tau} = 4.555$$

Anchor pin calculation results											
Force (W) (lbs)	Pin Length (l) (in)	Diameter (D) (in)	Cross Sectional Area (A) (in <sup>2</sup> )	Moment of Inertia (I) (in <sup>4</sup> )	Bending Moment (Mmax) (lb·in)	Transverse Shear (Vmax) (lb)	Displacement (vmax) (in)	Tangential Stress (tmax) (psi)	Tangential Factor of Safety	Shear Stress (tmax) (psi)	Shear Factor of Safety
5000	4		0.500	0.196	0.003	2500	-0.019	203718.327	0.285	16976.527	3.417
			0.625	0.307	0.007		-0.008	104303.784	0.556	10864.977	5.340
			0.750	0.442	0.016		-0.004	60360.986	0.961	7545.123	7.689
			0.875	0.601	0.029		-0.002	38011.583	1.526	5543.356	10.466
	6		1.000	0.785	0.049		-0.001	25464.791	2.278	4244.132	13.670
			0.500	0.196	0.003		-0.063	305577.491	0.190	16976.527	3.417
			0.625	0.307	0.007		-0.026	156455.675	0.371	10864.977	5.340
			0.750	0.442	0.016		-0.012	90541.479	0.641	7545.123	7.689
	8		0.875	0.601	0.029		-0.007	57017.374	1.018	5543.356	10.466
			1.000	0.785	0.049		-0.004	38197.186	1.519	4244.132	13.670
			0.500	0.196	0.003		-0.150	407436.654	0.142	16976.527	3.417
			0.625	0.307	0.007		208607.567	0.278	10864.977	5.340	
15000	4		0.750	0.442	0.016	120721.972	0.481	7545.123	7.689		
			0.875	0.601	0.029	76023.166	0.763	5543.356	10.466		
			1.000	0.785	0.049	50929.582	1.139	4244.132	13.670		
			0.500	0.196	0.003	611154.981	0.095	50929.582	1.139		
	6		0.625	0.307	0.007	312911.351	0.185	32594.932	1.780		
			0.750	0.442	0.016	181082.957	0.320	22635.370	2.563		
			0.875	0.601	0.029	114034.749	0.509	16630.068	3.489		
			1.000	0.785	0.049	76394.373	0.759	12732.395	4.557		
	8		0.500	0.196	0.003	916732.472	0.063	50929.582	1.139		
			0.625	0.307	0.007	469367.026	0.124	32594.932	1.780		
			0.750	0.442	0.016	271624.436	0.214	22635.370	2.563		
			0.875	0.601	0.029	171052.123	0.339	16630.068	3.489		
15000	6		1.000	0.785	0.049	-0.012	114591.559	0.508	12732.395	4.557	
			0.500	0.196	0.003	-0.449	1222309.963	0.047	50929.582	1.139	
			0.625	0.307	0.007	-0.184	625822.701	0.093	32594.932	1.780	
			0.750	0.442	0.016	-0.089	362165.915	0.160	22635.370	2.563	
	8		0.875	0.601	0.029	-0.048	228069.497	0.254	16630.068	3.489	
			1.000	0.785	0.049	-0.028	152788.745	0.380	12732.395	4.557	

## *Calculation for Anchor Plates*

Given:  $F := 15000\text{lb}$

Max design load on pin

$d := 1\text{in}$

Diameter of hole in the plate

$w := 4.0\text{in}$

Plate width

$t := 0.5\text{in}$

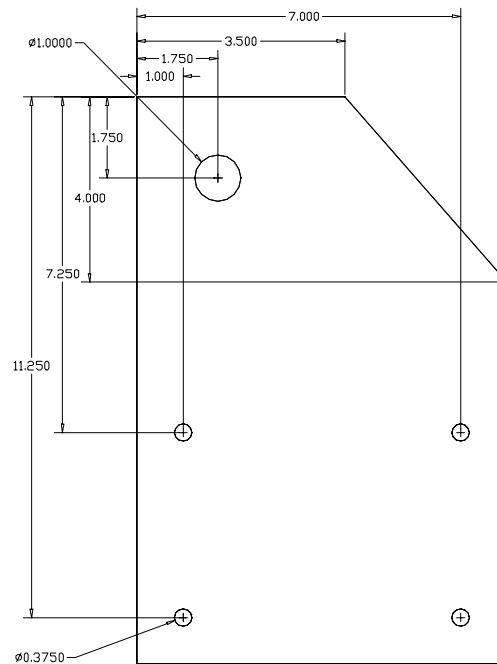
Plate thickness

$h := 1.75\text{in}$

Minimum distance from hole center to plate edge

- Find:
- (1) Maximum normal stresses,  $\sigma_{\max}$  due to the hole for securing the anchor pin
  - (2) Resultant load on each bolt,  $F_{a,b,c,d}$
  - (3) Maximum bolt shear stress,  $\tau_{\max}$
  - (4) Maximum bearing stress,  $\sigma_{\text{bear}}$
  - (5) Critical bending stress in the bar,  $\sigma_{\text{bend}}$

Diagram:





Solution: Part (1)

First calculate parameters to look up  $K_t$  from Frocht and Hill

$$\frac{d}{w} = 0.25$$

$$\frac{h}{w} = 0.438$$

$$K_t := 4.75$$

Next determine the nominal stresses  $\sigma_o$  and  $\tau_o$

$$\sigma_o := \frac{F}{(w - d) \cdot t}$$

$$\sigma_o = 1 \times 10^4 \frac{\text{lb}}{\text{in}^2}$$

$$\sigma_{\max} := K_t \cdot \sigma_o$$

$$\sigma_{\max} = 4.75 \times 10^4 \frac{\text{lb}}{\text{in}^2}$$

Part (2): First find the shear force V and moment M about point "O"

$$V := F$$

$$V = 1.5 \times 10^4 \text{ lb}$$

$$M := F \cdot 9.25 \text{ in}$$

$$M = 1.387 \times 10^5 \text{ lb} \cdot \text{in}$$

$$r := \sqrt{(2 \text{ in})^2 + (3 \text{ in})^2}$$

$$r = 3.606 \text{ in}$$

$$n := 4$$

Number of bolts used

Now, find the primary shear force F' and secondary shear force F''

$$F_{\text{prime}} := \frac{V}{n}$$

$$F_{\text{prime}} = 3.75 \times 10^3 \text{ lb}$$

$$F_{\text{DBLprime}} := \frac{M}{n \cdot r}$$

$$F_{\text{DBLprime}} = 9.621 \times 10^3 \text{ lb}$$

Adding the two force vectors using the parallelogram rule

$$\phi := \text{atan}\left(\frac{2 \text{ in}}{3 \text{ in}}\right)$$

$$\phi = 33.69 \text{ deg}$$

Angle between F' and r

$$\beta_{AB} := 90 \text{ deg} - \phi$$

$$\beta_{AB} = 56.31 \text{ deg}$$

Angle between F' and F''

$$\beta_{CD} := 90 \text{ deg} + \phi$$

$$\beta_{CD} = 123.69 \text{ deg}$$

Angle between F' and F''

$$F_A := \sqrt{F_{\text{prime}}^2 + F_{\text{DBLprime}}^2 + 2 \cdot F_{\text{prime}} \cdot F_{\text{DBLprime}} \cdot \cos(\beta_{AB})} \quad F_A = 1.211 \times 10^4 \text{ lb}$$

$$F_B := F_A \quad F_B = 1.211 \times 10^4 \text{ lb}$$

$$F_C := \sqrt{F_{\text{prime}}^2 + F_{\text{DBLprime}}^2 + 2 \cdot F_{\text{prime}} \cdot F_{\text{DBLprime}} \cdot \cos(\beta_{CD})} \quad F_C = 8.161 \times 10^3 \text{ lb}$$

$$F_D := F_C \quad F_D = 8.161 \times 10^3 \text{ lb}$$

Part (3): The bolt used is a flat head bolt with a size of 3/8"-16 x 1" made of steel

$$A_s := 0.0678 \text{ in}^2 \quad \text{Minor Pitch Diameter Area}$$

$$\tau_{\text{Bolt}} := \frac{F_A}{A_s} \quad \tau_{\text{Bolt}} = 1.786 \times 10^5 \frac{\text{lb}}{\text{in}^2}$$

Part (4): Since the web of the c-channel is thinner than the anchor plate the largest bearing force is due to the pressing of the bolt against the web of the c-channel

$$t_w := 0.314 \text{ in} \quad \text{Web thickness of C6x10.5 channel}$$

$$d_{\text{bolt}} := 0.375 \text{ in} \quad \text{Nominal diameter of the bolt}$$

$$A_b := d_{\text{bolt}} \cdot t_w \quad A_b = 0.118 \text{ in}^2 \quad \text{Bearing Area}$$

$$\sigma_{\text{bear}} := \frac{-F_A}{A_b} \quad \sigma_{\text{bear}} = -1.028 \times 10^5 \frac{\text{lb}}{\text{in}^2}$$

Part (5): The critical bending stress acts through bolts A and B

$$M_{AB} := F \cdot 7.25 \text{ in} \quad M_{AB} = 1.087 \times 10^5 \text{ lb} \cdot \text{in}$$

$$I_{\text{plate}} := \frac{t \cdot (8 \text{ in})^3}{12} \quad I_{\text{plate}} = 21.333 \text{ in}^4$$

$$I_{\text{holes}} := \frac{t \cdot d_{\text{bolt}}^3}{12} \quad I_{\text{holes}} = 2.197 \times 10^{-3} \text{ in}^4$$

$$I := I_{\text{plate}} - 2 \cdot \left[ I_{\text{holes}} + \left[ (3 \cdot \text{in})^2 \cdot t \cdot d_{\text{bolt}} \right] \right] \quad I = 17.954 \text{ in}^4$$

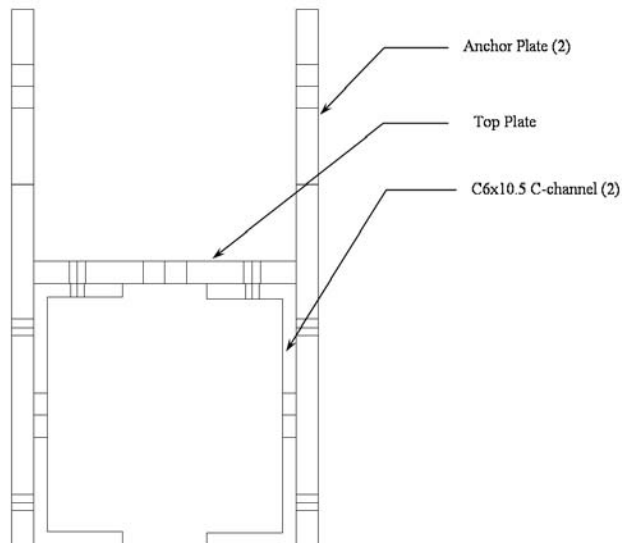
$$\sigma_{\text{bend}} := \frac{M_{AB} \cdot w}{I} \quad \sigma_{\text{bend}} = 2.423 \times 10^4 \frac{\text{lb}}{\text{in}^2}$$

## *Calculations for Structural Members*

### Given:

$F_{\max} := 15000\text{lb}$	Max tensile force based on hydraulics
$F_{\text{design}} := 5000\text{lb}$	Design tensile force
$w_p := 6\text{in}$	Width of top plate
$t_p := 0.5\text{in}$	Thickness of top plate
$l := 96\text{in}$	Overall length of structural members
$A_c := 3.09\text{in}^2$	Cross sectional area of C6x10.5 channel
$h_c := 6\text{in}$	Height of C6x10.5 channel
$h_{\text{pin}} := 4\text{in}$	Height of pin above the top plate
$E := 30 \cdot 10^6 \frac{\text{lb}}{\text{in}^2}$	Youngs Modulus for 1018 HR Steel
$\sigma_{\text{yield}} := 32000 \frac{\text{lb}}{\text{in}^2}$	Yield strength of 1018 HR Steel

### Diagram:



Please note the naming convention used is:

Top Plate is #1  
Left Channel is #2  
Right Channel is #3

- Find:
- (1) Max deflection angle,  $\theta_{\max}$
  - (2) Max deflection,  $y_{\max}$
  - (3) Max Stress,  $\sigma_{\max}$
  - (4) Associated Factors of Safety, SF

Solution: Part (1):

First determine the location of the Neutral Axis from the origin at the lower left corner of the cross section via geometry

<u>Componant</u>	<u>Area</u>	<u><math>x_{\text{bar}}</math></u>	<u><math>y_{\text{bar}}</math></u>	<u><math>x_{\text{bar}}A</math></u>	<u><math>y_{\text{bar}}A</math></u>
	(in <sup>2</sup> )	(in)	(in)	(in <sup>3</sup> )	(in <sup>3</sup> )
1	3.000	3.000	6.250	9.000	18.750
2	3.090	0.499	3.000	1.542	9.270
3	3.090	5.501	3.000	16.998	9.270
<b><u>Sums</u></b>	9.180	N/A	N/A	27.540	37.290

Solving for the centroids yeilds:

$$x_{\text{bar}} := \frac{27.540 \text{ in}^3}{9.180 \text{ in}^2}$$

$$x_{\text{bar}} = 3 \text{ in}$$

$$y_{\text{bar}} := \frac{37.290 \text{ in}^3}{9.180 \text{ in}^2}$$

$$y_{\text{bar}} = 4.062 \text{ in}$$

Now, find the moment of inertia for the composite beam:

$$I_{x,1} := \frac{w_p \cdot t_p^3}{12} + (3 \text{ in})^2 \cdot [(6.25 \text{ in}) - y_{\text{bar}}]^2$$

$$I_{x,1} = 14.423 \text{ in}^4$$

$$I_{x,2} := 15.2 \text{ in}^4 + 3.09 \text{ in}^2 \cdot (y_{\text{bar}} - 3.00 \text{ in})^2$$

$$I_{x,2} = 18.686 \text{ in}^4$$

$$I_{x,3} := 15.2 \text{ in}^4 + 3.09 \text{ in}^2 \cdot (y_{\text{bar}} - 3.00 \text{ in})^2$$

$$I_{x,3} = 18.686 \text{ in}^4$$

$$I_x := I_{x,1} + I_{x,2} + I_{x,3}$$

$$I_x = 51.795 \text{ in}^4$$

Calculate the moment produced:

$$L_{\text{arm}} := h_{\text{pin}} + [(t_p + h_c) - y_{\text{bar}}]$$

$$L_{\text{arm}} = 6.438 \text{ in}$$

$$M_{\text{design}} := L_{\text{arm}} \cdot F_{\text{design}}$$

$$M_{\text{design}} = 3.219 \times 10^4 \text{ lb}\cdot\text{in}$$

$$M_{\text{max}} := L_{\text{arm}} \cdot F_{\text{max}}$$

$$M_{\text{max}} = 9.657 \times 10^4 \text{ lb}\cdot\text{in}$$

If the beam were to be analyzed in two halves by superposition, each half would act like having one end fix and the other end free with a moment applied to the free end. Therefore the deflection angle is:

$$\theta_{\text{design}} := \frac{-M_{\text{design}} \cdot \left(\frac{1}{2}\right)}{E \cdot I_x}$$

$$\theta_{\text{design}} = -0.057 \text{ deg}$$

$$\theta_{\text{max}} := \frac{-M_{\text{max}} \cdot \left(\frac{1}{2}\right)}{E \cdot I_x}$$

$$\theta_{\text{max}} = -0.171 \text{ deg}$$

Part (2): By the same method as above the deflection magnitude equation can be written:

$$y_{\text{design}} := \frac{M_{\text{design}} \cdot \left(\frac{1}{2}\right)^2}{2 \cdot E \cdot I_x}$$

$$y_{\text{design}} = 0.024 \text{ in}$$

$$y_{\text{max}} := \frac{M_{\text{max}} \cdot \left(\frac{1}{2}\right)^2}{2 \cdot E \cdot I_x}$$

$$y_{\text{max}} = 0.072 \text{ in}$$

Part (3):

$$\sigma_{\text{design}} := \frac{-M_{\text{design}} \cdot y_{\text{bar}}}{I_x}$$

$$\sigma_{\text{design}} = -2.525 \times 10^3 \frac{\text{lb}}{\text{in}^2}$$

$$\sigma_{\text{max}} := \frac{-M_{\text{max}} \cdot y_{\text{bar}}}{I_x}$$

$$\sigma_{\text{max}} = -7.574 \times 10^3 \frac{\text{lb}}{\text{in}^2}$$

Part (4):

$$SF_{\text{design}} := \frac{\sigma_{\text{yield}}}{|\sigma_{\text{design}}|}$$

$$SF_{\text{design}} = 12.676$$

$$SF_{\text{max}} := \frac{\sigma_{\text{yield}}}{|\sigma_{\text{max}}|}$$

$$SF_{\text{max}} = 4.225$$

### *Calculations for Hydraulic Parts*

Given:

$$P_{des} := 1950\text{psi}$$

Design pressure output of power pack

$$P_{\max} := 5000 \text{ psi}$$

Maximum pressure output of power pack

$$Q := 19.8 \frac{\text{gal}}{\text{min}}$$

Flow output of power pack

$$V_{\text{cross\_head}} := 144 \frac{\text{in}}{\text{min}}$$

Velocity of the cross head

bore := 2.5in

Linear actuator piston diameter

stroke := 18in

Linear actuator stroke length

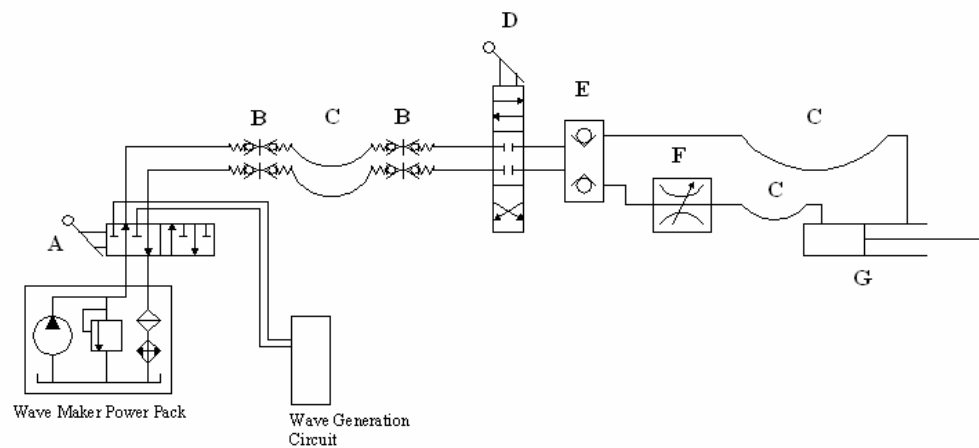
$$F_{des} := 5000\text{lbf}$$

Design tensile force

$$F_{\max} := 15000 \text{ lbf}$$

Max tensile force

Hydraulic Schematic:



- Find:
- (1) Horsepower output of power pack
  - (2) Flow/Pressure requirements of linear actuator (LA)
  - (3-8) Pressure loss, flow reductions, heat sources from:
    - (3) Flow Control valve (FCV)
    - (4) Load Check valve (LCV)
    - (5) Directional Control valve (DCV)
    - (6) Quick-Disconnects (QD)
    - (7) Selector valve (SV)
    - (8) All lines and hoses
  - (9) Total estimated losses

Solution: Part (1)

$$W_{hpdes} := P_{des} \cdot Q$$

$$W_{hpdes} = 22.523 \text{ hp}$$

$$W_{hpmax} := P_{max} \cdot Q$$

$$W_{hpmax} = 57.75 \text{ hp}$$

Part (2):

$$Q_{LA} := V_{cross\_head} \cdot \pi \cdot \left( \frac{\text{bore}}{2} \right)^2$$

$$Q_{LA} = 3.06 \frac{\text{gal}}{\text{min}}$$

$$P_{LAdes} := \frac{F_{des}}{\pi \cdot \left( \frac{\text{bore}}{2} \right)^2}$$

$$P_{LAdes} = 1.019 \times 10^3 \text{ psi}$$

$$P_{LAmax} := \frac{F_{max}}{\pi \cdot \left( \frac{\text{bore}}{2} \right)^2}$$

$$P_{LAmax} = 3.056 \times 10^3 \text{ psi}$$

Part (3): Since the flow remains constant calculate the pressure loss across the FCV ( $P_{fc}$ )

$$P_{fcman} := 150 \text{ psi}$$

$$P_{fcdes} := P_{des} - P_{LAdes}$$

$$P_{fcdes} = 931.408 \text{ psi}$$

$$P_{fcmax} := P_{max} - P_{LAmax}$$

$$P_{fcmax} = 1.944 \times 10^3 \text{ psi}$$

$$q_{FCVman} := P_{fcman} \cdot Q_{LA}$$

$$q_{FCVman} = 0.268 \text{ hp}$$

$$q_{FCVdes} := P_{fcdes} \cdot Q_{LA}$$

$$q_{FCVdes} = 1.663 \text{ hp}$$

$$q_{FCVmax} := P_{fcmax} \cdot Q_{LA}$$

$$q_{FCVmax} = 3.47 \text{ hp}$$

Part (4): From the manufacturer the pressure drop across the LCV is:

$$P_{LCV} := 5\text{psi}$$

$$q_{LCV} := P_{LCV} \cdot Q_{LA}$$

$$q_{LCV} = 8.925 \times 10^{-3} \text{ hp}$$

Part (5): From the manufacturer the pressure drop at the design flow rate is:

$$P_{DCV} := 2\text{psi}$$

$$q_{DCV} := P_{DCV} \cdot Q_{LA}$$

$$q_{DCV} = 3.57 \times 10^{-3} \text{ hp}$$

Part (6): From the manufacturer the pressure drop at the design flow rate is:

$$P_{QD} := 3\text{psi}$$

$$q_{QD} := P_{QD} \cdot Q_{LA}$$

$$q_{QD} = 5.355 \times 10^{-3} \text{ hp}$$

Part (7): From the manufacturer the pressure drop at the design flow rate is:

$$P_{SV} := 3\text{psi}$$

$$q_{SV} := P_{SV} \cdot Q_{LA}$$

$$q_{SV} = 5.355 \times 10^{-3} \text{ hp}$$

Part (8): Most of the pressure drop will be in the fifty foot sections of hose! So, first compute the Reynolds Number:

$$d_{ID} := 0.5\text{in}$$

Inside diameter of the hose

$$\nu := 665\text{stokes}$$

The kinematic viscosity of oil

$$V_{fl} := \frac{Q_{LA}}{\pi \cdot \frac{d_{ID}^2}{4}}$$

Velocity of the oil in the hose

$$N_r := \frac{7740 \cdot 6.65 \cdot 0.5}{4.998}$$

$$N_r = 5.149 \times 10^3$$

Since the Reynolds number is greater than 4000 the flow is considered to be turbulent. This means the friction factor for the hose is given by the Blasius equation:

$$f := \frac{0.3164}{N_r^{0.25}}$$

$$f = 0.037$$

Now the head loss can be calculated using the Darcy-Wabaush Equation:



$$h_l := f \cdot \left( \frac{50 \text{ ft}}{d_{ID}} \right) \cdot \left( \frac{V_{fl}^2}{2 \cdot g} \right)$$

$$h_l = 17.414 \text{ ft}$$

Now calculate the pressure loss

$$\gamma_{H2O} := 62.4 \frac{\text{lbf}}{\text{ft}^3}$$

Specific weight of water

$$S_g := 0.876$$

Specific gravity of oil used

$$P_{hose} := \gamma_{H2O} \cdot S_g \cdot h_l$$

$$P_{hose} = 6.61 \text{ psi}$$

$$q_{hose} := P_{hose} \cdot Q_{LA}$$

$$q_{hose} = 0.012 \text{ hp}$$

Part (9): Sum all the pressure losses and heat generation factors:

$$P_{total} := P_{fcman} + P_{LCV} + P_{DCV} + 8 \cdot P_{QD} + P_{SV} + 2 \cdot P_{hose}$$

$$P_{total} = 197.22 \text{ psi}$$

Estimated total system pressure loss

$$q_{total} := q_{FCVman} + q_{LCV} + q_{DCV} + 8 \cdot q_{QD} + q_{SV} + 2 \cdot q_{hose}$$

$$q_{total} = 0.352 \text{ hp}$$

Estimated total system heat production

**APPENDIX B:**  
**AutoCAD Fabrication Drawings**


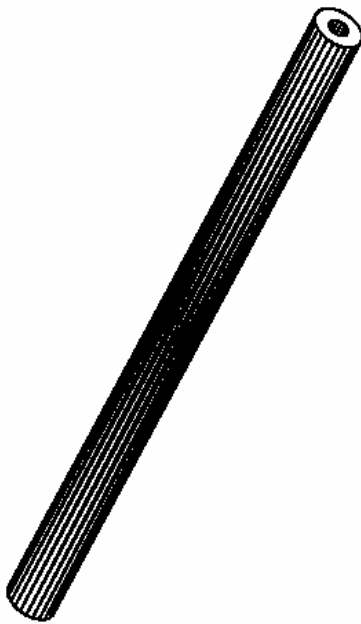




REVISIONS		ZONE		REV		DESCRIPTION		DATE		APPROVED	
<div style="display: flex; justify-content: space-between;"> <div style="width: 45%;"> </div> <div style="width: 45%;"> </div> </div>											

APPLICATION		DO NOT SCALE DRAWING		UNLESS OTHERWISE SPECIFIED DIMENSIONS ARE IN INCHES		TOLERANCES ARE:		XREF = 11.0 XREF = N/A XREF = 4.000 ANGLES = N/A		MATERIAL AND TREATMENT	
THIS ITEM IS USED ON SUBASSEMBLIES		DRAWING NO.		PER ASSY		TOTAL		XREF = 11.0 XREF = N/A XREF = 4.000 ANGLES = N/A		12x8x1/8 1018 HR Plate	
WSR9001		2		1		2					
TO MAKE FINAL ASSEMBLY TOTAL REQ'D		2									


PARTS LIST		DESCRIPTION		SPECIFICATION		QTY		REV	
UNIVERSITY of NEW HAMPSHIRE		JERE A CHASE OCEAN ENGINEERING LABORATORY							
TITLE		Anchor Plate		SIZE		FSCM NO.		DNG NO.	
A		A		WSR0001				REV	
SCALE Not to Scale		DRAWN BY: GMC		SHEET		1 OF 1			

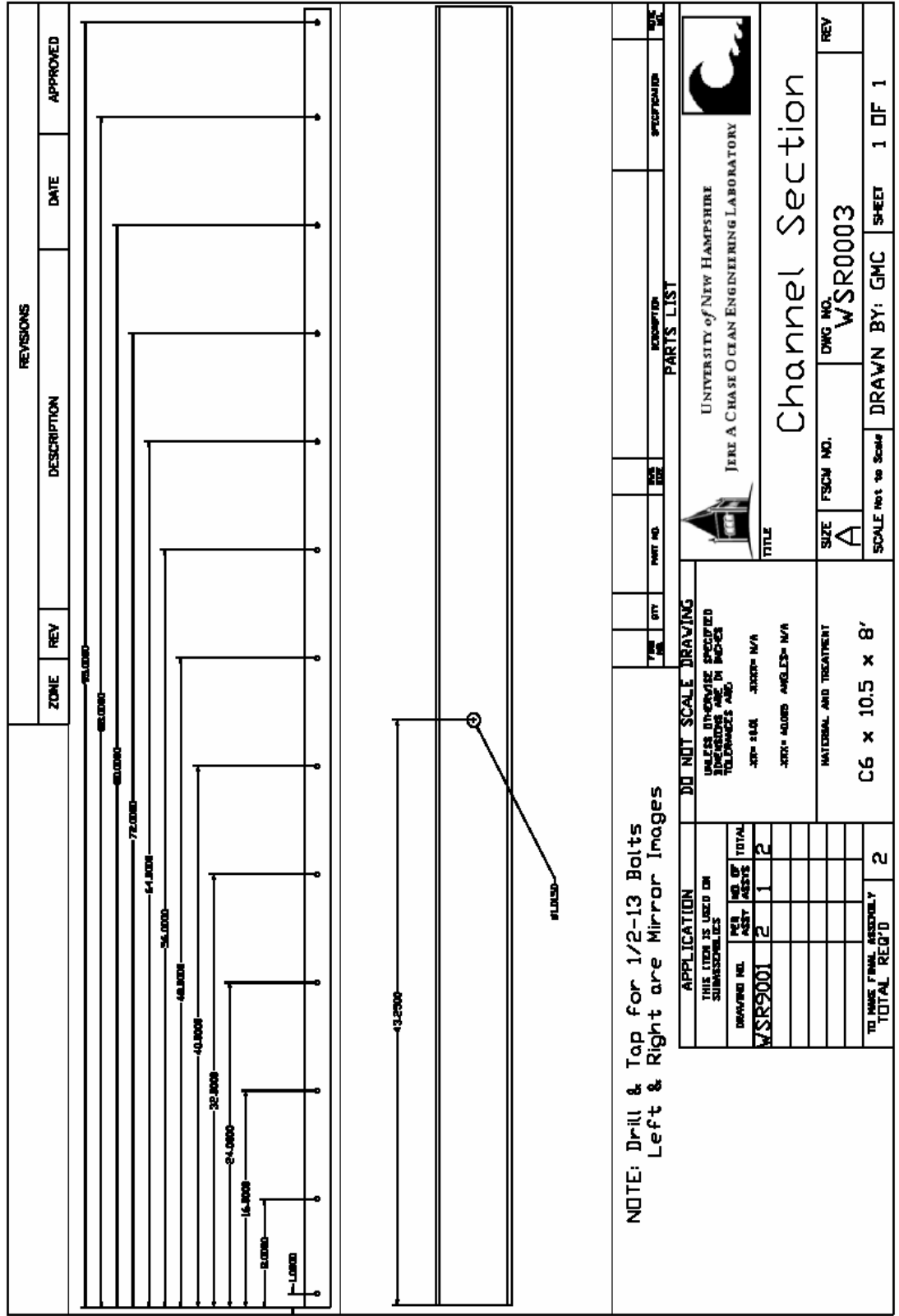
		REVISIONS			
		ZONE	REV	DESCRIPTION	DATE
					
<p><b>NOTE:</b> Drill &amp; Tap 1/4-20 x 3/8 DP Both Ends</p>					

APPLICATION		DO NOT SCALE DRAWING		UNLESS OTHERWISE SPECIFIED DIMENSIONS ARE IN INCHES TOLERANCES ARE:	
THIS ITEM IS USED ON SUBASSEMBLIES	PER NO. OF ASSEMBLY	PER NO. OF ASSEMBLY	PER NO. OF ASSEMBLY	PER NO. OF ASSEMBLY	PER NO. OF ASSEMBLY
WSR9001	4	1	4		
TOTAL		4			
TO MAKE FINAL ASSEMBLY TOTAL REQ'D		4			

PARTS LIST		UNIVERSITY of NEW HAMPSHIRE		JERE A CHASE OCEAN ENGINEERING LABORATORY	
ITEM NO.	QTY	PART NO.	DESCRIPTION	SPECIFICATION	REV
					
<b>Bearing Axle</b>					
SIZE		FSCM NO.		DWG NO.	
A				WSR0002	
SCALE Not to Scale		DRAWN BY: GMC		SHEET 1 OF 1	



REVISIONS				
ZONE	REV	DESCRIPTION	DATE	APPROVED

0.25 Thru - Two Places

APPLICATION		DO NOT SCALE		DRAWING	
THIS ITEM IS USED IN SUBASSEMBLIES		UNLESS OTHERWISE SPECIFIED DIMENSIONS ARE IN INCHES TOLERANCES ARE:			
DRAWING NO.	PER ASSY	NO OF ASSYS	TOTAL		
WSR9001	1	1	1		
TO MAKE FINAL ASSEMBLY TOTAL REQ'D			1		

PARTS LIST					
ITEM NO.	QTY	PART NO.	DESCRIPTION	SPECIFICATION	MATERIAL

 UNIVERSITY of NEW HAMPSHIRE JERE A CHASE OCEAN ENGINEERING LABORATORY		 UNIVERSITY of NEW HAMPSHIRE JERE A CHASE OCEAN ENGINEERING LABORATORY	
TITLE <h2 style="margin: 0;">Cylinder Pin</h2>		DWG NO. <h2 style="margin: 0;">WSR0004</h2>	
SIZE FSCM NO. <h2 style="margin: 0;">A</h2>		REV 	
SCALE Not to Scale DRAWN BY: GMC		SHEET 1 OF 1	



REVISIONS				
ZONE	REV	DESCRIPTION	DATE	APPROVED

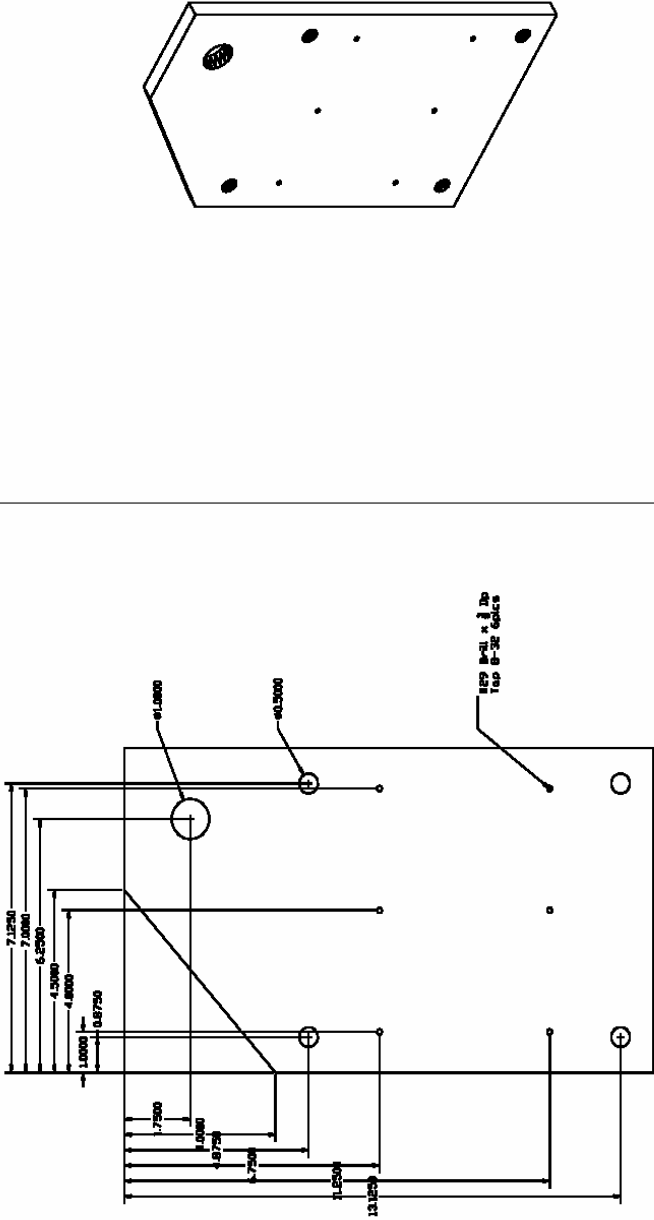
ITEM NO.	QTY	PART NO.	DATE	DESCRIPTION	SPECIFICATION	DATE
PARTS LIST						

APPLICATION		DO NOT SCALE DRAWING	
THIS ITEM IS USED ON SUBASSEMBLIES		UNLESS OTHERWISE SPECIFIED DIMENSIONS ARE IN INCHES TOLERANCES ARE:	
DRAWING NO.	PER ASSY	NO OF TOTAL	
WSR9001	2	1	2
TO MAKE FINAL ASSEMBLY TOTAL REQ'D		2	

UNIVERSITY of NEW HAMPSHIRE JERE A CHASE OCEAN ENGINEERING LABORATORY	
TITLE: Side Bearing Plate	
SIZE: A	FSCM NO. WSR0005
MATERIAL AND TREATMENT: 6½x8x½ MDS Filled Nylon	
SCALE: Not to Scale	DRAWN BY: GMC
SHEET 1 OF 1	

		REVISIONS			
ZONE	REV	DESCRIPTION	DATE	APPROVED	
					
Note: Two Plates are Mirror Images					
APPLICATION		DO NOT SCALE DRAWING		PARTS LIST	
THIS ITEM IS USED ON SUBASSEMBLIES		UNLESS OTHERWISE SPECIFIED DIMENSIONS ARE IN INCHES TOLERANCES ARE:		UNLESS OTHERWISE SPECIFIED	
DRAWING NO.	REV	QTY	SIZE	DESCRIPTION	DATE
WSR9001	2	1	2		
TO MAKE FINAL ASSEMBLY TOTAL REQ'D		2			
MATERIAL AND TREATMENT		14x8x1/8 1018 HR Plate		TITLE	
				CROSS HEAD PLATE	
				UNIVERSITY OF NEW HAMPSHIRE JERE A CHASE OCEAN ENGINEERING LABORATORY	
				DRAWN BY: GMC	
				SHEET 1 OF 1	



		REVISIONS																																
		ZONE	REV	DATE																														
<p><b>NOTE: Center Holes</b></p>		<table border="1" style="width: 100%; border-collapse: collapse;"> <thead> <tr> <th colspan="2">APPLICATION</th> <th colspan="2">DO NOT SCALE</th> <th colspan="2">DRAWING</th> </tr> <tr> <th colspan="2">THIS ITEM IS USED IN SUBASSEMBLIES</th> <th colspan="2">UNLESS OTHERWISE SPECIFIED DIMENSIONS ARE IN INCHES</th> <th colspan="2">TOLERANCES ARE:</th> </tr> <tr> <th>DRAWING NO.</th> <th>PER ASSY</th> <th>NO OF ASSYS</th> <th>TOTAL</th> <th>XX= ±0.01</th> <th>XXX= N/A</th> </tr> </thead> <tbody> <tr> <td>WSR9001</td> <td>2</td> <td>1</td> <td>2</td> <td></td> <td></td> </tr> <tr> <td colspan="2">TO MAKE FINAL ASSEMBLY TOTAL REQ'D</td> <td>2</td> <td></td> <td></td> <td></td> </tr> </tbody> </table>			APPLICATION		DO NOT SCALE		DRAWING		THIS ITEM IS USED IN SUBASSEMBLIES		UNLESS OTHERWISE SPECIFIED DIMENSIONS ARE IN INCHES		TOLERANCES ARE:		DRAWING NO.	PER ASSY	NO OF ASSYS	TOTAL	XX= ±0.01	XXX= N/A	WSR9001	2	1	2			TO MAKE FINAL ASSEMBLY TOTAL REQ'D		2			
APPLICATION		DO NOT SCALE		DRAWING																														
THIS ITEM IS USED IN SUBASSEMBLIES		UNLESS OTHERWISE SPECIFIED DIMENSIONS ARE IN INCHES		TOLERANCES ARE:																														
DRAWING NO.	PER ASSY	NO OF ASSYS	TOTAL	XX= ±0.01	XXX= N/A																													
WSR9001	2	1	2																															
TO MAKE FINAL ASSEMBLY TOTAL REQ'D		2																																
		<table border="1" style="width: 100%; border-collapse: collapse;"> <thead> <tr> <th>FORM NO.</th> <th>QTY</th> <th>PART NO.</th> <th>SIZE</th> <th>DESCRIPTION</th> <th>SPECIFICATION</th> <th>DATE</th> </tr> </thead> <tbody> <tr> <td colspan="7" style="text-align: center;">PARTS LIST</td> </tr> </tbody> </table>			FORM NO.	QTY	PART NO.	SIZE	DESCRIPTION	SPECIFICATION	DATE	PARTS LIST																						
FORM NO.	QTY	PART NO.	SIZE	DESCRIPTION	SPECIFICATION	DATE																												
PARTS LIST																																		
		<div style="display: flex; justify-content: space-between; align-items: center;"> <div style="text-align: center;">               UNIVERSITY of NEW HAMPSHIRE              JERE A CHASE OCEAN ENGINEERING LABORATORY           </div> <div style="text-align: center;">   <b>Thrust Plate Bearing</b>              SIZE: FSCM NO. A              DWG NO. WSR0008              SCALE: Not to Scale              DRAWN BY: GMC              SHEET 1 OF 1           </div> </div>																																

REVISIONS				
ZONE	REV	DESCRIPTION	DATE	APPROVED

PARTS LIST					
ITEM NO.	QTY	PART NO.	DESCRIPTION	SPECIFICATION	MATERIAL
<div> <div>           UNIVERSITY OF NEW HAMPSHIRE            JERE A CHASE OCEAN ENGINEERING LABORATORY         </div> </div>					
<div> <div> <div>           TITLE  <b>Thrust Plate</b> </div> </div> <div>           SIZE  <b>A</b> </div> <div>           FSCM NO.  <b>WSR0009</b> </div> <div>           DWG NO.  <b>WSR0009</b> </div> </div>					
SCALE: Not to Scale DRAWN BY: GMC SHEET 1 OF 1					

APPLICATION		DO NOT SCALE		DRAWING	
THIS ITEM IS USED ON SUBASSEMBLIES		UNLESS OTHERWISE SPECIFIED DIMENSIONS ARE IN INCHES		TOLERANCES ARE:	
DRAWING NO.	PER ASSY	NO OF TOTAL			
WSR9001	1	1	.XX = ±0.01    .XXX = N/A .XXX = ±0.005    ANGLES = N/A		
MATERIAL AND TREATMENT		10x8x1 1018 HR Plate			
TO MAKE FINAL ASSEMBLY TOTAL REQ'D		1			

NOTE: Both Slots are 0.125 DP  
Radius all internal corners





REVISIONS				
ZONE	REV	DESCRIPTION	DATE	APPROVED

APPLICATION		DO NOT SCALE		DRAWING	
THIS ITEM IS USED IN SUBASSEMBLIES		UNLESS OTHERWISE SPECIFIED DIMENSIONS ARE IN INCHES TOLERANCES ARE:			
DRAWING NO.	PER ASSY	NO OF ASSYS	TOTAL		
WSR9001	2	1	2		
TO MAKE FINAL ASSEMBLY TOTAL REQ'D			2		

PARTS LIST					
ITEM NO.	QTY	PART NO.	DESCRIPTION	SPECIFICATION	MATERIAL
<div style="display: flex; justify-content: space-between; align-items: center;"> <div> <p>UNIVERSITY of NEW HAMPSHIRE JERE A CHASE OCEAN ENGINEERING LABORATORY</p> </div> <div> <p>Leg Plate</p> </div> </div>					
TITLE		SIZE	FSCM NO.	DWG NO.	REV
		A		WSR0012	
MATERIAL AND TREATMENT					
C6 x 10.5 x 12"					
SCALE Not to Scale			DRAWN BY: GMC		
			SHEET 1 OF 1		



REVISIONS				
ZONE	REV	DESCRIPTION	DATE	APPROVED

TYPE	QTY	PART NO.	SIZE	DESCRIPTION	SPECIFICATION	DATE	REV
PARTS LIST							

APPLICATION THIS ITEM IS USED ON SUBASSEMBLIES		DO NOT SCALE DRAWING UNLESS OTHERWISE SPECIFIED DIMENSIONS ARE IN INCHES TOLERANCES ARE: .XX = ±0.01    .XXX = M/A .XXX = ±0.005    ANGLES = M/A	
DRAWING NO.	WSR9001	PER ASSY	1
		OF ASSYS	1
		TOTAL	1
TO MAKE FINAL ASSEMBLY		TOTAL REQ'D	
		1	

UNIVERSITY of NEW HAMPSHIRE JERE A CHASE OCEAN ENGINEERING LABORATORY			
TITLE Load Cell Plate			
SIZE	FSCM NO.	DWG NO.	REV
A		WSR0013	
SCALE Not to Scale		DRAWN BY: GMC    SHEET 1 OF 1	

## **APPENDIX C:**

### **MatLab Code**

```

%%%%%%%%%%%%%%%%%%%%%%%%%%%%%%%%%%%%%%%%%%%%%%%%%%%%%%%%%%%%%%%%%%%%%%%%
%WSR_main processes the raw data from rope breaking experiments one at a time or in a bundle.
% WSR_main takes in four arguments
% (1) The first is the Synchro file containing the LANC info and Load Cell data
% (2) The right or left camera image text file as output by Ropemovie program and automatically loads both the left and right
% (3) The last input file is the excel file containing the sample S/N with the starting frame for both the left and right video captures
% WSR_main outputs a variety of graphs including the raw engineering stress-strain, elongation and delta elongation vs sample #, stress and delta stress verses sample #, and various curve fits for the data.
% WSR_main calls the following functions:
% (1) Datamatch.m
% (2) LANCadj.m
% (3) FitIndicies.m
% (4) WSRCurveFit.m
% (5) WSRStats.m
% (6) PlotStruct.m
% By Glenn McGillicuddy
% Date: 8/25/05
%%%%%%%%%%%%%%%%%%%%%%%%%%%%%%%%%%%%%%%%%%%%%%%%%%%%%%%%%%%%%%%%%%%%%%%%

```

```

close all;
clear all;
clc;

```

```

numfiles = 1;          %Number of files to process(files must be listed in the reference file)
limit = 2;             %Number of Standard deviations to include in the setting of the fit limits
ITp = 200*0.375^2;     %Initial Tension based on diameter to calculate the starting point of all fits
%strand_dia = 0.165;   %Strand diameter of the rope under analysis

```

```

% Prompt the user for the starting files and directories

```

```

[synfile,synpath] = uigetfile('C:\MATLAB6p5\work\WSR\Data\*.syn',...
    'Select the first SYNCRO file to be processed');
[imagefile,imagepath] = uigetfile('C:\MATLAB6p5\work\WSR\Data\*.txt',...
    'Select the associated IMAGE text file (Right or Left)');
[reffile,refpath] = uigetfile('C:\MATLAB6p5\work\WSR\Data\*.txt',...
    'Select the TEXT file that contains the frame references');
check = strcmp(synfile(1,end-8:end-4),imagefile(1,1:5));
if check == 0
    error('Synchro file does not match specified Image text file')
end
clear check;

```

```

% Load the Text reference file for the starting points of the Video captures.

```

```

[sample, LcamM, LcamS, LcamF, RcamM, RcamS, RcamF] = textread(strcat(refpath,reffile),...
    '%5c %*2c %2c %2c %2c %*2c %2c %2c %2c %*6c');
Lcam_cap = strcat('0:', LcamM, ':', LcamS, ':', LcamF);
Rcam_cap = strcat('0:', RcamM, ':', RcamS, ':', RcamF);
clear LcamM LcamS LcamF RcamM RcamS RcamF;

```

```

% Load the Synchro file and the Ropemovie text files (for loop iterates for the specified number of

```

```

%      files)

for m = 1:numfiles
    if m == 1
        [Lcam, Rcam, Data_raw(:,1)] = textread(strcat(synpath,synfile),...
            '%*26c %10c %*5c %10c %*10c %f %*26c');
        [Lcam_image(:,1), Lcam_image(:,2), Lcam_image(:,3), Lcam_image(:,4)] =...
            textread(strcat(imagepath,imagefile(1:end-5),'L.txt'), '%u %f %f %f');
        [Rcam_image(:,1), Rcam_image(:,2), Rcam_image(:,3), Rcam_image(:,4)] =...
            textread(strcat(imagepath,imagefile(1:end-5),'R.txt'), '%u %f %f %f');
    else
        file_index = strmatch(synfile(1,end-8:end-4),sample, 'exact') + 1;
        synfile = strcat(synfile(1,1:end-9),sample(file_index,:),'syn');
        imagefile = strcat(sample(file_index,:), 'L.txt');
        check = strcmp(synfile(1,end-8:end-4),imagefile(1,1:5));
        if check == 0
            error('Syncro file does not match specified Image text file')
        end
        clear check file_index;
        [Lcam, Rcam, Data_raw(:,1)] = textread(strcat(synpath,synfile),...
            '%*26c %10c %*5c %10c %*10c %f %*26c');
        [Lcam_image(:,1), Lcam_image(:,2), Lcam_image(:,3), Lcam_image(:,4)] =...
            textread(strcat(imagepath,imagefile(1:end-5),'L.txt'), '%u %f %f %f');
        [Rcam_image(:,1), Rcam_image(:,2), Rcam_image(:,3), Rcam_image(:,4)] =...
            textread(strcat(imagepath,imagefile(1:end-5),'R.txt'), '%u %f %f %f');
    end

    % Down sample the data such that there is only one data point per LANC change

    rec_index = max(strmatch(Lcam(1,:),Lcam)) + 1;
    ovr_samp = strncmp(Lcam(rec_index,:), Lcam(rec_index+1,:),10);
    if ovr_samp == 0
        LC_data = Data_raw;
        cam_LANC(:,1:10) = Lcam;
        cam_LANC(:,12:21) = Rcam;
    else
        [row col] = size(Lcam);
        datapts = fix(row/9);
        index = 1;
        for n = 1:datapts
            LC_data(index,:) = Data_raw((n*9),:);
            cam_LANC(index,1:10) = Lcam((n*9),:);
            cam_LANC(index,12:21) = Rcam((n*9),:);
            index = index + 1;
        end
    end
end

clear Data_raw Lcam Rcam row col datapts index n rec_index ovr_samp;

% Match the image data up with the load cell data using the LANC info and the reference text file.

Lcam_strt = Lcam_cap(strmatch(synfile(1,end-8:end-4),sample, 'exact'),:);
Lcam_strt = LANCadj(Lcam_strt,Lcam_image(1,1));
Rcam_strt = Rcam_cap(strmatch(synfile(1,end-8:end-4),sample, 'exact'),:);
Rcam_strt = LANCadj(Rcam_strt,Rcam_image(1,1));

```

```

Aligned_data = Datamatch(Lcam_strt,Rcam_strt,cam_LANC,LC_data,Lcam_image, Rcam_image);
clear Lcam_strt Rcam_strt ans cam_LANC;

% Now apply corrections to the Load cell data

Corrected_data(:,1) = (Aligned_data(:,1)+0.0003)/0.0033;
test_stats = max(Corrected_data(:,1));
test_stats(1,2) = mean((LC_data(end-10:end,1)+0.0003)/0.0033);

% Convert transition point from a pixel to an actual distance using the ruler of the image file.

Aligned_data(:,4:5) = 0;
for n=1:length(Aligned_data(2:end,1))
    Aligned_data(n+1,4) = (Aligned_data(n,2) - Aligned_data(n+1,2)) + Aligned_data(n,4);
    Aligned_data(n+1,5) = (Aligned_data(n,3) - Aligned_data(n+1,3)) + Aligned_data(n,5);
end

clear n;
ruler = 2/2.54; %Stripes on ruler are 2cm wide convert to inches
test_stats(2,1) = ruler/(mean(Lcam_image(:,4))); %Determine the inches per pixels
test_stats(2,2) = std(Lcam_image(:,4));
Corrected_data(:,2) = Aligned_data(:,4) * test_stats(2,1);

test_stats(3,1) = ruler/(mean(Rcam_image(:,4)));
test_stats(3,2) = std(Rcam_image(:,4));
Corrected_data(:,3) = Aligned_data(:,5) * test_stats(3,1);

% Compute the Engineering stress-strain for the data points and plot the unfitted data

Lo = 12; %Original gauge length
Ao = .11044; %3*((pi*(strand_dia^2))/4); %Cross-sectional area of WSR
s = Corrected_data(:,1) / Ao;
e = (Corrected_data(:,2)-Corrected_data(:,3))/Lo;

figure(1)
title('Engineering Stress-Strain');
xlabel('Strain ( in / in )');
ylabel('Stress ( lbs / in^2 )');
grid on
hold on
plot(e,s,'bo','Tag',synfile(1,end-8:end-4));

% Call function to determine indicies for curve fitting

[DervData, indicies] = FitIndicies(limit,ITp,synfile,Ao,e,s);

% Fit a curve to the stress-strain data points

[s_fit, e_fit] = WSRCurveFit(e,s,DervData,indicies,synfile);

% Store the data

processed_data(m) = struct('Experiment', synfile(1,end-8:end-4), 'Stress', s, 'Derivative_Stress',...
    DervData, 'Strain', e, 'Test_Stats', test_stats, 's_Curve_Fits', s_fit, 'e_Curve_Fits', e_fit,...
    'Curve_Indicies', indicies);
clear Aligned_data Corrected_data DervData LC_data Lcam_image Lo Rcam_image e_fit...

```

```

        indices ruler s test_stats;
    end

clear Lcam_cap Rcam_cap imagefile imagepath m n numfiles reffile reffpath sample synfile synpath;

%Determine the stats for the curve fits

[s_avg_val, s_avg_val_std, s_avg_fit, s_avg_fit_std] = WSRStats(processed_data, 's');
[e_avg_val, e_avg_val_std, e_avg_fit, e_avg_fit_std] = WSRStats(processed_data, 'e');

% Fit the average elongation data

s = [0.1,0.5,0.9]*s_avg_val(4,3);
for n = 1:length(processed_data)
    e(n,1) = (polyval(processed_data(n).e_Curve_Fits(1,:),s(1)));
    e(n,2) = processed_data(n).e_Curve_Fits(2,2)+processed_data(n).e_Curve_Fits(2,3)*s(2);
    e(n,3) = polyval(processed_data(n).e_Curve_Fits(3,:),s(3));
end
e_mean = mean(e)*12;
e_std = std(e*12);

% Call a plotting function to produce the plots

PlotStruct(s_avg_fit,s_avg_fit_std,s_avg_val,s_avg_val_std,processed_data);

strcat('Average Mechanical Settling Point is: ', num2str(s_avg_val(2,3)*Ao), ' lbs')
strcat('Average Yield Point is: ', num2str(s_avg_val(3,3)*Ao), ' lbs')
strcat('Average Ultimate Tensile Point is:', num2str(s_avg_val(4,3)*Ao), ' lbs')
strcat('Average Young's Modulus is: ', num2str(s_avg_fit(2,3)), ' psi')

```

```

function [Aligned_data] = Datamatch(Lcam_strt,Rcam_strt,cam_LANC,LC_data,Lcam_image,
                                   Rcam_image)
%%%%%%%%%%%%%%%%%%%%%%%%%%%%%%%%%%%%%%%%%%%%%%%%%%%%%%%%%%%%%%%%%%%%%%%%%%%%%%
%Datamatch complies the Load cell and the Left and Right Transition pixels into one array
% The first two input arguments are character strings that represent the Left and Right
%   starting LANCs from the image processing
% The third input argument is the Left and Right LANC strings from the SYNCRO file
% The fourth input argument is a double array which represents the load cell data from
%   the SYNCRO file
% The fifth and sixth input parameters are double arrays containing the results of the
%   image processing (Relative Frame#, Transition Pixel, Robustness, and Ruler Pixel)
% The function outputs a double array containing the Load cell data and the transition
%   pixels of the Left and Right cameras
%
% By Glenn McGillicuddy
% Date: 8/20/05
%%%%%%%%%%%%%%%%%%%%%%%%%%%%%%%%%%%%%%%%%%%%%%%%%%%%%%%%%%%%%%%%%%%%%%%%%%%%%%

% Matching the Left camera LANC from SYNCRO data and the image processing starting point and
%   returning the index

Lcam_index = strmatch(Lcam_strt,cam_LANC(:,1:10), 'exact');
tf = isempty(Lcam_index);
if tf == 1
    Lcam_strt = LANCadj(Lcam_strt,1);
    Lcam_index = strmatch(Lcam_strt,cam_LANC(:,1:10), 'exact');
    tf = isempty(Lcam_index);
    if tf == 1
        Aligned_data = 0;
        error('Can not match up LANC data and Left camera frame starting point!!')
    end
    clear tf;
    Lcam_image(1,:) = [];
end
clear tf;

% Matching the Right camera LANC from SYNCRO data and the image processing starting point and
%   returning the index

Rcam_index = strmatch(Rcam_strt,cam_LANC(:,12:21), 'exact');
tf = isempty(Rcam_index);
if tf == 1
    Rcam_strt = LANCadj(Rcam_strt,1);
    Rcam_index = strmatch(Rcam_strt,cam_LANC(:,12:21), 'exact');
    tf = isempty(Rcam_index);
    if tf == 1
        Aligned_data = 0;
        error('Can not match up LANC data and Right camera frame starting point!!')
    end
    clear tf;
    Rcam_image(1,:) = [];
end
clear tf;

% Truncate the start of the image data file that starts first such that the Left and Right

```

```

%      cameras start at the same point in the SYNCRO file

if Lcam_index > Rcam_index
    abs_index = Lcam_index;
    Rcam_image(1:((Lcam_index - Rcam_index)*2),:) = [];
elseif Rcam_index > Lcam_index
    abs_index = Rcam_index;
    Lcam_image(1:((Rcam_index - Lcam_index)*2),:) = [];
else
    abs_index = Lcam_index;
end

% Combining the Load Cell data and the Left and Right camera transition tracking data
%      Remembering that the image data is at 30Hz and the Syncro data is at 15Hz so, you
%      must down sample the image data

Aligned_data = LC_data(abs_index:end,1);
if length(Lcam_image) >= length(Rcam_image)
    i = fix(length(Rcam_image)/2);
else
    i = fix(length(Lcam_image)/2);
end

Aligned_data(1,2) = Lcam_image(1,2);
Aligned_data(1,3) = Rcam_image(1,2);
for j = 1:i-1
    Aligned_data(j+1,2) = Lcam_image(((j*2)+1),2);
    Aligned_data(j+1,3) = Rcam_image(((j*2)+1),2);
end

% Now remove all data points without any transition data

if length(Aligned_data) > i
    Aligned_data(i+1:end,:) = [];
end

clear Lcam_index Rcam_index Lcam_strt Rcam_strt abs_index i j;

```



```

function [cam_index] = LANCadj(cam_index,offset)
%%%%%%%%%%%%%%%%%%%%%%%%%%%%%%%%%%%%%%%%%%%%%%%%%%%%%%%%%%%%%%%%%%%%%%%%
%LANCadj changes the LANC string
% LANCadj takes in two arguments
% The first argument is the character array containing the LANC string to be adjusted
% The last argument is a 1x1 double array representing the number of frames to
% offset the LANC string by
% This function outputs a character array that represents the H:MM:SS:FF of the adjusted
% LANC string
%
% By Glenn McGillicuddy
% Date: 8/20/05
%%%%%%%%%%%%%%%%%%%%%%%%%%%%%%%%%%%%%%%%%%%%%%%%%%%%%%%%%%%%%%%%%%%%%%%%

```

```

% Convert the strings to numbers and add the offset to the frame number

```

```

camM = str2num(cam_index(1,3:4));
camS = str2num(cam_index(1,6:7));
camF = str2num(cam_index(1,9:10)) + offset;

```

```

% Check to ensure that values are in the correct quantities

```

```

if camF >= 30
    camS = camS + fix(camF/30);
    if camS >= 60
        camM = camM + fix(camS/60);
        camS = camS - (fix(camS/60)*60);
    end
    camF = camF - (fix(camF/30)*30);
end

```

```

% Convert the adjusted numbers back to a character string

```

```

if camF <= 9
    camF = strcat('0', num2str(camF));
else
    camF = num2str(camF);
end

```

```

if camS <= 9
    camS = strcat('0', num2str(camS));
else
    camS = num2str(camS);
end

```

```

if camM <= 9
    camM = strcat('0', num2str(camM));
else
    camM = num2str(camM);
end

```

```

% Form a character string in the H:MM:SS:FF format

```

```

cam_index = strcat('0:', camM, ':', camS, ':', camF);
clear camM camS camF;

```

```

function [DervData, indices] = FitIndices(limit,ITp,synfile,Ao,e,s)
%%%%%%%%%%%%%%%%%%%%%%%%%%%%%%%%%%%%%%%%%%%%%%%%%%%%%%%%%%%%%%%%%%%%%%%%%%
%FitIndices determines the linear indices of the mechanical and strain hardening regions
% The first input argument is the number of STD to define the allowable data spread when
% determining the indices
% The second input argument is the calculated initial tension based on the CI guidelines
% The third input argument is the SYNCRO file name
% The fourth input parameter is the cross sectional area of the rope
% The fifth and sixth input arguments are the corrected strain and stress data
% The function outputs a double array containing the derivative of stress data and a
% matrix containing the indices for the start, mechanical, yield, and UTS along
% with the stress and strain values at these indices
%
% By Glenn McGillicuddy
% Date: 09/01/05
%%%%%%%%%%%%%%%%%%%%%%%%%%%%%%%%%%%%%%%%%%%%%%%%%%%%%%%%%%%%%%%%%%%%%%%%%%

% Find the starting point in the stress data that exceeds the Initial Tension criterion

strt = find(s >= ITp/Ao);

% Determine the first derivative of stress and plot

for n = 1:length(s)-1
    ds(n,1) = s(n+1,1)-s(n,1);
    if ds(n,1) < 0
        ds(n,1) = 0;
    end
end

% Detect and note any data spikes

dsmean = mean(ds(20:60,1));
k = 1;
spike_index = [];
for n = 10:length(ds)-10
    if ds(n,1) > dsmean+150 || ds(n,1) < dsmean-150
        spike_index(k,1) = n;
        k = k + 1;
    end
end

% Remove any data spikes by placing the values at the mean value

clear k n;
if isempty(spike_index)
    'No data spikes within set limits'
else
    for n = 1:length(spike_index)
        ds(spike_index(n,1),1) = dsmean;
    end
end

% Run a boxcar filter forwards and backwards to smooth the data and plot

windowSize = 5;

```

```

dsfilt = filtfilt(ones(1,windowSize)/windowSize,1,ds);

figure(2)
title('First Derivative of Stress');
xlabel('Linear Index Number');
ylabel('d\sigma');
grid on
hold on
plot(ds,'bo','Tag',synfile(1,end-8:end-4))
plot(dsfilt,'r*--','Tag',strcat(synfile(1,end-8:end-4),' Filtered'))

% Determine the second derivative of stress, filter, and plot

for r = 1:length(dsfilt)-1
    d2s(r,1) = dsfilt(r+1,1) - dsfilt(r,1);
end

d2sfilt = filtfilt(ones(1,windowSize)/windowSize,1,d2s);
d2smean = mean(d2sfilt(20:60,1));
d2sstd = std(d2sfilt(20:60,1));

figure(3)
title('Second Derivative of Stress');
xlabel('Linear Index Number');
ylabel('d^2\sigma');
grid on
hold on
plot(d2s,'bo','Tag',synfile(1,end-8:end-4))
plot(d2sfilt,'r*--','Tag',strcat(synfile(1,end-8:end-4),' Filtered'))

% Working from index of 20 back to one find the point at which the 2nd derivative
% of stress is outside of plus or minus one two standard derivations of the mean

i = 20;
k = 0;
while k == 0 && i > 0
    if d2sfilt(i-1,1) <= d2smean+(limit*d2sstd) && d2sfilt(i-1,1) >= d2smean-(limit*d2sstd)
        i = i-1;
    else
        k = 1;
        i_mech = i;
    end
    if i == 1
        'WARNING: No Mechanical limit Found'
        i_mech = 20;
    end
end

% Working from index of 60 forward to end of data find the point at which the 2nd
% derivative of stress is outside of plus or minus one two standard derivations of the mean

i = 60;
k = 0;
while k == 0 && i < length(d2sfilt)
    if d2sfilt(i+1,1) <= d2smean+(limit*d2sstd) && d2sfilt(i+1,1) >= d2smean-(limit*d2sstd)
        i = i+1;
    end
end

```

```

else
    k = 1;
    i_yield = i;
end
if i == length(d2sfilt)-1
    'WARNING: No Yield Point Found'
    i_yield = 75;
end
end

% Find the ultimate breaking strength and the associated index

[UTS i_UTS] = max(s);

% Plot the indicies

figure(3)
plot(i_mech,[-20:0.1:20], 'm')
plot(i_yield,[-20:0.1:20], 'm')
figure(2)
plot(i_mech,[150:0.1:250], 'm')
plot(i_yield,[150:0.1:250], 'm')

% Format the data to be returned to the calling program

indicies(1,1) = strt(2);
indicies(1,2) = e(strt(2));
indicies(1,3) = s(strt(2));

indicies(2,1) = i_mech;
indicies(2,2) = e(i_mech);
indicies(2,3) = s(i_mech);

indicies(3,1) = i_yield;
indicies(3,2) = e(i_yield);
indicies(3,3) = s(i_yield);

indicies(4,1) = i_UTS;
indicies(4,2) = e(i_UTS);
indicies(4,3) = s(i_UTS);

DervData(:,1) = dsfilt;
DervData(2:end,2) = d2sfilt;

clear UTS ans d2s d2filt d2smean d2sstdd ds dsfilt dsmean i i_UTS i_mech i_yield k...
    limit r spike_index strt windowSize;

```

```

function [s_fit, e_fit] = WSRCurveFit(e,s,DervData,indicies,synfile)
%%%%%%%%%%%%%%%%%%%%%%%%%%%%%%%%%%%%%%%%%%%%%%%%%%%%%%%%%%%%%%%%%%%%%%%%%%%%%%
%WSRCurveFit determines calculates a number of piecewise fit for each of the data plots %
% The first and second input arguments are the corrected strain and stress data %
% The third input argument is derivative data from FitIndicies.m %
% The fourth input parameter is the matrix of indices from FitIndicies.m %
% The fifth input argument is the name of the file under investigation %
% The function outputs two double array containing the associated fits for the stress and %
% strain data for the engineering stress-strain, 1st derivative of stress and the %
% 2nd derivative of stress %
% %
% By Glenn McGillicuddy %
% Date: 09/01/05 %
%%%%%%%%%%%%%%%%%%%%%%%%%%%%%%%%%%%%%%%%%%%%%%%%%%%%%%%%%%%%%%%%%%%%%%%%%%%%%%

% Break out the indices and data

strt = indicies(1,1);
i_mech = indicies(2,1);
i_yield = indicies(3,1);
i_UTS = indicies(4,1);

dsfilt = DervData(:,1);
d2sfilt = DervData(2:end,2);

% Perform a linear fit to the second derivative between the extracted mech and yield points

d2sfit = robustfit([i_mech:1:i_yield]',d2sfilt(i_mech:i_yield,1));

% Now find the approach slope, max value, and decending slope of the first derivative

k = 0;
n = 20;
while k == 0 && n < i_yield
    if d2sfilt(n,1) + d2sfilt(n+1,1) <= 0
        zerocross = n;
        k = 1;
    end
    n = n + 1;
end

dsappfit = robustfit([i_mech:1:zerocross]', dsfilt(i_mech:zerocross,1));
dsdecfit = robustfit([zerocross:1:i_yield]', dsfilt(zerocross:i_yield,1),1);
dsinter = (dsappfit(1)-dsdecfit(1))/(dsdecfit(2)-dsappfit(2));

% Now fit the raw Stress-Strain data using the mech and yield indices

mechreg_s = polyfit(e(strt:20),s(strt:20),2);
mechreg_e = polyfit(s(strt:20),e(strt:20),2);
elasreg_s = robustfit(e(i_mech:i_yield),s(i_mech:i_yield));
elasreg_e = robustfit(s(i_mech:i_yield),e(i_mech:i_yield));
strnhard_s = polyfit(e(i_yield:i_UTS),s(i_yield:i_UTS),2);
strnhard_e = polyfit(s(i_yield:i_UTS),e(i_yield:i_UTS),2);

% Plot these fits on the associated figures

```

```

figure(1)
f1 = polyval(mechreg,e(1:i_mech));
f2 = elasreg(1)+elasreg(2)*e(i_mech:i_yield);
f3 = polyval(strnhard,e(i_yield:i_UTS));
plot(e(1:i_mech),f1,'g','Tag',strcat(synfile(1,end-8:end-4),' Mechanical'))
plot(e(i_mech:i_yield),f2,'r','Tag',strcat(synfile(1,end-8:end-4),' Elastic'))
plot(e(i_yield:i_UTS),f3,'c','Tag',strcat(synfile(1,end-8:end-4),' Strain Hardened'))

figure(2)
plot([1:1:zerocross+10]',dsappfit(1)+dsappfit(2)*[1:1:zerocross+10]','k-','Tag',...
    strcat(synfile(1,end-8:end-4),' Approach'))
plot([zerocross-10:1:length(dsfilt)]',dsdecfit(1)+dsdecfit(2)*[zerocross-10:1:length(dsfilt)]',...
    'k-','Tag',strcat(synfile(1,end-8:end-4),' Descending'))
plot(dsinter,dsdecfit(1)+dsdecfit(2)*dsinter,'c*','Tag',strcat(synfile(1,end-8:end-4),...
    'Intersection'))

figure(3)
plot([1:1:length(d2sfit)]',d2sfit(1)+d2sfit(2)*[1:1:length(d2sfit)]','k-','Tag',...
    strcat(synfile(1,end-8:end-4),' Area Slope'))

% Format the data to be returned to the calling program

s_fit(1,:) = mechreg_s;
s_fit(2,2:3) = elasreg_s';
s_fit(3,:) = strnhard_s;

s_fit(4,2:3) = dsappfit';
s_fit(5,2:3) = dsdecfit';
s_fit(6,3) = dsinter;

s_fit(7,2:3) = d2sfit';
s_fit(8,3) = zerocross;

e_fit(1,:) = mechreg_e;
e_fit(2,2:3) = elasreg_e';
e_fit(3,:) = strnhard_e;

e_fit(4,2:3) = dsappfit';
e_fit(5,2:3) = dsdecfit';
e_fit(6,3) = dsinter;

e_fit(7,2:3) = d2sfit';
e_fit(8,3) = zerocross;

clear d2sfit d2sfit dsappfit dsdecfit dsfilt dsinter elasreg f1 f2 f3 i_UTS i_mech...
    i_yield k mechreg n strnhard strt zerocross

```

```

function [avg_val, avg_val_std, avg_fit, avg_fit_std] = WSRStats(processed_data, type);
%%%%%%%%%%%%%%%%%%%%%%%%%%%%%%%%%%%%%%%%%%%%%%%%%%%%%%%%%%%%%%%%%%%%%%%%%%%%%%
%WSRStats determines the statistical parameters associated with the fits in each replicate
% The first input argument is the struct containing all the processed data
% The second input argument is a character that determines what fits are analyzed (stress
% or strain).
% The function outputs four double arrays containing the mean and standard deviations
% of the values associated with the fit indices. It also outputs the mean and
% standard deviations of the fits
%
% By Glenn McGillicuddy
% Date: 09/01/05
%%%%%%%%%%%%%%%%%%%%%%%%%%%%%%%%%%%%%%%%%%%%%%%%%%%%%%%%%%%%%%%%%%%%%%%%%%%%%%

```

% Determine the average mechanical settling point, yield point, and ultimate tensile strength

```

for i = 1:length(processed_data)
    i_strt(i,1:3) = processed_data(i).Curve_Indices(1,1:3);
    i_mech(i,1:3) = processed_data(i).Curve_Indices(2,1:3);
    i_yield(i,1:3) = processed_data(i).Curve_Indices(3,1:3);
    i_UTS(i,1:3) = processed_data(i).Curve_Indices(4,1:3);

    mech_fit(i,1:3) = eval(strcat('processed_data(i).',type,'_Curve_Fits(1,1:3)'));
    elas_fit(i,1:3) = eval(strcat('processed_data(i).',type,'_Curve_Fits(2,1:3)'));
    hard_fit(i,1:3) = eval(strcat('processed_data(i).',type,'_Curve_Fits(3,1:3)'));
    appr_fit(i,1:3) = eval(strcat('processed_data(i).',type,'_Curve_Fits(4,1:3)'));
    dec_fit(i,1:3) = eval(strcat('processed_data(i).',type,'_Curve_Fits(5,1:3)'));
    inter_fit(i,1:3) = eval(strcat('processed_data(i).',type,'_Curve_Fits(6,1:3)'));
    d2s_fit(i,1:3) = eval(strcat('processed_data(i).',type,'_Curve_Fits(7,1:3)'));
    zcross_fit(i,1:3) = eval(strcat('processed_data(i).',type,'_Curve_Fits(8,1:3)'));

    load(i,1) = processed_data(i).Test_Stats(1,1);
end

```

% Organize the data to be transferred back to calling program

```

avg_val(1,1:3) = mean(i_strt);
avg_val(2,1:3) = mean(i_mech);
avg_val(3,1:3) = mean(i_yield);
avg_val(4,1:3) = mean(i_UTS);
avg_val(1:4,1) = round(avg_val(1:4,1));

avg_val_std(1,1:3) = std(i_strt);
avg_val_std(2,1:3) = std(i_mech);
avg_val_std(3,1:3) = std(i_yield);
avg_val_std(4,1:3) = std(i_UTS);

avg_fit(1,1:3) = mean(mech_fit);
avg_fit(2,1:3) = mean(elas_fit);
avg_fit(3,1:3) = mean(hard_fit);
avg_fit(4,1:3) = mean(appr_fit);
avg_fit(5,1:3) = mean(dec_fit);
avg_fit(6,1:3) = mean(inter_fit);
avg_fit(7,1:3) = mean(d2s_fit);
avg_fit(8,1:3) = round(mean(zcross_fit));

```

```
avg_fit_std(1,1:3) = std(mech_fit);  
avg_fit_std(2,1:3) = std(elas_fit);  
avg_fit_std(3,1:3) = std(hard_fit);  
avg_fit_std(4,1:3) = std(appr_fit);  
avg_fit_std(5,1:3) = std(dec_fit);  
avg_fit_std(6,1:3) = std(inter_fit);  
avg_fit_std(7,1:3) = std(d2s_fit);  
avg_fit_std(8,1:3) = std(zcross_fit);
```



```

function PlotStruct(avg_fit,avg_fit_std,avg_val,avg_val_std,processed_data);
%%%%%%%%%%%%%%%%%%%%%%%%%%%%%%%%%%%%%%%%%%%%%%%%%%%%%%%%%%%%%%%%%%%%%%%%
%PlotStruct graphs the corrected data along with the fits and their confidence intervals
% The first four input arguments are the parameters output from WSRStats.m
% The fifth input parameter structure containing the processed data
%
% By Glenn McGillicuddy
% Date: 09/01/05
%%%%%%%%%%%%%%%%%%%%%%%%%%%%%%%%%%%%%%%%%%%%%%%%%%%%%%%%%%%%%%%%%%%%%%%%

% Plot the raw data for the Engineering Stress-Strain, delta stress, and delta2 stress

figure(1)
axis([0 0.3 0 28000])
title('Engineering Stress-Strain');
xlabel('Strain ( in / in )');
ylabel('Stress ( lbs / in^2 )');
box on
grid on
hold on

figure(2)
title('First Derivative of Stress');
xlabel('Linear Index Number');
ylabel('ds');
box on
grid on
hold on

figure(3)
title('Second Derivative of Stress');
xlabel('Linear Index Number');
ylabel('d^2 s');
box on
grid on
hold on

for n = 1:length(processed_data)
    figure(1)
    plot(processed_data(n).Strain(avg_val(1,1):end),processed_data(n).Stress(avg_val(1,1):end),...
        'bo','Tag',processed_data(n).Experiment);
    figure(2)
    plot(processed_data(n).Derivative_Stress(:,1),'bo','Tag',processed_data(n).Experiment);
    figure(3)
    plot(processed_data(n).Derivative_Stress(2:end,2),'bo','Tag',processed_data(n).Experiment);
end

%Create an array of strain values in order to plot the fits

e = 0:avg_val(4,2)/(avg_val(4,1)+10):avg_val(4,2);

% Evaluate the average fit values based on the above stain matrix

f1 = polyval(avg_fit(1,:),e(1:avg_val(2,1)));
f2 = avg_fit(2,2)+avg_fit(2,3)*e(avg_val(2,1):avg_val(3,1));
f3 = polyval(avg_fit(3,:),e(avg_val(3,1):end));

```

```

f4 = avg_fit(4,2)+avg_fit(4,3)*[1:1:avg_fit(8,3)+10]';
f5 = avg_fit(5,2)+avg_fit(5,3)*[avg_fit(8,3)-10:1:avg_val(4,1)]';
f6 = avg_fit(5,2)+avg_fit(5,3)*avg_fit(6,3);
f7 = avg_fit(7,2)+avg_fit(7,3)*[1:1:avg_val(4,1)]';

```

% Compute the upper 95% Confidence Interval

```

f1u = f1 + (1.96*(avg_fit_std(1,3)/sqrt(length(processed_data))));
f2u = f2 + (1.96*(avg_fit_std(2,3)/sqrt(length(processed_data))));
f3u = f3 + (1.96*(avg_fit_std(3,3)/sqrt(length(processed_data))));
f4u = f4 + (1.96*(avg_fit_std(4,2)/sqrt(length(processed_data))));
f5u = f5 + (1.96*(avg_fit_std(5,2)/sqrt(length(processed_data))));
f6u = f6 + (1.96*(avg_fit_std(6,3)/sqrt(length(processed_data))));
f7u = f7 + (1.96*(avg_fit_std(7,2)/sqrt(length(processed_data))));

```

% Compute the lower 95% Confidence Interval

```

f1l = f1 - (1.96*(avg_fit_std(1,3)/sqrt(length(processed_data))));
f2l = f2 - (1.96*(avg_fit_std(2,3)/sqrt(length(processed_data))));
f3l = f3 - (1.96*(avg_fit_std(3,3)/sqrt(length(processed_data))));
f4l = f4 - (1.96*(avg_fit_std(4,2)/sqrt(length(processed_data))));
f5l = f5 - (1.96*(avg_fit_std(5,2)/sqrt(length(processed_data))));
f6l = f6 - (1.96*(avg_fit_std(6,3)/sqrt(length(processed_data))));
f7l = f7 - (1.96*(avg_fit_std(7,2)/sqrt(length(processed_data))));

```

% Plot the various fits and tier confidence intervals

```

figure(1)
plot(e(1:avg_val(2,1)),f1,'g','Tag','Mechanical Region Fit','LineWidth',2)
plot(e(1:avg_val(2,1)),f1u,'k--','Tag','Mechanical Region Fit + STD')
plot(e(1:avg_val(2,1)),f1l,'k--','Tag','Mechanical Region Fit - STD')
plot(e(avg_val(2,1):avg_val(3,1)),f2,'r','Tag','Elastic Region Fit','LineWidth',2)
plot(e(avg_val(2,1):avg_val(3,1)),f2u,'k--','Tag','Elastic Region Fit + STD','LineWidth',2)
plot(e(avg_val(2,1):avg_val(3,1)),f2l,'k--','Tag','Elastic Region Fit - STD','LineWidth',2)
plot(e(avg_val(3,1):end),f3,'c','Tag','Strain Hardened Region Fit','LineWidth',2)
plot(e(avg_val(3,1):end),f3u,'k--','Tag','Strain Hardened Region Fit + STD')
plot(e(avg_val(3,1):end),f3l,'k--','Tag','Strain Hardened Region Fit - STD')
hgsave(gcf,'Stress_Strain_RefComp.fig')
print('-dtiff','-r400','Stress_Strain_POLY_CI')

```

```

figure(2)
plot([1:1:avg_fit(8,3)+10]',f4,'r-','Tag','Approach Slope Fit','LineWidth',2)
plot([1:1:avg_fit(8,3)+10]',f4u,'k--','Tag','Approach Slope Fit + STD','LineWidth',2)
plot([1:1:avg_fit(8,3)+10]',f4l,'k--','Tag','Approach Slope Fit - STD','LineWidth',2)
plot([avg_fit(8,3)-10:1:avg_val(4,1)]',f5,'r-','Tag','Decending Slope Fit','LineWidth',2)
plot([avg_fit(8,3)-10:1:avg_val(4,1)]',f5u,'k--','Tag','Decending Slope Fit + STD','LineWidth',2)
plot([avg_fit(8,3)-10:1:avg_val(4,1)]',f5l,'k--','Tag','Decending Slope Fit - STD','LineWidth',2)
plot(avg_fit(6,3),f6,'g*','Tag','Intersection Point','LineWidth',2)
plot(avg_val(2,1),[f6-100:0.1:f6+100], 'c-','LineWidth',2)
plot(avg_val(3,1),[f6-100:0.1:f6+100], 'c-','LineWidth',2)
hgsave(gcf,'Delta_Stress_RefComp.fig')
print('-dtiff','-r400','Delta_Stress_POLY_CI')

```

```

figure(3)
plot([1:1:avg_val(4,1)]',f7,'r-','Tag','Cross Sectional Area Slope','LineWidth',2)
plot([1:1:avg_val(4,1)]',f7u,'k--','Tag','Cross Sectional Area Slope + STD','LineWidth',1)

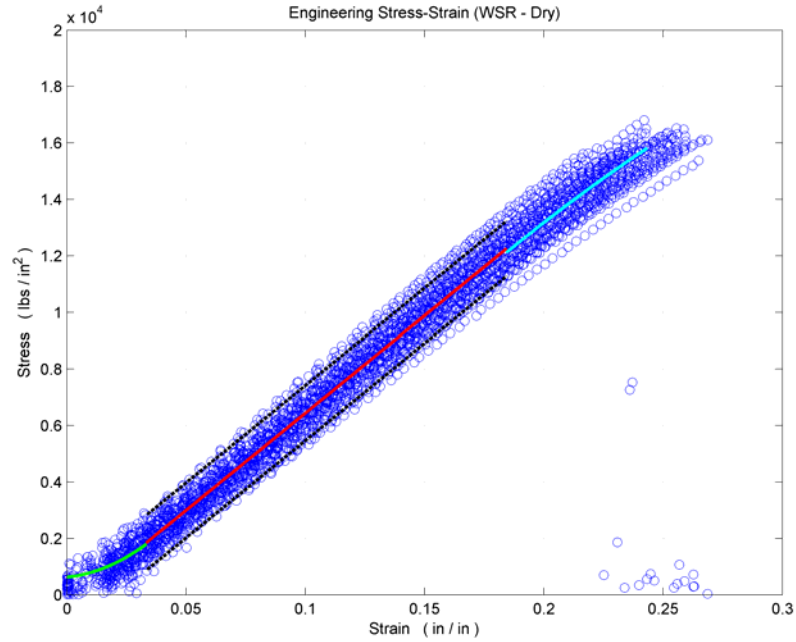
```

```

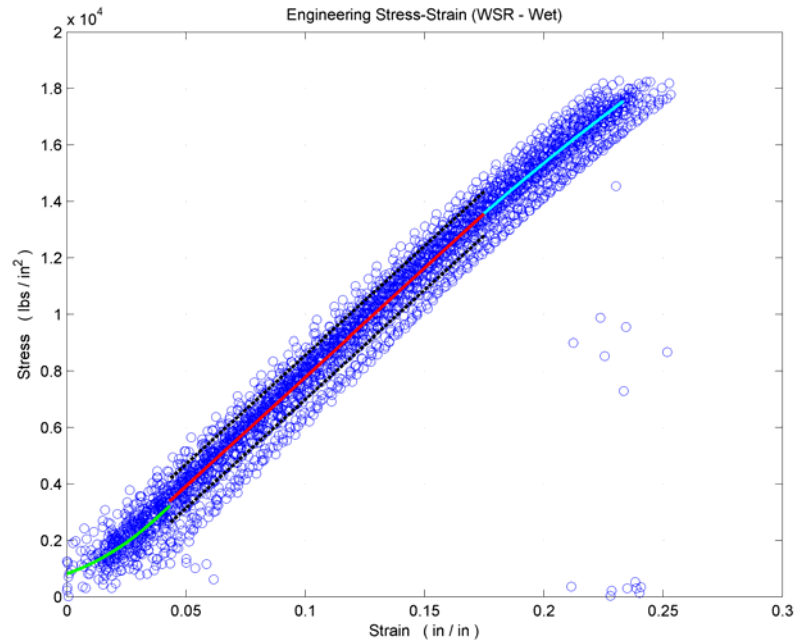
plot([1:1:avg_val(4,1)]',f7l,'k--','Tag','Cross Sectional Area Slope - STD','LineWidth',1)
plot(avg_val(2,1),[-20:0.1:20], 'c-','LineWidth',2)
plot(avg_val(3,1),[-20:0.1:20], 'c-','LineWidth',2)
hgsave(gcf,'Delta2_Stress_RefComp.fig')
print('-dtiff','-r400','Delta2_Stress_WSRW_CI')

```

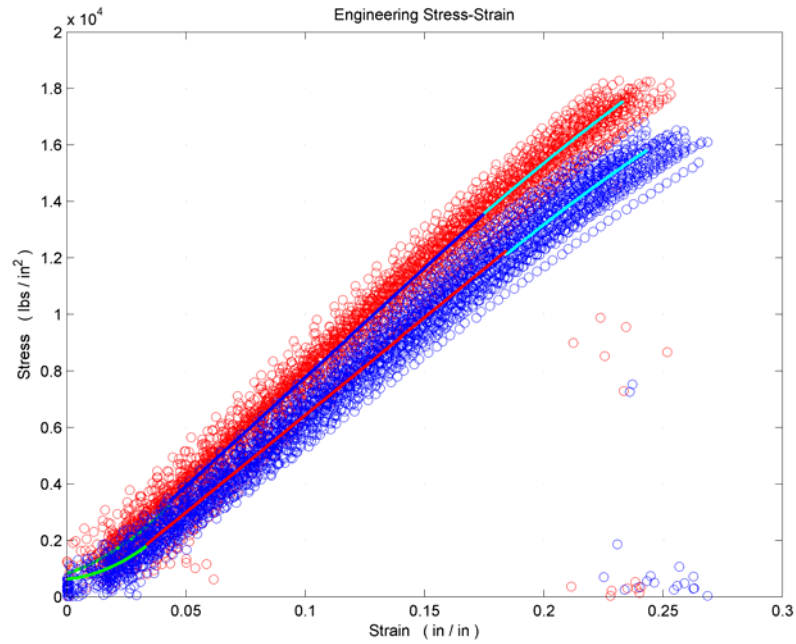
**APPENDIX D:**  
**Engineering Stress-Strain Plots**



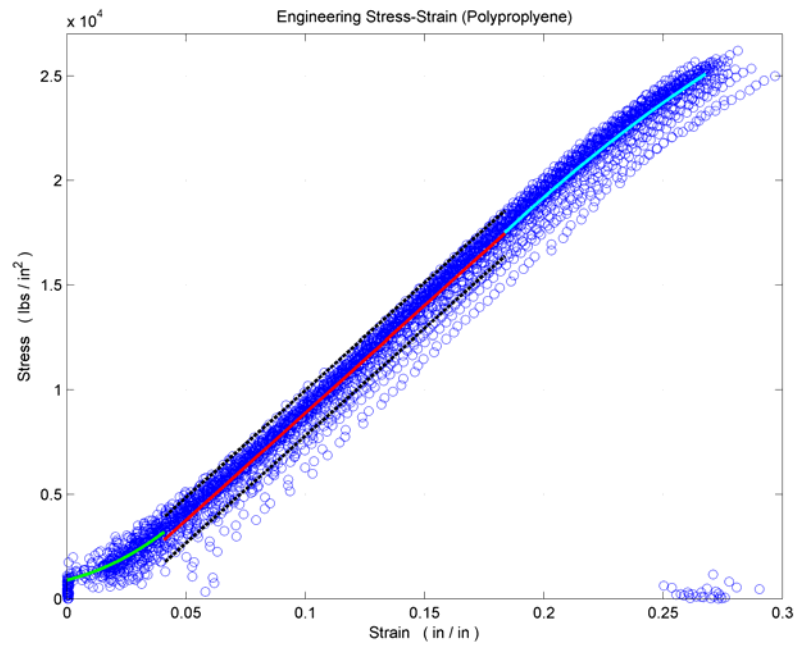
**Figure D.1: Engineering Stress-Strain of WSR - Dry. Raw data for each replicate (blue), Mechanical settling curve fit (green), Linear-elastic region curve fit (red), Strain-hardening region curve fit (cyan), and 95% Confidence interval (black dash).**



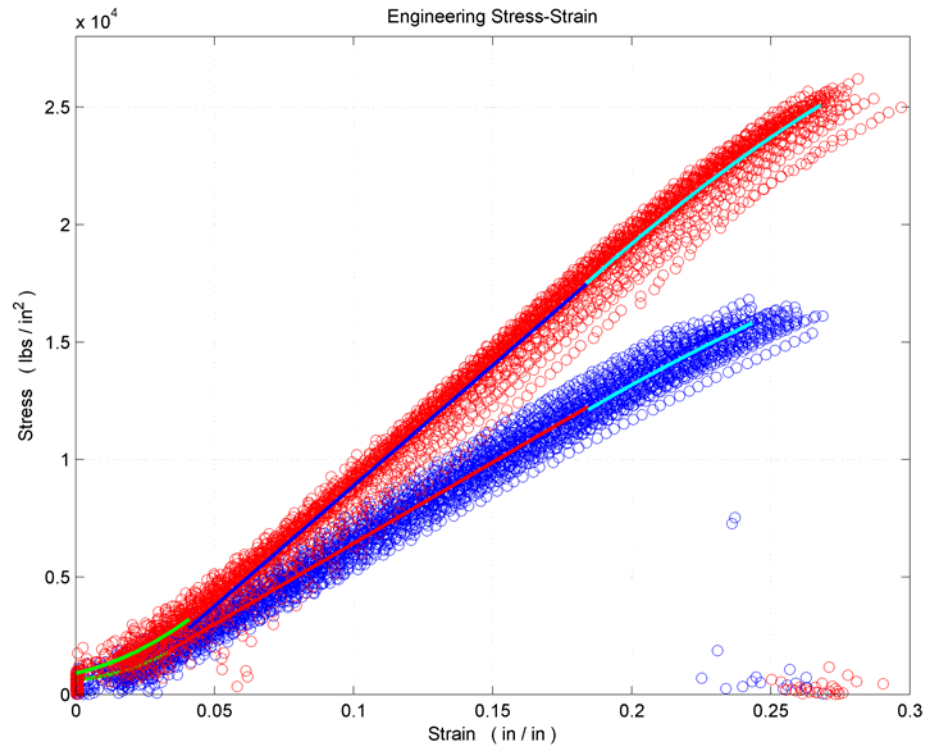
**Figure D.2: Engineering Stress-Strain of WSR – Wet. Raw data for each replicate (blue), Mechanical settling curve fit (green), Linear-elastic region curve fit (red), Strain-hardening region curve fit (cyan), and 95% Confidence interval (black dash).**



**Figure D.3: Engineering Stress-Strain Comparison of Wet and Dry WSR. Dry case is represented in blue and Wet case is represented in red.**



**Figure D.4: Engineering Stress-Strain of Polypropylene. Raw data for each replicate (blue), Mechanical settling curve fit (green), Linear-elastic region curve fit (red), Strain-hardening region curve fit (cyan), and 95% Confidence interval (black dash).**

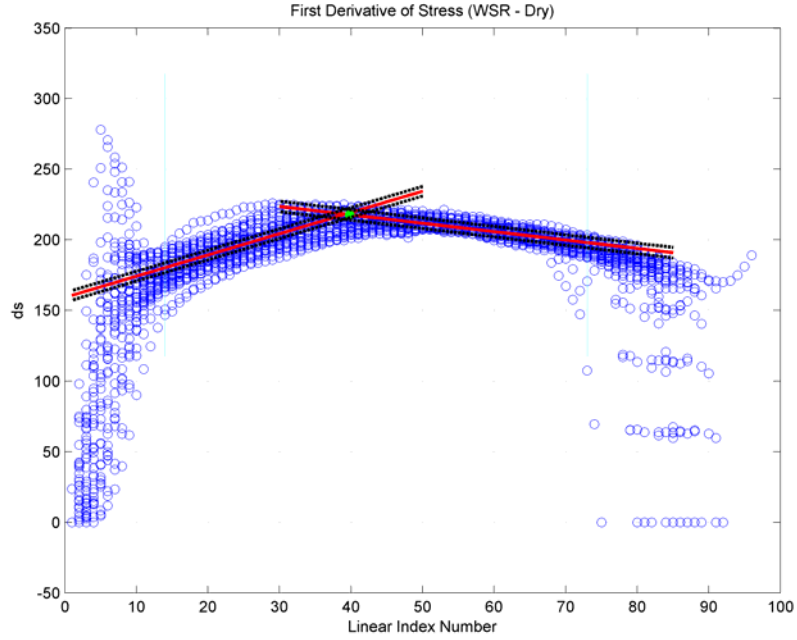


**Figure D.5: Engineering Stress-Strain Comparison of WSR - Dry (blue) and Standard Polypropylene (red). Note the significant difference in the slope of the linear elastic region fit. Also note the flatness of WSR's strain-hardening region in comparison to the polypropylene.**

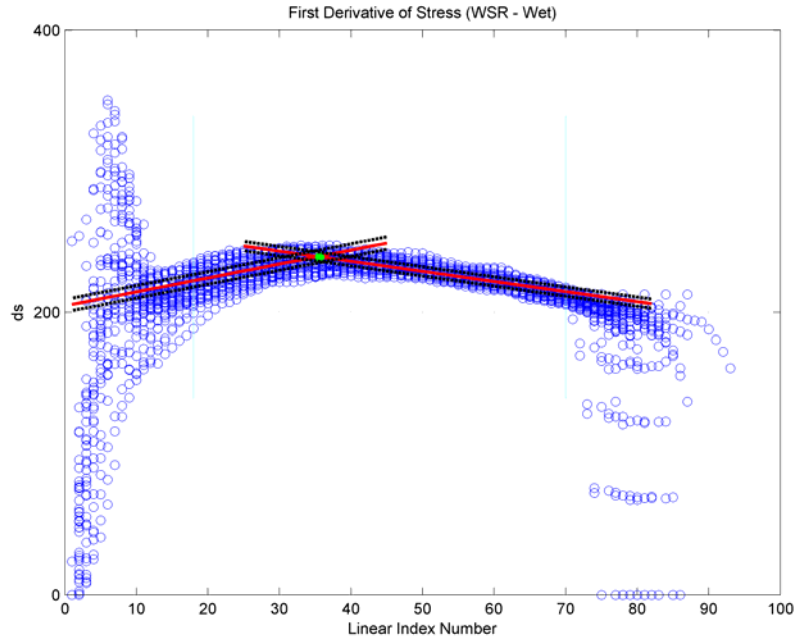
## **APPENDIX E:**

### **First Derivative of Stress with Respect to Time**

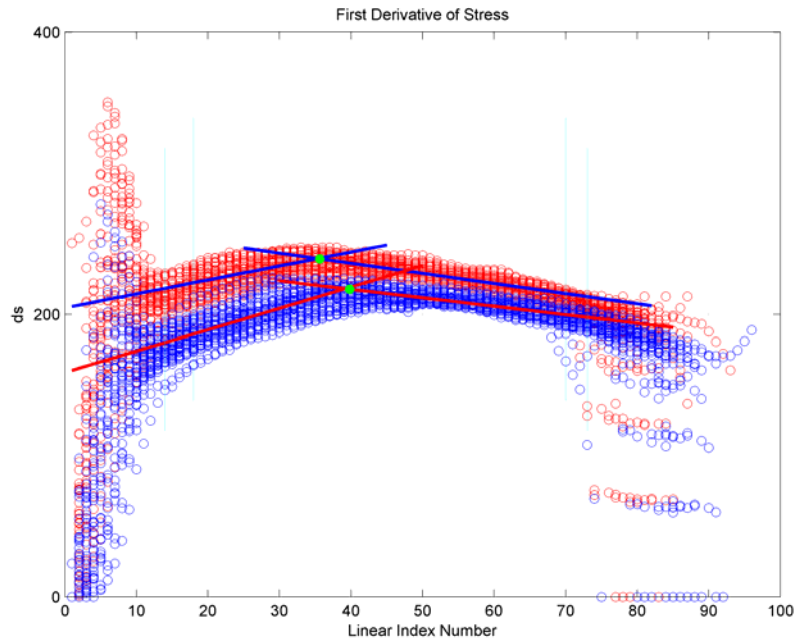




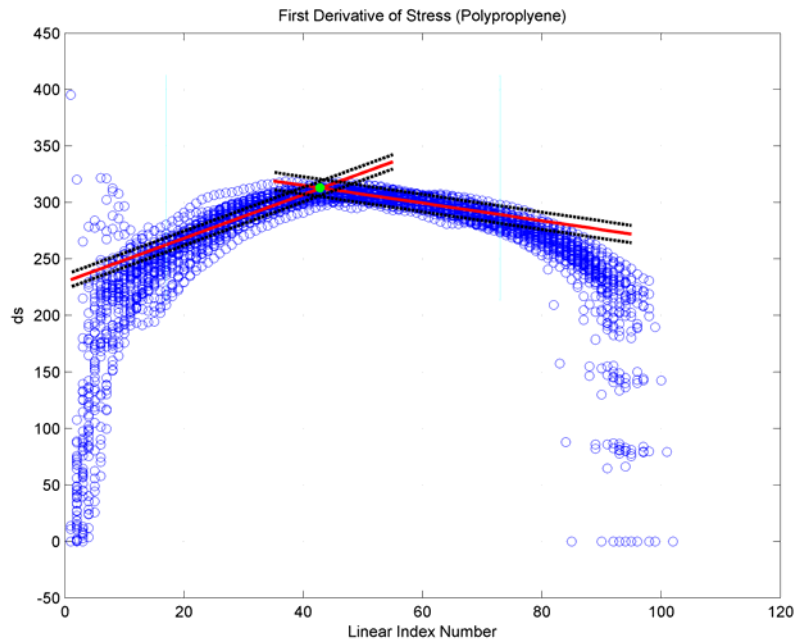
**Figure E.1: First Derivative of Stress for WSR-Dry. Raw data for each replicate (blue), piecewise fits for the positive and negative sections (red), the intersection of the fits (green), and the 95% Confidence interval (black dash)**



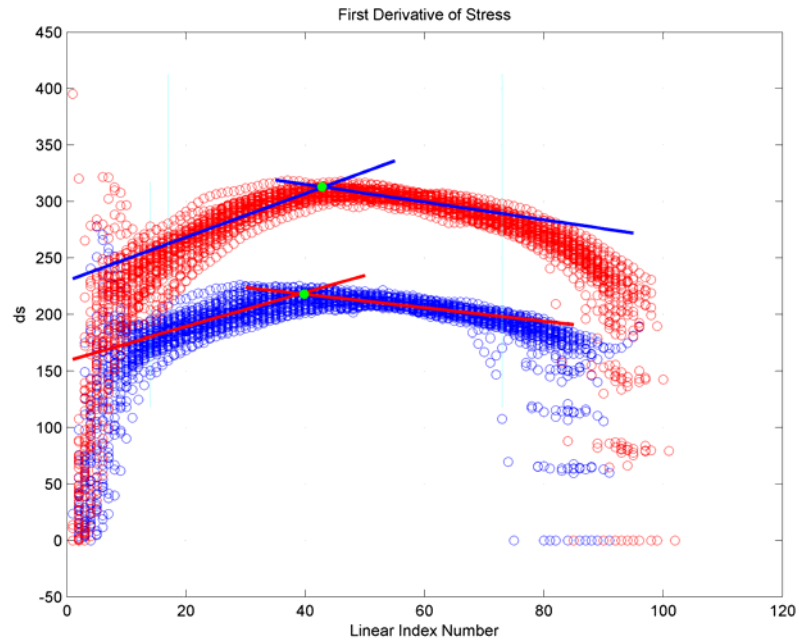
**Figure E.2: First Derivative of Stress for WSR-Wet. Raw data for each replicate (blue), piecewise fits for the positive and negative sections (red), the intersection of the fits (green), and the 95% Confidence interval (black dash).**



**Figure E.3: First derivative of stress comparison between dry (blue) and wet (red) WSR.**



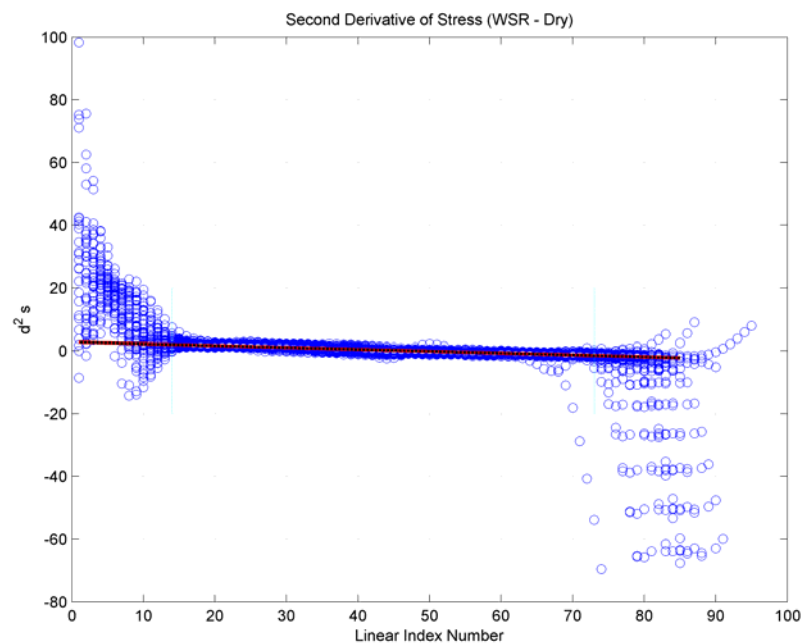
**Figure E.4: First Derivative of Stress for Polypropylene. Raw data for each replicate (blue), piecewise fits for the positive and negative sections (red), the intersection of the fits (green), and the 95% Confidence interval (black dash).**



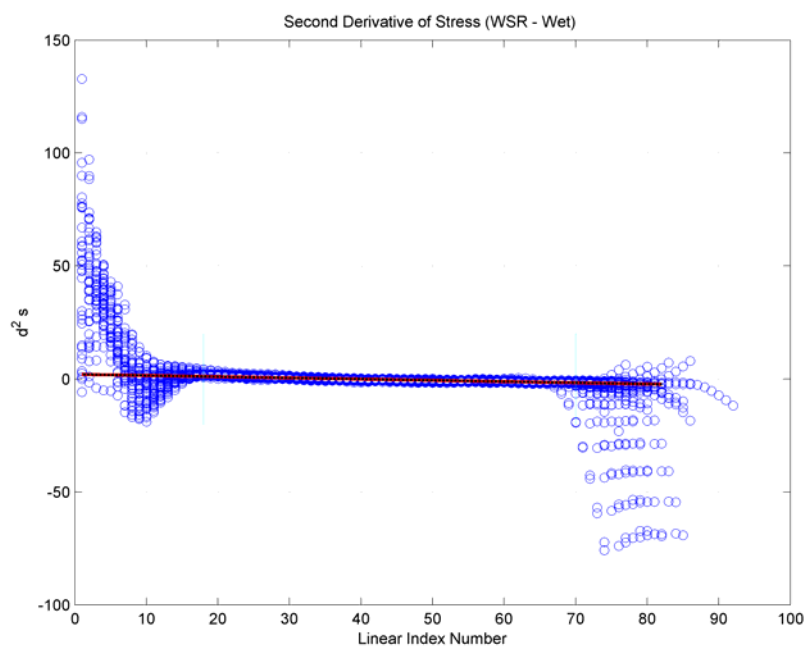
**Figure E.5: First derivative of stress comparison between WSR-Dry (blue) and Standard Polypropylene (red). Note that the WSR is much flatter as compared to the polypropylene.**

## **APPENDIX F:**

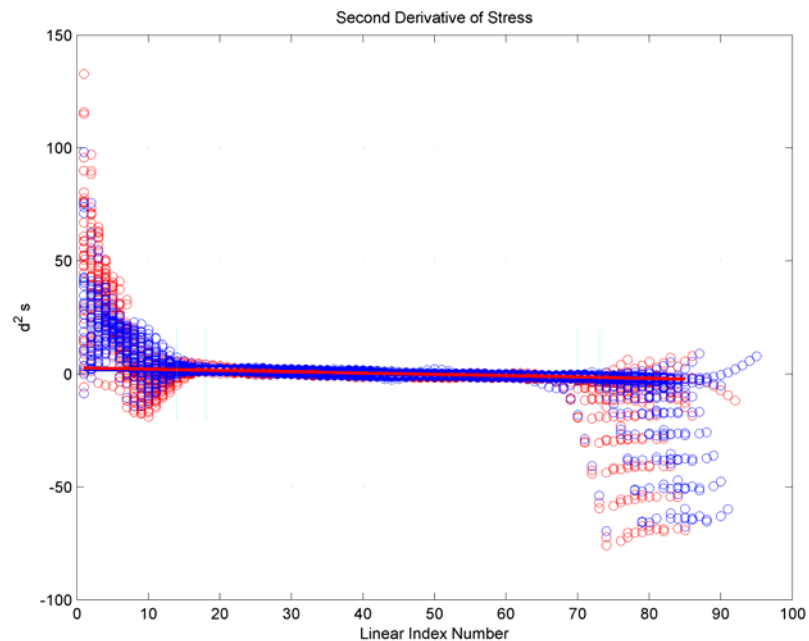
### **Second Derivative of Stress with Respect to Time**



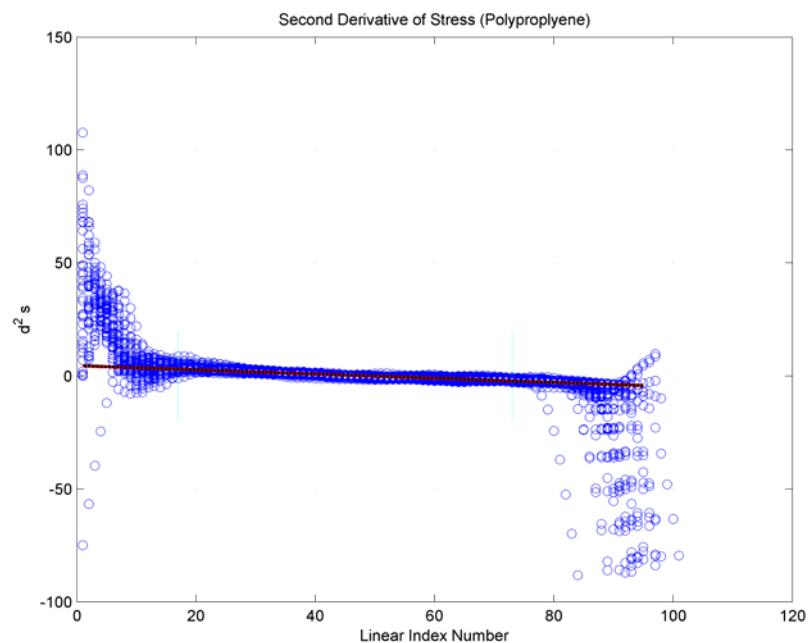
**Figure F.1: Second derivative of stress for WSR-Dry. Raw data for each replicate (blue), curve fit of the data (red), and 95% Confidence interval (black dash). Note the negative slope of the fit line.**



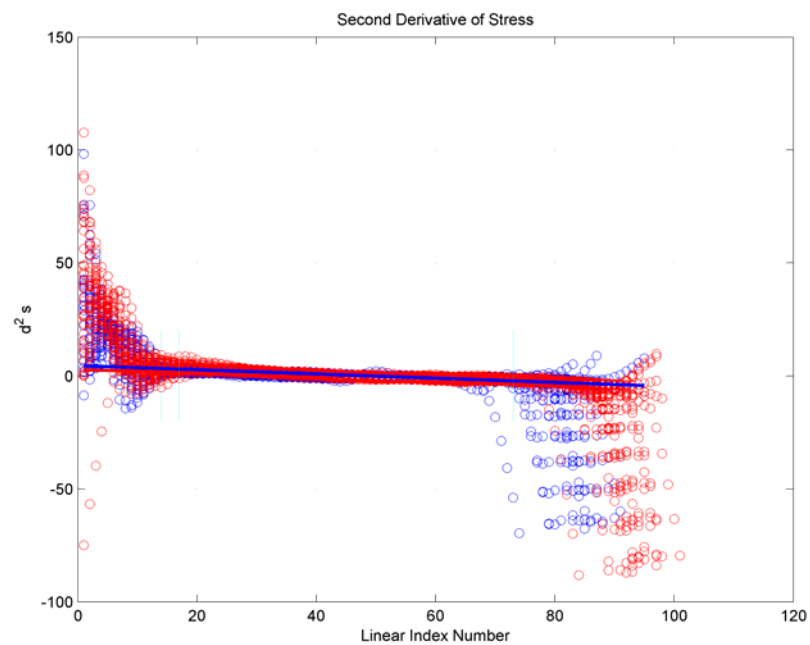
**Figure F.2: Second derivative of stress for WSR-Wet. Raw data for each replicate (blue), curve fit of the data (red), and 95% Confidence interval (black dash). Note the negative slope of the fit line.**



**Figure F.3: Comparison between the dry (blue) and wet (red) WSR second derivative of stress.**



**Figure F.4: Second derivative of stress for polypropylene. Raw data for each replicate (blue), curve fit of the data (red), and 95% Confidence interval (black dash). Note the negative slope of the fit line.**



**Figure F.5: Comparison of the second derivative of stress between WSR-dry (blue) and standard polypropylene (red)**